nature cell biology

ARTICLES

https://doi.org/10.1038/s41556-021-00688-9

Check for updates

ELOF1 is a transcription-coupled DNA repair factor that directs RNA polymerase II ubiquitylation

Yana van der Weegen[1,10], Klaas de Lint[2,10], Diana van den Heuvel[1], Yuka Nakazawa[3,4], Tycho E. T. Mevissen[5], Janne J. M. van Schie[2], Marta San Martin Alonso[1,6], Daphne E. C. Boer[1], Román González-Prieto[7], Ishwarya V. Narayanan[8], Noud H. M. Klaassen[1], Annelotte P. Wondergem[1], Khashayar Roohollahi[2], Josephine C. Dorsman[2], Yuichiro Hara[3,4], Alfred C. O. Vertegaal[7], Job de Lange[2], Johannes C. Walter[5], Sylvie M. Noordermeer[1,6], Mats Ljungman[8,9], Tomoo Ogi[3,4], Rob M. F. Wolthuis[2]✉ and Martijn S. Luijsterburg[1]✉

Cells employ transcription-coupled repair (TCR) to eliminate transcription-blocking DNA lesions. DNA damage-induced binding of the TCR-specific repair factor CSB to RNA polymerase II (RNAPII) triggers RNAPII ubiquitylation of a single lysine (K1268) by the CRL4^{CSA} ubiquitin ligase. How CRL4^{CSA} is specifically directed towards K1268 is unknown. Here, we identify ELOF1 as the missing link that facilitates RNAPII ubiquitylation, a key signal for the assembly of downstream repair factors. This function requires its constitutive interaction with RNAPII close to K1268, revealing ELOF1 as a specificity factor that binds and positions CRL4^{CSA} for optimal RNAPII ubiquitylation. Drug–genetic interaction screening also revealed a CSB-independent pathway in which ELOF1 prevents R-loops in active genes and protects cells against DNA replication stress. Our study offers key insights into the molecular mechanisms of TCR and provides a genetic framework of the interplay between transcriptional stress responses and DNA replication.

Transcription of protein-coding and noncoding genes requires RNA polymerase II (RNAPII), which synthesizes RNA transcripts complementary to the DNA template strand. The presence of DNA lesions in the template strand causes stalling of elongating RNAPII (RNAPIIo), which leads to genome-wide transcriptional arrest[1–3]. It is essential that cells overcome this arrest and restore transcription. The transcription-coupled repair (TCR) pathway efficiently removes transcription-blocking DNA lesions through the proteins CSB, CSA and UVSSA[4–6]. Inactivating mutations in *CSB* and *CSA* cause Cockayne syndrome (CS), which is characterized by severe neurological dysfunction related to persistent RNAPII arrest at DNA lesions[2,7].

The sequential and cooperative actions of CSB, CSA and UVSSA recruit TFIIH to DNA damage-stalled RNAPII to initiate DNA repair[6]. In addition to protein–protein contacts, efficient transfer of TFIIH onto RNAPII requires ubiquitylation of a single lysine on the largest subunit of RNAPII (RPB1-K1268), which is essential for efficient TCR[2]. This DNA damage-induced modification of RNAPII is dependent on cullin-ring type E3-ligases (CRLs) and is strongly decreased in CSA-deficient cells[2], which indicates that the CRL4^{CSA} E3 ligase complex drives RNAPII ubiquitylation.

CSB binds to DNA upstream of RNAPII[8] (Extended Data Fig. 1a) and recruits the CRL4^{CSA} complex through an evolutionarily conserved motif in its carboxy terminus[6]. However, how the activity of CRL4^{CSA} ubiquitin ligase is specifically directed towards the K1268 site remains to be elucidated.

Results

A CRISPR screen identifies *ELOF1* as a putative TCR gene. To identify unknown TCR genes, we performed a genome-wide CRISPR screen in the presence of the compound illudin S, which induces transcription-blocking DNA lesions that are eliminated by TCR[9]. RPE1-iCas9 cells were transduced with the pLCKO-TKOv3 library, which contains 70,948 single guide RNAs (sgRNAs) targeting open reading frames[10], and cultured for 12 population doublings, after which sgRNA contents were analysed (Extended Data Fig. 1b).

Using a false-discovery rate (FDR) cut-off of 0.01, we found 104 sensitizer hits and 18 hits conferring resistance to illudin S. The strongest resistance was conferred by guide RNAs (gRNAs) targeting *PTGR1*, which is in line with its known role in bioactivating illudin S[11] (Fig. 1a and Extended Data Fig. 1c). Nine known core TCR genes, including *CSB*, *CSA* and *UVSSA*, but also genes connected to transcription recovery after UV irradiation (*HIRA*[12], *DOT1L*[13] and *STK19* (ref. [14]) (Fig. 1a,b), were required for illudin S tolerance. Consistent with known effects of illudin S on replication[9], we found the 9-1-1 complex, translesion synthesis and sister-chromatid cohesion components (Fig. 1b). Our screen also identified the

[1]Department of Human Genetics, Leiden University Medical Center, Leiden, The Netherlands. [2]Department of Clinical Genetics, Section Oncogenetics, Cancer Center Amsterdam, Amsterdam University Medical Center, Amsterdam, The Netherlands. [3]Department of Genetics, Research Institute of Environmental Medicine (RIeM), Nagoya University, Nagoya, Japan. [4]Department of Human Genetics and Molecular Biology, Nagoya University Graduate School of Medicine, Nagoya, Japan. [5]Howard Hughes Medical Institute and Department of Biological Chemistry and Molecular Pharmacology, Harvard Medical School, Boston, MA, USA. [6]Oncode Institute, Utrecht, The Netherlands. [7]Department of Cell and Chemical Biology, Leiden University Medical Center, Leiden, The Netherlands. [8]Department of Radiation Oncology, University of Michigan, Ann Arbor, MI, USA. [9]Department of Environmental Health Sciences, Rogel Cancer Center and Center for RNA Biomedicine, University of Michigan, Ann Arbor, MI, USA. [10]These authors contributed equally: Yana van der Weegen, Klaas de Lint. ✉e-mail: r.wolthuis@amsterdamumc.nl; m.luijsterburg@lumc.nl

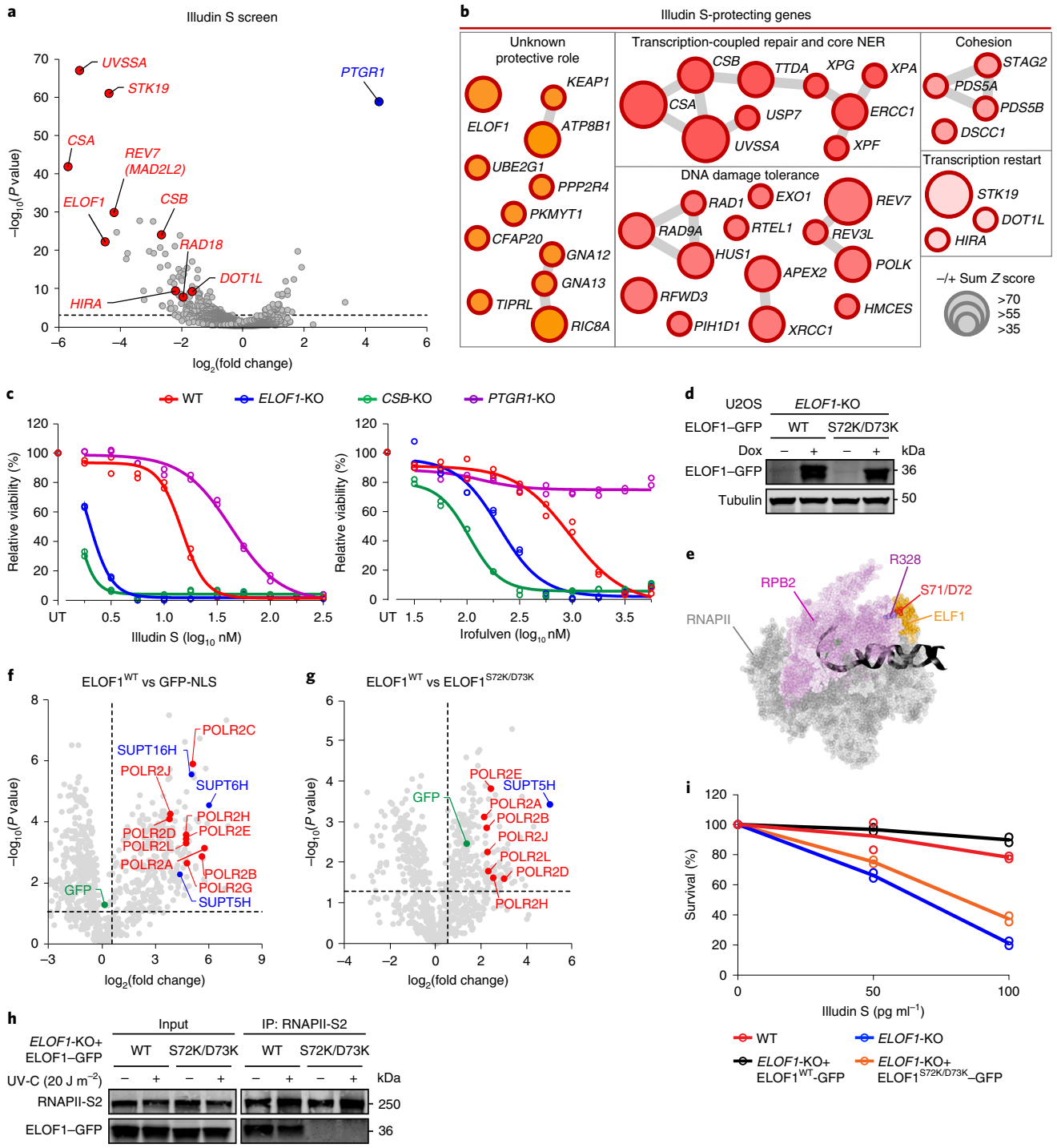

Fig. 1 | RNAPII-associated *ELOF1* is a putative TCR gene. a, Volcano plot depicting gene KOs sensitizing (red) or conferring resistance (blue) to illudin S. Fold changes ($\log_2$) are plotted on the *x* axis and significance ($-\log_{10}$(*P* value)) is plotted on the *y* axis (full analysis results are in the source data). **b**, Network analysis of highly significant hits representing genes essential for illudin S resistance. Grey lines reflect known protein–protein interactions (Cytoscape, BioGRID). NER, nucleotide excision repair. **c**, Drug-sensitivity assays (72 h) of indicated RPE1-iCas9 cells. The experiment was performed twice and each symbol represents the median of six technical replicates of an independent experiment. UT, untreated. **d**, Western blot analysis of U2OS (FRT) *ELOF1*-KO cells complemented with inducible GFP-tagged versions of ELOF1. Data shown represent three independent experiments. **e**, Side view of the structure (Protein Data Bank ID: 5XOG) of *Komagataella pastoris* ELF1 (orange) bound to RNAPII (grey) with RPB2 in purple. Residues important for the ELF1-RNAPII interaction are indicated. **f**,**g**, Volcano plots depicting the statistical differences between four replicates of the MS analysis after GFP immunoprecipitation of mock-treated cells comparing ELOF1^{WT}–GFP with GFP-NLS (**f**) or ELOF1^{WT}–GFP with ELOF1$^{S72K/D73K}$–GFP (**g**). The fold change ($\log_2$) is plotted on the *x* axis and the significance (*t*-test $-\log_{10}$(*P* value)) is plotted on the *y* axis. RNAPII subunits are indicated in red, elongation factors are indicated in blue, and GFP is indicated in green. **h**, Endogenous RNAPIIo co-immunoprecipitation (co-IP) on U2OS (FRT) *ELOF1*-KO cells complemented with ELOF1^{WT}–GFP and ELOF1$^{S72K/D73K}$–GFP. Data shown represent four independent experiments. **i**, Clonogenic illudin S survival of U2OS (FRT) WT, *ELOF1*-KO and GFP-tagged ELOF1 rescue cell lines. The experiment was performed twice and each symbol represents the mean of two technical replicates of an independent experiment. Uncropped blots and numerical data are provided in the source data.

uncharacterized *ELOF1* gene as a top hit, which we decided to study in detail (Fig. 1a,b).

We generated single *PTGR1*, *ELOF1* and *CSB* knockouts (KOs) in RPE1-iCas9 cells (Extended Data Fig. 1d) and exposed these to compounds that generate transcription stress. Drug-sensitivity assays confirmed that single *ELOF1*-KO and *CSB*-KO clones were highly sensitive to illudin S, irofulven and cisplatin, while *PTGR1*-KO cells were resistant to illudin S and irofulven (Fig. 1c and Extended Data Fig. 1e). Clonogenic survival experiments confirmed that *ELOF1*-KO cells are nearly as sensitive to illudin S as *CSB*-KO cells (Extended Data Fig. 1f). Re-expression of green fluorescent protein (GFP)-tagged ELOF1 in *ELOF1*-KO U2OS cells completely restored their illudin S tolerance (Fig. 1d and Extended Data Fig. 2a,b).

ELOF1 interacts with RNAPII through conserved residues. ELOF1 is a small zinc-finger protein that is evolutionarily conserved across eukaryotes, except for its C-terminal acidic tail, which is absent in metazoan orthologues[15] (Extended Data Fig. 2c). ELF1, the yeast orthologue of ELOF1, is a putative transcription elongation factor that interacts with RNAPII through a central RNAPII-binding helix (Fig. 1e) and promotes passage through nucleosomes[16,17]. Mutations in residues that disrupt this interaction (ELF1$^{S71K/D72K}$) compromise its function[16,17].

To study human ELOF1, we immunoprecipitated GFP-tagged ELOF1 variants followed by mass spectrometry (MS). Pull-down of wild-type ELOF1 (ELOF1^{WT}) revealed an interaction with nine RNAPII subunits and three transcription elongation factors (Fig. 1f and Extended Data Fig. 2d). The ELOF1$^{S72K/D73K}$ (S71K/D72K in yeast) mutant showed a severely reduced interaction with RNAPIIo (Fig. 1g and Extended Data Fig. 2d), which was confirmed by reciprocal pull-down of RNAPIIo (Fig. 1h). The RNAPIIo–ELOF1 interaction was constitutive and not affected by UV irradiation (Fig. 1h and Extended Data Fig. 2e). Re-expression of ELOF1^{WT}, but not ELOF1$^{S72K/D73K}$, fully rescued the illudin S-sensitive phenotype of *ELOF1*-KO cells (Fig. 1i and Extended Data Fig. 2f). These findings reveal similar RNAPII-binding modes between yeast ELF1 and human ELOF1 and show that the ELOF1–RNAPII interaction protects against transcription-blocking DNA damage.

Loss of ELOF1 decreases RNAPII elongation rates. To identify the framework of genetic interactions with ELOF1, we performed a genome-wide CRISPR screen in *ELOF1*-KO RPE1-iCas9 cells. This approach identified synthetic lethality between *ELOF1* and several transcription elongation factors, including *SUPT4H1*, *TCEA1*, *SUPT6H* and the PAF1 complex subunits *CTR9* and *LEO1* (Fig. 2a,b). This is consistent with genetic studies showing that deletion of yeast ELF1 causes synthetic lethality with mutations in elongation factors[18], which is probably caused by functional redundancy[16,17]. Several of these elongation factors also reside in a protein complex with ELOF1 (Fig. 1f).

To investigate the role of ELOF1 in transcription elongation, we performed genome-wide BruDRB-seq[19]. Cells were treated with the transcription inhibitor 5,6-dichlorobenzimidazole1-β-D-ribofuranoside (DRB) for 3.5 h followed by its removal to trigger synchronized transcription elongation into gene bodies. Nascent transcripts were labelled with bromouridine (BrU), isolated and deep-sequenced[19]. Averaging nascent RNA profiles of 400 genes revealed that RNAPII progressed ~60 kb within 30 min in both WT and *ELOF1*-KO cells (Fig. 2c–e). Within 60 min, RNAPII progressed ~120 kb in WT cells, but only ~90 kb in *ELOF1*-KO cells (Fig. 2c–e). Transcription wave-front measurements revealed that RNAPII elongates with ~2 kb min^{-1} in WT cells and ~1.5 kb min^{-1} in *ELOF1*-KO cells (Extended Data Fig. 3a).

Basal transcription after 5-ethynyluridine (5-EU) incorporation was reduced to ~40% in *ELOF1*-KO cells compared with WT cells (Fig. 2f,g). An analysis of 400 genes of at least 100 kb by Bru-seq revealed no difference in initiation, while transcription progressively decreased towards the end of longer genes in *ELOF1*-KO cells (Fig. 2h), which was milder for shorter genes (Extended Data Fig. 3b). Consistently, *ELOF1*-KO cells did not display differences in chromatin accessibility at transcription start sites (TSSs) of ~3,000 genes measured by ATAC-seq (Extended Data Fig. 3c). These findings show that human ELOF1 acts as a transcription elongation factor.

ELOF1 is required for transcription restart following UV irradiation. TCR-deficient cells fail to resume transcription following genotoxic stress[20]. To assess whether ELOF1 is involved in transcription restart, we measured the recovery of RNA synthesis (RRS) by 5-EU labelling after UV irradiation. Transcriptional arrest was visible 3 h after UV irradiation in WT, *ELOF1*-KO and *CSB*-KO cells. Although WT cells completely recovered RNA synthesis within 24 h after UV exposure, both *CSB*-KO and *ELOF1*-KO cells failed to restart transcription (Fig. 3a,b and Extended Data Fig. 4a). Importantly, this defect is not due to decreased transcription elongation since *ELOF1*-KO cells were able to restart transcription after treatment with the transcription inhibitor DRB (Extended Data Fig. 4b). Re-expression of ELOF1^{WT} fully rescued transcription restart after UV irradiation in *ELOF1*-KO cells, while expression of ELOF1$^{S72K/D73K}$ did not (Fig. 3a,b and Extended Data Fig. 4c).

To explore the RRS in a genome-wide manner, we labelled nascent transcripts with BrU after UV irradiation followed by RNA isolation and sequencing. At 3 h after UV treatment, nascent transcription was strongly reduced at TSSs and progressively decreased further into gene bodies, with a loss beyond 100 kb in both WT and *ELOF1*-KO cells (Fig. 3c,d). Although milder, a similar loss of nascent transcription was observed towards the end of shorter genes (25–50 kb and 50–100 kb; Extended Data Fig. 4d), which fits with the distribution of photolesions[21] and the probability that RNAPII encounters them. Nascent transcription was partially resumed at 8 h and fully restored at 24 h after UV irradiation in WT cells, while *ELOF1*-KO cells failed to recover transcription at both time points (Fig. 3c–e).

Loss of ELOF1 causes stalling of RNAPII after UV irradiation. Genotoxic stress induces expression of the transcriptional repressor ATF3, which downregulates ~5,000 genes[22]. Both CSB and CSA promote ATF3 degradation, thereby relieving its inhibitory impact on transcription initiation[22]. Western blot analysis revealed an increase in steady-state ATF3 levels 7 h after UV treatment in WT, *ELOF1*-KO and *CSB*-KO cells (Fig. 3f). ATF3 protein levels decreased in WT cells within 48 h after UV exposure, while ATF3 levels strongly increased in both *ELOF1*-KO and *CSB*-KO cells at 24 h and 48 h after UV irradiation (Fig. 3f). These findings may explain the reduced RNA synthesis at TSSs following UV irradiation in *ELOF1*-KO cells (Fig. 3d and Extended Data Fig. 4d). RNA-sequencing (RNA-seq) showed that ATF3 transcript levels were strongly upregulated 24 h after UV exposure in *ELOF1*-KO and *CSB*-KO cells compared with WT cells (Extended Data Fig. 5a–c), which indicates that UV-mediated ATF3 induction is at least in part controlled at the mRNA synthesis level. While *ELOF1*-KO and *CSB*-KO cells showed a strong upregulation of short pro-survival genes, such as *CDKN1A*[23], a set of longer genes was downregulated at 24 h after UV treatment (Extended Data Fig. 5a–d), which is consistent with the RNA synthesis recovery defect in these cells (Fig. 3a,b).

To monitor genome-wide occupancy of RNAPII after UV irradiation, we performed chromatin immunoprecipitation with sequencing (ChIP-seq) using antibodies against unmodified RNAPII (pan-RNAPII). Heatmaps around the TSS showed a strong signal for ~3,000 genes around the promoter in non-irradiated cells, which

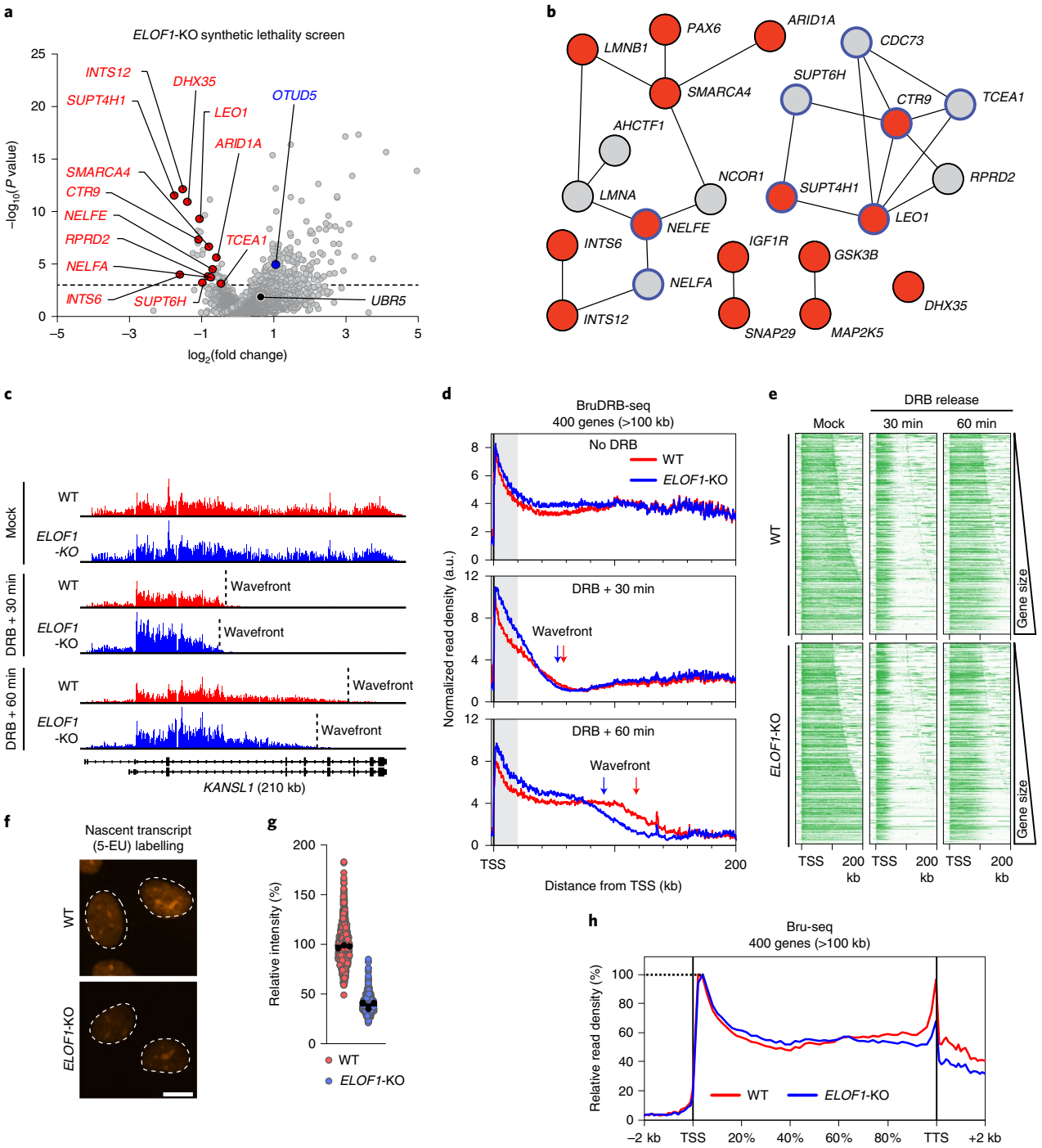

Fig. 2 | ELOF1 is required for efficient transcription elongation. a, Volcano plot depicting gene KOs depleted (red) or enriched (blue) in proliferating *ELOF1*-KO cells compared with WT cells. The fold change ($\log_2$) is plotted on the *x* axis and significance ($-\log_{10}$(*P* value)) is plotted on the *y* axis (full analysis results are in the source data). **b**, Network of interacting hit genes (FDR < 0.1, red) depleted in *ELOF1*-KO cells compared with WT cells, and depleted interactors (normalized *Z*-score ≤ 3, grey). Blue edges reflect RNAPII interactors and elongation factors, grey lines indicate other protein–protein interactions. **c**, UCSC genome browser track showing read densities of BrU signals across the *KANSL1* gene after mock treatment or after DRB wash-out (30 min or 60 min) showing transcription wavefronts in WT (red) and *ELOF1*-KO cells (blue). **d**, Metaplots of nascent transcription in 400 genes of >100 kb in WT (red) or *ELOF1*-KO (blue) cells after mock treatment or after DRB wash-out (30 min or 60 min). Wavefronts are defined as the distance from the TSS where the BrU signal drops below 20% of the positive signal. a.u., arbitrary units. **e**, Heatmaps of Bru-seq data from the TSS into the first 200 kb of 400 genes of >100 kb with the highest Bru-seq signal. Genes are ranked according to gene length (left panel). Heatmaps of the same genes after DRB wash-out (30 min or 60 min) in WT and *ELOF1*-KO cells. **f**,**g**, Representative images (**f**) and quantification (**g**) of 5-EU levels of RPE1-iCas9 *ELOF1*-KO cells normalized to RPE1-iCas9 WT cells. The experiment was performed three times and each black circle represents the median of two technical replicates of an independent experiment, with >80 cells collected per technical replicate. The black line represents the median of all the cells collected. Scale bar, 10 µm. **h**, Metaplots of BrU signal (nascent transcription) from 2 kb before the TSS to 2 kb after the TTS in 400 genes of >100 kb in WT (red) or *ELOF1*-KO (blue) cells. Profiles are normalized to 100% at promoter-proximal BrU peaks instead of area under the curve for better comparison of transcription profiles. Profiles are averages of two independent replicates. Numerical data are provided in the source data.

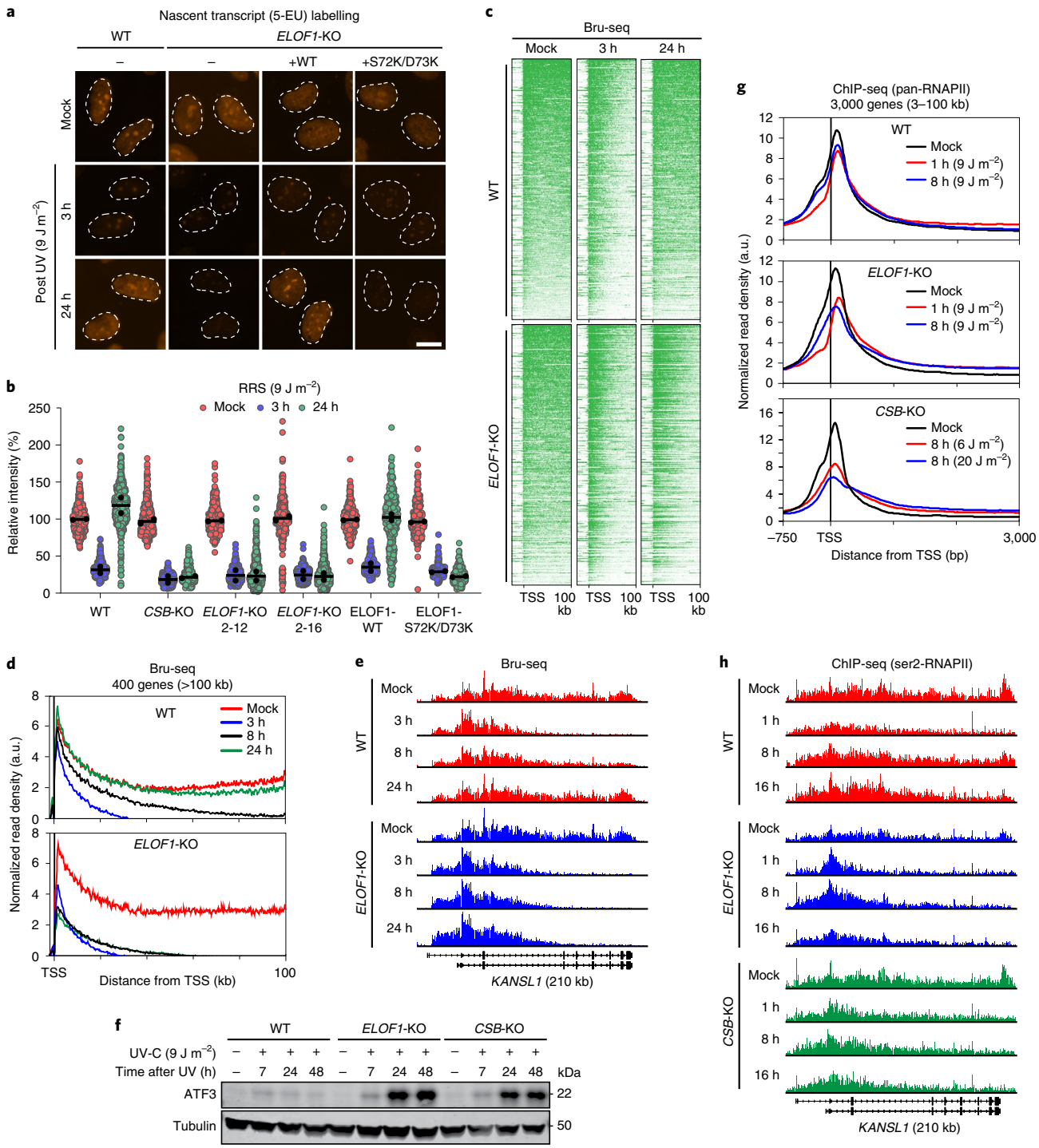

Fig. 3 | ELOF1 is essential for transcription recovery after UV irradiation. a,**b**, RRS in the indicated RPE1-iCas9 cells following UV irradiation (3 h or 24 h; 9 J m^{-2}). Representative images (**a**) and (**b**) quantification of 5-EU levels normalized to mock treatment for each cell line. The experiment was performed twice and each black circle represents the median of two technical replicates of an independent experiment, with >80 cells collected per technical replicate. The black line represents the median of all cells. Scale bar, 10 µm. **c**, Heatmaps of Bru-seq data from the TSS into the first 100 kb of 400 genes of >100 kb ranked according to the BrU signal in mock-treated cells (left panel). Heatmaps of the same genes after UV irradiation (9 J m^{-2}). **d**, Metaplots of BrU signals in 400 genes of >100 kb in WT (upper) or *ELOF1*-KO (lower) cells after mock treatment or UV irradiation (9 J m^{-2}). **e**, UCSC genome browser track showing BrU read densities across the *KANSL1* gene after mock treatment or UV irradiation (9 J m^{-2}) in WT (red) and *ELOF1*-KO cells (blue). **f**, Western blot analysis of ATF3 protein levels in the indicated RPE1-iCas9 cell lines after mock treatment or UV irradiation (9 J m^{-2}). Data shown represent four independent experiments for WT and *ELOF1*-KO cells, and three independent experiments for *CSB*-KO cells. **g**, Averaged metaplots of pan-RNAPII ChIP-seq of 3,000 genes of 3–100 kb around the TSS in RPE1-iCas9 WT (upper) and RPE1 *ELOF1*-KO (middle) cells after mock treatment (black) or at 1 h (red) or 8 h (blue) after UV irradiation (9 J m^{-2}). The lower panel shows metaplots in U2OS *CSB*-KO cells after mock treatment (black) or 8 h after UV irradiation with either 6 J m^{-2} (red) or 20 J m^{-2} (blue). **h**, UCSC genome browser track showing the read density of the ser2-RNAPII signal across the *KANSL1* gene after mock treatment or UV irradiation (9 J m^{-2}) in WT (red), *ELOF1*-KO (blue) and *CSB*-KO cells (green). Uncropped blots and numerical data are provided in the source data.

was comparable between WT and *ELOF1*-KO cells (Extended Data Fig. 6a). At 1 h and 8 h after UV treatment, we detected a striking reduction in RNAPII binding at TSSs in *ELOF1*-KO cells, but not in WT cells, which was accompanied by an increase in RNAPII reads in the gene body (Fig. 3g and Extended Data Fig. 6a,b). A similar redistribution of RNAPII after UV irradiation was detected in *CSB*-KO cells, which suggests that this corresponds to increased stalling at DNA lesions in gene bodies (Fig. 3g). This is consistent with our Bru-seq data showing that RNA synthesis is already largely restored around TSSs at 8 h after UV exposure in WT cells, but not in *ELOF1*-KO cells (Fig. 3c,d).

We also detected enrichment of pan-RNAPII after transcription termination sites (TTSs) in non-irradiated cells, which reflects post-transcriptional pausing before dissociation (Extended Data Fig. 6b,c). *ELOF1*-KO cells showed poor TTS enrichment at 8 h after UV irradiation compared with WT cells, which suggests that fewer transcripts reach the end of genes (Fig. 2h and Extended Data Fig. 6b,c). ChIP-seq experiments using antibodies against elongating RNAPII (Ser2-RNAPII) revealed that reads throughout gene bodies and at TTSs indeed recovered within 16 h after UV treatment in WT cells, but not in *ELOF1*-KO and *CSB*-KO cells (Fig. 3h).

TCR-seq reveals that ELOF1 is an essential TCR factor. To determine whether ELOF1 is directly involved in repair or regulates subsequent restart of transcription, we measured genome-wide TCR kinetics using our recently developed strand-specific ChIP-seq technology (TCR-seq)[2]. The DNA fragments that are co-purified with RNAPIIo are highly enriched for UV-induced photolesions specifically in the transcribed (template) strand, but not in the coding strand[1]. TCR-seq allows strand-specific PCR amplification of fragments without DNA damage, enabling genome-wide quantification of TCR kinetics (Fig. 4a).

Metaplots revealed a strong strand-bias in WT, *ELOF1*-KO and *CSB*-KO cells 1 h after UV irradiation, which was fully resolved in WT cells over the course of 16 h, while both *ELOF1*-KO and *CSB*-KO cells displayed a strong strand-bias at all time points analysed (Fig. 4b,c and Extended Data Fig. 7a). Resolving the strand-bias in WT cells was accompanied by the reappearance of Ser2-RNAPII reads throughout gene bodies and after the TTS, which did not occur in the absence of *ELOF1* or *CSB* (Fig. 4b,c and Extended Data Fig. 7a). An analysis of the genome-wide removal of DNA lesions from transcribed strands (Extended Data Fig. 8a) showed that WT cells cleared DNA lesions within 16 h, while *ELOF1*-KO and *CSB*-KO cells did not display significant repair within this time frame (Fig. 4d). Strand-specific analysis after ChIP-seq with another (pan-RNAPII) antibody confirmed these results (Extended Data Fig. 9a,b). Importantly, *ELOF1*-KO cells were fully capable of removing UV-induced DNA lesions by global genome repair (Extended Data Fig. 10a,b), thereby demonstrating that ELOF1 is specifically involved in TCR-mediated removal of DNA lesions.

ELOF1 is required for RNAPII ubiquitylation. To monitor whether ELOF1 is involved in TCR complex assembly, we immunoprecipitated endogenous RNAPIIo to isolate intact TCR complexes[6]. Both CSB and CSA associated with RNAPII in a UV-specific manner in WT and *ELOF1-KO* cells, while the association of CSA with RNAPIIo was completely abolished in cells lacking *CSB*[6] (Fig. 5a). The constitutive interaction between ELOF1 and RNAPII was not affected by CSB depletion (Extended Data Fig. 10c). The TFIIH subunits (p89 and p62) showed a UV-induced interaction with RNAPIIo in WT cells, while this interaction was severely reduced in cells lacking *ELOF1* (Fig. 5a,b). Importantly, re-expressing ELOF1–GFP in *ELOF1-KO* cells restored TFIIH recruitment (Fig. 5b).

RNAPII ubiquitylation on K1268 (RPB1-K1268) in response to UV irradiation is required for the recruitment of the TFIIH complex[2]. Considering that TFIIH recruitment is reduced in *ELOF1*-KO cells, we asked whether ELOF1 is involved in the UV-induced ubiquitylation of RNAPII. Immunoprecipitation showed that RNAPII is robustly ubiquitylated in response to UV treatment in WT cells, which was largely absent in cells lacking either *ELOF1* or *CSB* (Fig. 5c,d). The association of endogenous UVSSA with DNA damage-stalled RNAPIIo was strongly decreased in *ELOF1-KO* cells compared with WT cells, and was virtually absent in *CSB-KO* cells (Fig. 5c). In agreement, the accompanying paper by Geijer et al.[24] shows similarly defective UVSSA recruitment by live-cell imaging after UV irradiation. Interestingly, recruitment of monoubiquitylated UVSSA was particularly affected in *ELOF1*-KO cells[2] (Fig. 5c). This is in line with previous work demonstrating that RNAPII ubiquitylation supports the ubiquitylation of UVSSA and that, in turn, UVSSA ubiquitylation is required for TFIIH recruitment[2]. The loss of UV-induced RNAPII ubiquitylation and UVSSA monoubiquitylation and the reduced association of TFIIH with DNA damage-stalled RNAPIIo in *ELOF1*-KO cells were fully restored by stable expression of ELOF1^{WT}, while expression of ELOF1$^{S72K/D73K}$ failed to do so (Fig. 5e).

ELOF1 interacts with the CRL4^{CSA} complex. The UVSSA-binding partner USP7 was previously found to protect CSB from UV-induced degradation[5,25,26]. Considering that UVSSA recruitment is decreased in *ELOF1*-KO cells, we hypothesized that ELOF1 may indirectly affect RNAPII ubiquitylation by affecting CSB levels. Western blot analysis revealed that CSB is not degraded in response to UV irradiation in any of the cell lines (WT, *CSA*-KO, *ELOF1*-KO or *UVSSA*-KO), but we noted that CSA is degraded in response to UV irradiation in *ELOF1-KO* cells and *UVSSA*-KO cells, but not in WT or *CSB-KO* cells (Fig. 6a and Extended Data Fig. 10d). It is feasible that CSA is no longer deubiquitylated by the UVSSA-binding partner USP7 in *ELOF1*-KO cells. Indeed, WT cells treated with the USP7 inhibitor FT671 were unable to recover transcription after UV irradiation[25] (Extended Data Fig. 10e) and showed increased degradation of CSA after UV irradiation, but not to the same extent as in *ELOF1*-KO cells (Extended Data Fig. 10f). This suggests that there are both USP7-dependent and -independent mechanisms. Treatment of *ELOF1*-KO cells with the proteasome inhibitor MG132 fully restored CSA protein levels after UV irradiation, but failed to rescue RNAPII ubiquitylation in *ELOF1*-KO cells (Fig. 6b,c), thereby demonstrating that this is not an indirect effect caused by CSA degradation.

The yeast orthologue ELF1 is bound to RNAPII in close proximity to the K1268 ubiquitylation site (K1264 in *Komagataella pastoris*; Fig. 6d). We therefore hypothesized that ELOF1 brings the ubiquitin ligase activity of the CRL4^{CSA} complex in close proximity to the K1268 site on RNAPII. To test this, we employed a recombinant approach using purified *Xenopus laevis* (xl) proteins. Immobilized glutathione *S*-transferase (GST)-tagged xlELOF1 robustly interacted with purified xlRNAPII in vitro (Fig. 6e), while it failed to associate with the global genome repair factor xlRAD23B (Extended Data Fig. 10g). A robust interaction was detected between immobilized xlELOF1 and the xlCRL4^{CSA} complex, which consists of CSA, DDB1, CUL4A and RBX1 (Fig. 6f). Despite this direct interaction, the CRL4^{CSA} complex did not ubiquitylate xlELOF1 in vitro, whereas xlCSB was efficiently ubiquitylated (Extended Data Fig. 10h). To verify the interaction between ELOF1 and CRL4^{CSA}, we applied an in situ proximity-ligation assay (PLA) between TY1-epitope-tagged ELOF1 and the RBX1 subunit of CRL4^{CSA}. Nuclear TY1 staining was detected in *ELOF1*-KO cells rescued with stable expression of ELOF1–TY1 (Extended Data Fig. 10i), which fully restored their illudin S resistance (Extended Data Fig. 2f). Endogenous RBX1, but not ELOF1–TY1, was recruited to sites of local UV-induced DNA damage (Extended Data Fig. 10j). In 50% of the cells, an increased PLA signal between RBX1 and ELOF1 was detected at these DNA damage sites (Fig. 6g,h), which was approximately twofold

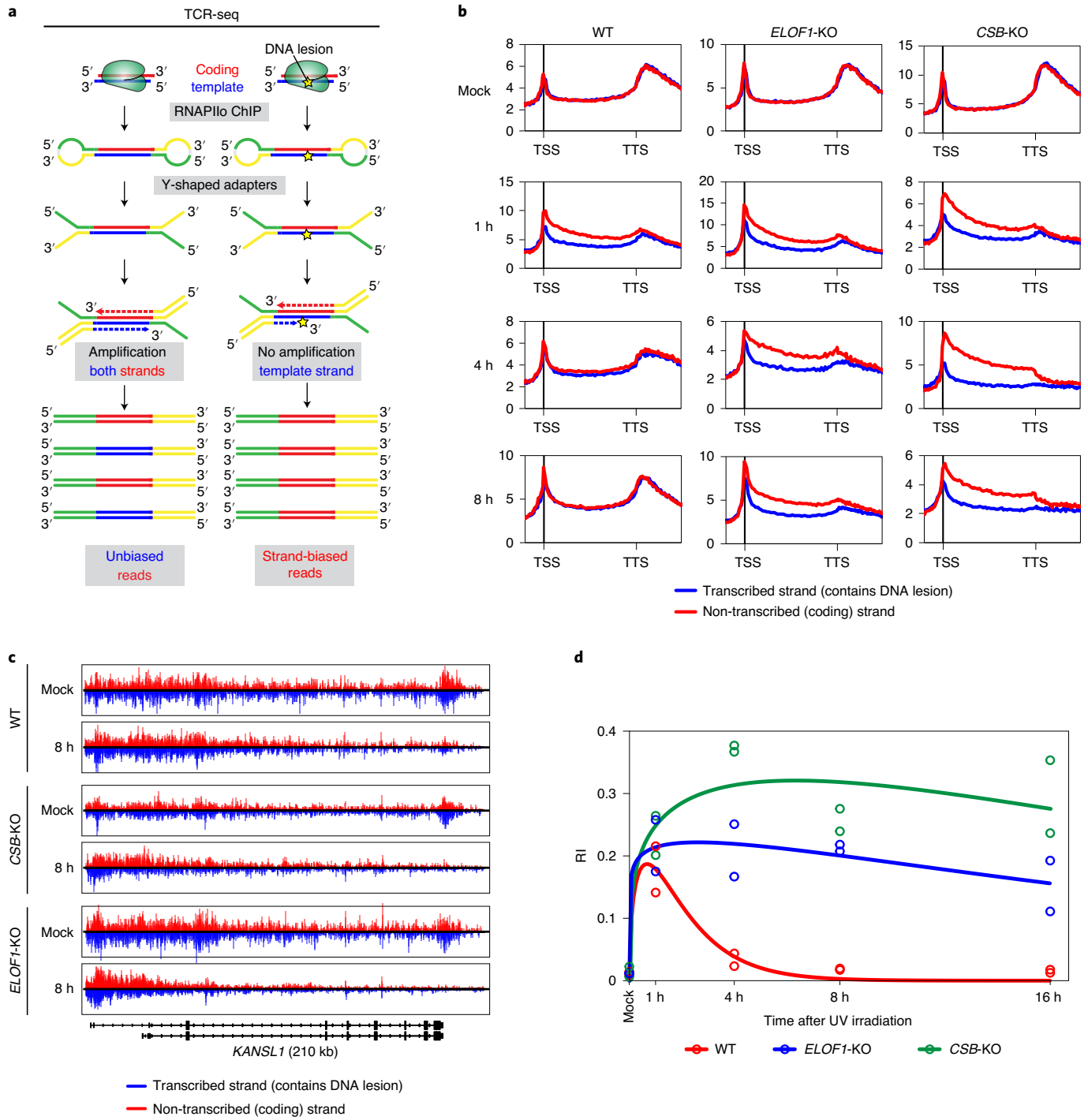

Fig. 4 | ELOF1 is essential for repair of transcription-blocking DNA damage. a, Schematic representation of TCR-seq. The use of asymmetrical adapters allows the preservation of strand-specific information. Without UV irradiation, the reads in the transcribed strand are similar to the reads in the non-transcribed strand (unbiased reads). After UV irradiation, the DNA that is co-purified with RNAPIIo after ChIP is highly enriched for DNA lesions in the transcribed strand, but not in the non-transcribed strand. These DNA lesions prevent PCR amplification during library preparation, resulting in fewer reads in the transcribed strand compared with the non-transcribed strand (biased reads). **b**, Averaged metaplots of ser2-RNAPII TCR-seq of 3,000 genes from the TSS until the TTS (−5 kb and +5 kb, respectively) in the indicated RPE1-iCas9 cells after mock treatment or at 1 h, 4 h or 8 h after UV irradiation (9 J m^{-2}). The experiment was performed twice. See Extended Data Fig. 6a for individual replicates and additional time points. **c**, UCSC genome browser tracks showing read densities of TCR-seq data based on strand-specific ser2-RNAPII signals across the *KANSL1* gene after mock treatment or at 8 h after UV irradiation (9 J m^{-2}) in WT, *CSB*-KO and *ELOF1*-KO cells. **d**, Time course of the indicated RPE1-iCas9 cells showing the recovery index (RI), representing genome-wide TCR repair kinetics. Per sample, a frequency distribution plot was generated of the per-gene strand-specificity index (SSI; defined as the relative difference in read density between the transcribed and non-transcribed strands) of 3,000 genes of 3–100 kb. The RI is subsequently obtained by fitting a mixture of three Gaussian distributions, corresponding to undamaged gene fractions (SSI = 0) and two unrepaired gene fractions (that is, |SSI|<>0). The RI was calculated from duplicate time-course experiments shown in Extended Data Fig. 8a.

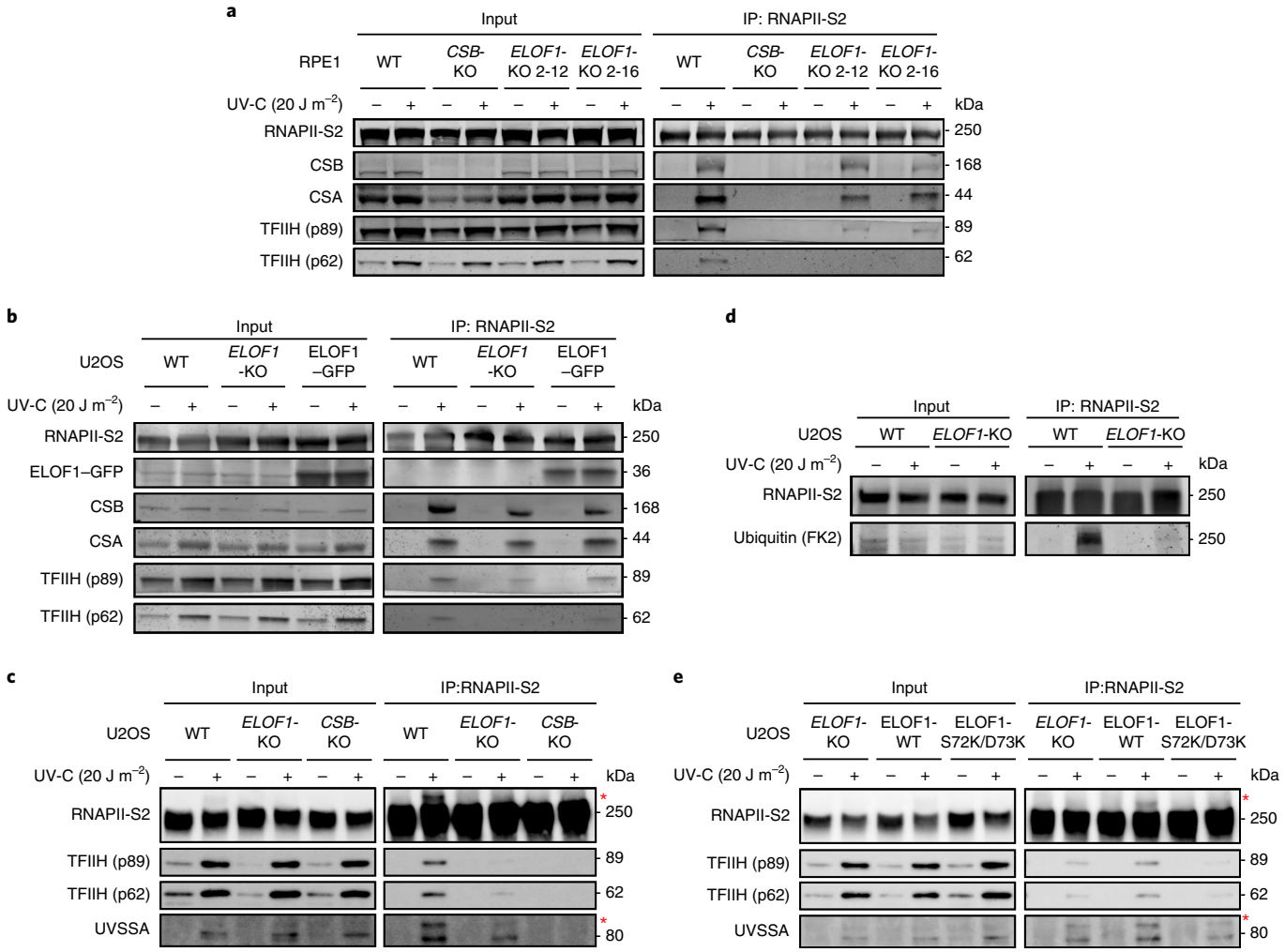

Fig. 5 | ELOF1–RNAPII interaction is required for RNAPII ubiquitylation. a, Endogenous RNAPIIo co-IP of RPE1-iCas9 WT, *CSB*-KO and *ELOF1*-KO clones. **b**, Endogenous RNAPIIo co-IP of U2OS (FRT) WT, *ELOF1*-KO and *ELOF1*-KO cells complemented with ELOF1^{WT}–GFP. **c**, Endogenous RNAPIIo co-IP of U2OS (FRT) WT, *ELOF1*-KO and *CSB*-KO clones. **d**, Endogenous RNAPIIo co-IP of U2OS (FRT) cells (WT and *ELOF1*-KO) in the presence of the deubiquitylase inhibitor *N*-ethylmaleimide (NEM). The ubiquitylated form of RNAPII was detected using an anti-FK2 antibody. **e**, Endogenous RNAPIIo co-IP of U2OS (FRT) *ELOF1*-KO and *ELOF1*-KO cells complemented with ELOF1^{WT}–GFP or ELOF1$^{S72K/D73K}$–GFP. For **c** and **e**, the ubiquitylated form of RNAPII and UVSSA, detected as higher migrating bands, are indicated with a red asterisk. Data shown represent three independent experiments for **a** and **d** and two experiments for **b**, **c** and **e**. Uncropped blots are provided in the source data.

higher than at other nuclear areas (Fig. 6i). Our findings suggest that ELOF1 interacts directly with CRL4^{CSA} and stimulates the CRL4^{CSA}-dependent ubiquitylation of RNAPII K1268 (Fig. 6j).

ELOF1 is involved in a CSB-independent repair pathway. To further compare the roles of CSB and ELOF1 in response to DNA damage, we performed CRISPR screens in *CSB*-KO and *ELOF1*-KO cells in the presence of illudin S. Loss of *CSA* and *UVSSA* in *CSB*-KO cells was epistatic, while loss of *ELOF1* caused an additive sensitivity to illudin S (FDR < 0.001; Fig. 7a). The screen in *ELOF1*-KO cells confirmed that loss of the core TCR genes *CSA*, *CSB* and *UVSSA* caused an additive sensitivity to illudin S (FDR < 0.01). Loss of *STK19*, which has been previously linked to transcription recovery after UV irradiation[14] and sensitizing RPE1 cells to illudin S[27] (Fig. 1a,b), did not cause additional illudin S sensitivity in either *CSB*-KO or *ELOF1*-KO cells (Fig. 7a,b). Both *CSB*-KO and *ELOF1*-KO cells revealed a strong dependency on *REV7* (also known as *MAD2L2*) and the 9-1-1 complex (Fig. 7a,b), which suggests that these KO cells require translesion synthesis to deal with unresolved DNA damage during replication. Loss of the tumour suppressor *PTEN* reduced the cytotoxic effects of transcriptional stress in both *ELOF1*-KO and *CSB*-KO cells (Fig. 7a,b). Furthermore, loss of the deubiquitylase *OTUD5*, which inhibits RNAPII elongation in response to DNA double-strand breaks[28], alleviated the sensitivity of *ELOF1*-KO cells to illudin S, while its loss had the opposite impact on *CSB*-KO cells (Fig. 7a,b).

To validate these genetic interactions, we generated *CSB/ELOF1* and *CSB/CSA* double knockout (dKO) cells. Drug-sensitivity assays confirmed that *CSB/ELOF1*-dKO cells were more sensitive to illudin S and irofulven than either single KO, while this was not the case for *CSB/CSA*-dKO cells (Fig. 7c,d). We propose that *ELOF1*-KO cells are not fully TCR deficient, as they still benefit from remaining CSB expression. Conversely, *CSB*-KO cells rely on ELOF1 for proliferation in the presence of illudin S-induced DNA damage. Our network analyses showed that *CSB*-KO and *ELOF1*-KO cells have overlapping, but also unique, genetic dependencies (Fig. 7e). Based on these observations, we hypothesize that in addition to its role in canonical TCR, ELOF1 acts in a second DNA repair pathway.

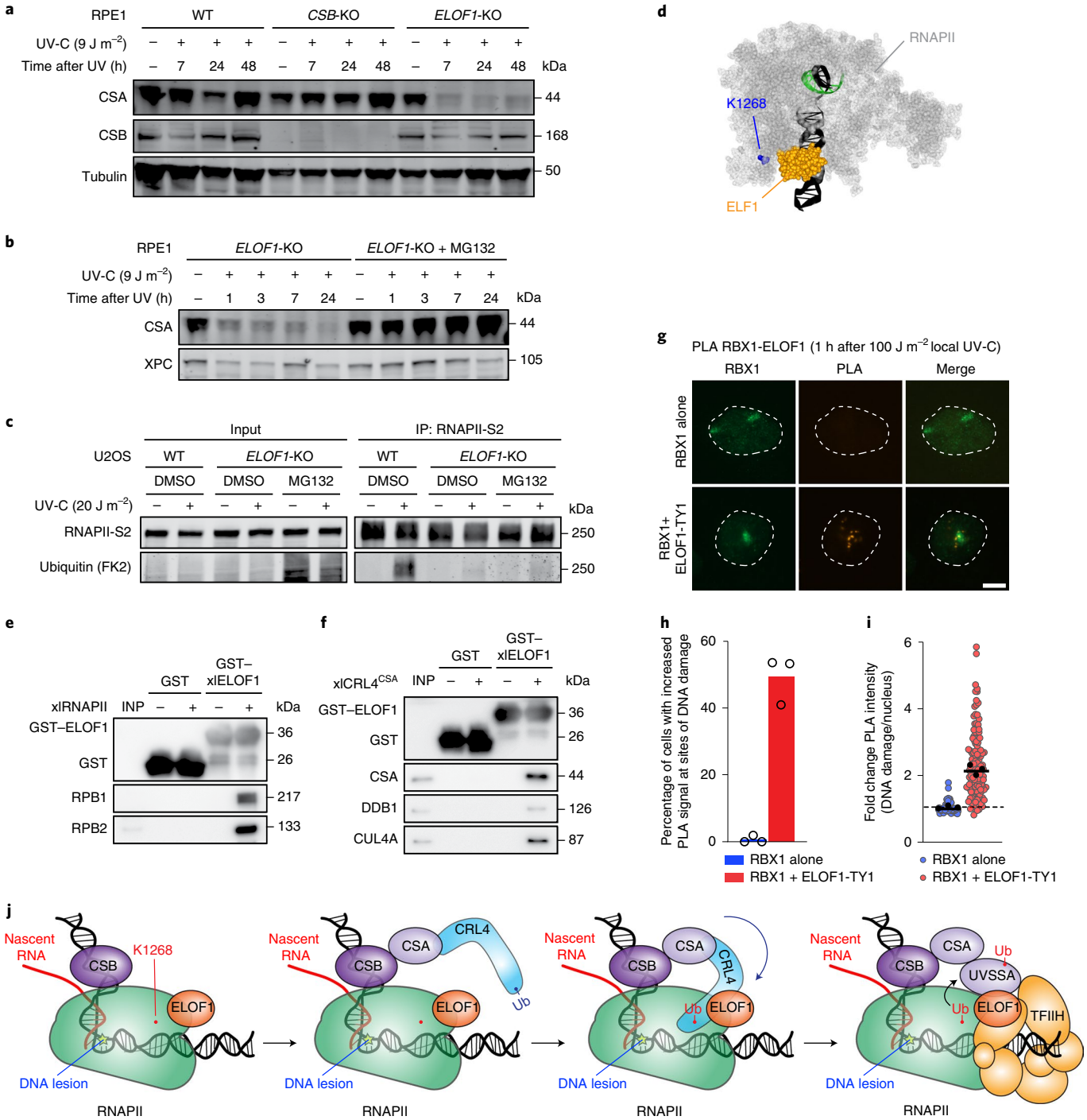

Fig. 6 | ELOF1 interacts with the CRL4^{CSA} complex. a,**b**, Western blot analysis of protein levels (CSA and CSB (**a**); CSA (**b**)) of the indicated RPE1-iCas9 cell lines after mock treatment or UV irradiation (9 J m^{-2}). MG-132 (20 μM) was added to the indicated cells 1 h before UV irradiation. Tubulin (**a**) or XPC (**b**) serve as a loading control. **c**, Endogenous RNAPIIo co-IP of U2OS (FRT) cells (WT and *ELOF1*-KO) in the presence of NEM. MG-132 (20 μM) was added to the indicated cells 1 h before UV irradiation. DMSO, dimethylsulfoxide. **d**, Top view of the structure (Protein Data Bank ID: 5XOG) of *Komagataella pastoris* ELF1 (orange) bound to RNAPII (grey). The RPB1-K1268 ubiquitylation site (K1264 in *Komagataella pastoris*) is indicated in blue. **e**,**f**, GST pull-down of immobilized recombinant *X. laevis* (xl) ELOF1 incubated with purified xlRNAPII (**e**) or recombinant xlCRL4^{CSA} complex (**f**). INP, input. Data in **a**–**c**, **e** and **f** represent two independent experiments. **g**–**i**, PLA signal between RBX1 and ELOF1-TY1 at sites of local DNA damage (1 h; 100 J m^{-2}). DNA damage was identified by RBX1 staining and RBX1 alone is a single antibody control. **g**, Representative images of PLA. Scale bar, 5 μm. **h**, Quantification of the percentage of cells with increased PLA signals at sites of local DNA damage. The experiment was performed three times and each symbol represents the mean of an independent experiment (>30 cells collected per experiment). **i**, Quantification of the fold change of PLA signal intensities at sites of local DNA damage compared with other nuclear areas. The experiment was performed three times and each symbol presents the median of an independent experiment and the median of all cells collected is shown as a black line (>30 cells collected per experiment). **j**, Model of how ELOF1 serves as a specificity factor for RNAPII ubiquitylation during TCR. Ub, ubiquitin. Uncropped blots and numerical data are provided in the source data.

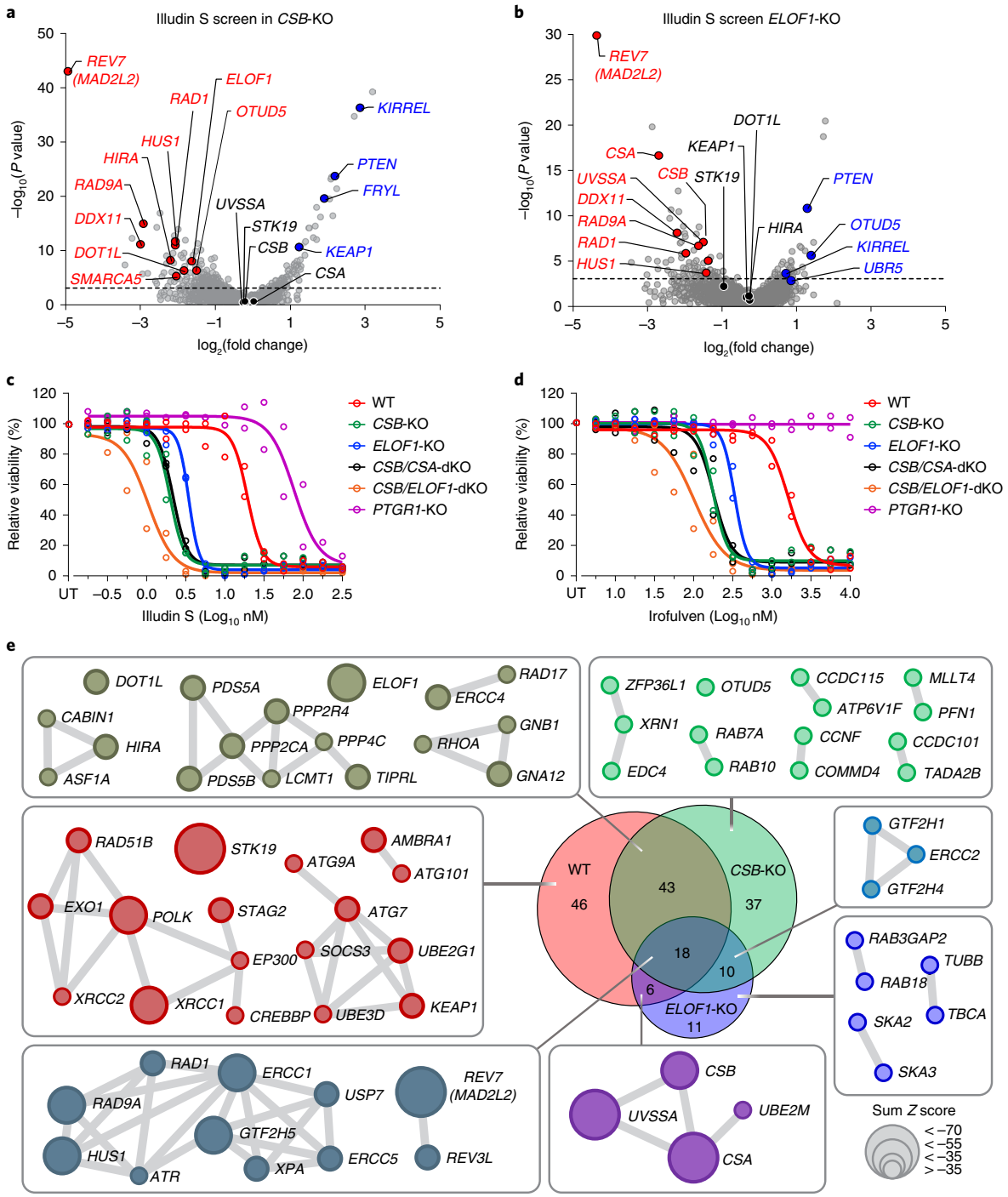

Fig. 7 | CRISPR screens identify determinants of illudin S sensitivity in the absence of ELOF1 or CSB. a,**b**, Volcano plots depicting gene KOs sensitizing (red) or conferring resistance (blue) to illudin S. *CSB*-KO (IC_{40}; 2 nM illudin S; **a**) or *ELOF1*-KO (IC_{40}; 5 nM illudin S; **b**) cells. The fold change (log_2) is plotted on the *x* axis and the significance ($-log_{10}$(*P* value)) is plotted on the *y* axis (full analysis results in the source data). **c**,**d**, Drug-sensitivity assays (72 h) in the indicated RPE1-iCas9 single KO and dKO clones exposed to illudin S (**c**) or irofulven (**d**). The experiment was performed twice and each symbol represents the median of four technical replicates of an independent experiment. UT, untreated. **e**, Venn diagram and network analysis of overlapping and unique hits in the illudin S screens of RPE1-iCas9 WT, *CSB*-KO and *ELOF1*-KO cell lines. Grey lines reflect known protein–protein interactions (Cytoscape, BioGRID). Numerical data are provided in the source data.

ELOF1 regulates a replication-stress pathway. Recently published genome-wide CRISPR screens in the presence of 27 genotoxic agents suggested that loss of *ELOF1*, but not of *CSB*, *CSA* or *UVSSA*, causes sensitivity to compounds that interfere with DNA replication[27] (Extended Data Fig. 10k). In line with this, we found that *ELOF1*-KO cells showed increased sensitivity to a specific inhibitor of DNA polymerase α (CD437) in clonogenic survival experiments, while WT and *CSB*-KO cells were similarly sensitive to CD437 (Fig. 8a). To investigate S-phase-specific DNA repair functions of ELOF1, we monitored γH2AX foci in 5-ethynyl-2′-deoxyuridine

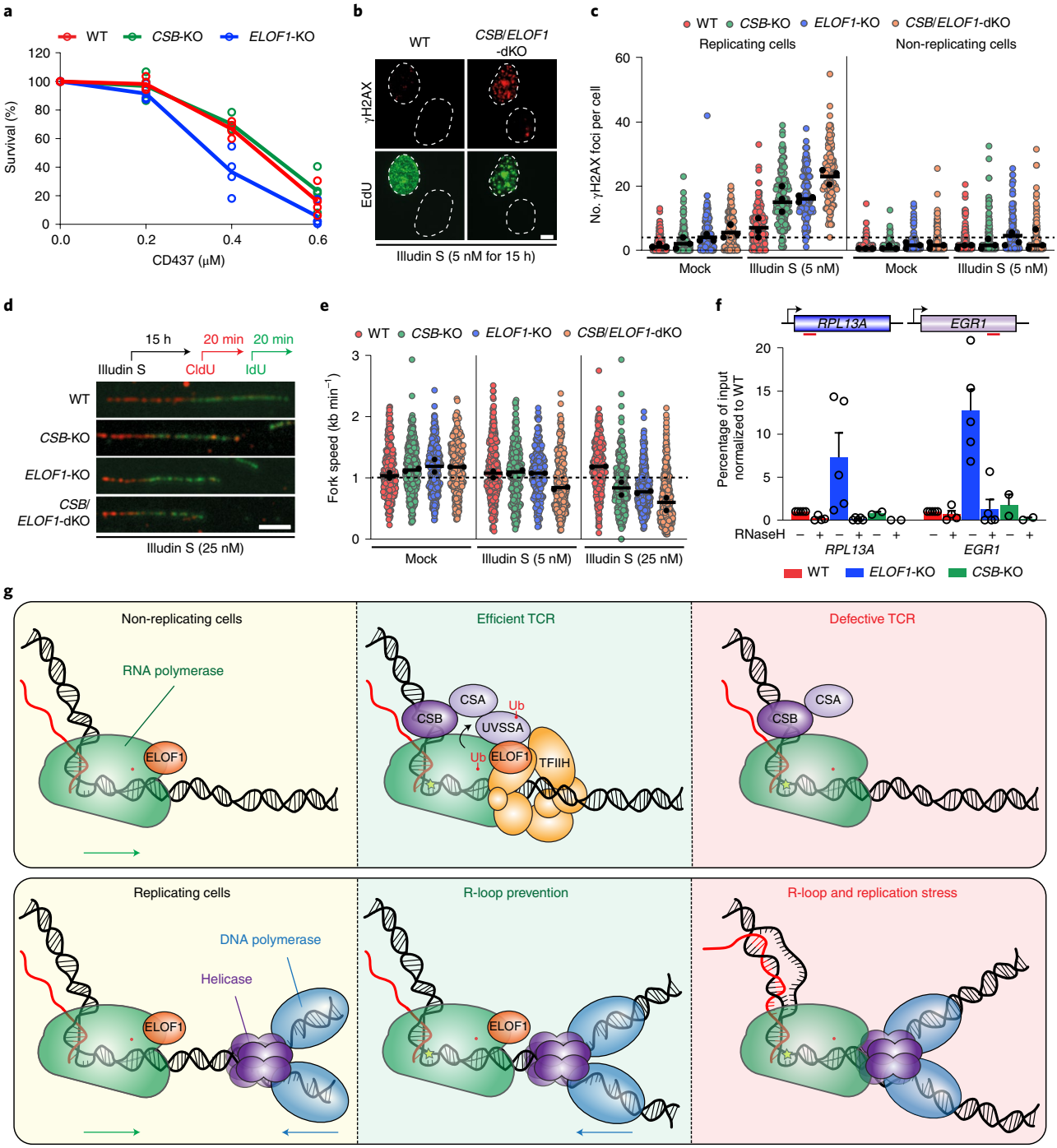

Fig. 8 | ELOF1 protects cells against DNA damage during replication. a, Clonogenic survival of the indicated RPE1-iCas9 cells after treatment with CD437. The experiment was performed four times and each symbol represents the mean of two technical replicates of an independent experiment. **b**,**c**, Representative images (**b**) and quantification (**c**) of γH2AX foci in the indicated RPE1-iCas9 cells after treatment with illudin S (5 nM). Replicating cells were identified by EdU labelling. The experiment was performed three times and black circles represent the median of an independent experiment (>26 cells collected per experiment). The black line represents the median of all the cells collected. Scale bar, 5 μm. **d**, Top: schematic representation of the DNA fibre assay. Cells were mock treated or treated with illudin S (5 nM or 25 nM) for 15 h, followed by sequential incubation with CldU (red) and IdU (green), each for 20 min. Bottom: representative images of DNA fibres in the indicated RPE1-iCas9 KO clones after treatment with illudin S (25 nM). Scale bar, 5 μm. **e**, Quantification of DNA replication fork speed in the indicated RPE1-iCas9 KO clones after mock treatment and illudin S treatment (5 nM or 25 nM). The experiment was performed twice and black circles represent the median of an independent experiment (>100 forks scored per experiment). The black line represents the median of all the scored forks. **f**, Top: a schematic representation of the *RPL13A* and *EGR1* loci depicting the relative position of primer pairs used for DRIP-qPCR (red). Bottom: DRIP-qPCR analysis of the *RPL13A* and *EGR1* genes in the indicated RPE1-iCas9 cells with and without RNaseH treatment. Each symbol represents the relative level of DNA–RNA hybrids normalized to input and WT without RNaseH per independent experiment. The bars indicate the mean + s.e.m. of all the experiments ($n = 5$ for WT and *ELOF1*-KO, $n = 2$ for *CSB*-KO). **g**, Model of the role of ELOF1 in non-replicating and replicating cells showing how ELOF1 depletion leads to defective TCR, R-loop accumulation and replication stress after encountering transcription-blocking DNA damage. Numerical data are provided in the source data.

(EdU)-positive cells. Both *CSB*-KO and *ELOF1*-KO cells showed a marked increase in γH2AX foci in S-phase cells after illudin S treatment. This induction increased even further in *CSB/ELOF1*-dKO cells (Fig. 8b,c). Formation of γH2AX foci in non-replicating cells was much lower and poorly induced in *CSB*-KO, *ELOF1*-KO and *CSB*/*ELOF1*-dKO cells (Fig. 8b,c). DNA fibre analyses demonstrated that DNA replication forks progressed at normal rates (~1 kb min^{-1}) in mock-treated cells. However, fork speed declined after 25 nM illudin S treatment in *CSB*-KO and *ELOF1*-KO cells, but not in WT cells. Importantly, knocking out *CSB* and *ELOF1* together significantly reduced fork speed even at low illudin S concentrations (5 nM; Fig. 8d,e).

To test whether a role of ELOF1 in DNA replication is linked to transcription, we monitored R-loop accumulation after UV irradiation by DNA–RNA immunoprecipitation and quantitative PCR (DRIP–qPCR) in actively transcribed *RPL13A* and *EGR1* genes. Both genes showed increased R-loops in *ELOF1*-KO cells, while *CSB*-KO cells showed levels comparable to WT cells (Fig. 8f). The R-loop signal in *ELOF1*-KO cells was completely lost after RNase H treatment. These findings reveal a second TCR-independent role of ELOF1 in protecting cells against DNA damage during replication, which becomes particularly important when canonical TCR fails (Fig. 8g).

Discussion

In this study, we identified and characterized human ELOF1 as an RNAPII-associated transcription elongation factor that is also a core component of the transcription-coupled DNA repair machinery with an additional role in preventing DNA damage during DNA replication.

The UV-induced ubiquitylation of RNAPII (RPB1-K1268) by the $CRL4^{CSA}$ complex is important for TCR[2,3]. Yeast ELF1 binds to a central cleft in front of RNAPII close to this ubiquitylation site[17] (Fig. 6d). Our findings suggest that loss of ELOF1 does not affect the recruitment of either CSB or $CRL4^{CSA}$ to lesion-stalled RNAPII (Fig. 5a,b), but rather that ELOF1 interacts with $CRL4^{CSA}$ through direct protein–protein contacts and directs the catalytic site of the $CRL4^{CSA}$ complex into close proximity to the K1268 site (Fig. 6e–i). By serving as a specificity factor for RNAPII ubiquitylation, ELOF1 subsequently promotes the recruitment and ubiquitylation of UVSSA, which in turn transfers the TFIIH complex from UVSSA onto DNA damage-stalled RNAPIIo to initiate repair (Fig. 6j).

The importance of ELOF1 in TCR is evident from the following findings: (1) the inability of *ELOF1*-KO cells to remove UV-induced lesions from transcribed strands (Fig. 4 and Extended Data Figs. 7–9); (2) the persistent stalling of RNAPII throughout the genome after UV irradiation (Fig. 3g,h and Extended Data Fig. 6b); and (3) the inability of *ELOF1*-KO cells to recover RNA synthesis following UV irradiation, similar to TCR-deficient *CSB*-KO cells[20] (Fig. 3a–d and Extended Data Fig. 4a,d). We therefore propose that ELOF1 is a core TCR factor and hypothesize that hypomorphic *ELOF1* mutations may cause a CS-like phenotype.

Our genetic-interaction network indicated that ELOF1 is not only involved in TCR but also in a CSB-independent repair pathway (Fig. 7a,b). Consistently, we found that *ELOF1*-deficient cells but not *CSB*-deficient cells are sensitive to replication stress triggered by DNA polymerase α inhibition (Fig. 8a), and accumulate R-loops in transcribed regions (Fig. 8f). Although the precise nature of this pathway remains to be elucidated, these findings suggest that ELOF1 helps prevent DNA damage during replication and might prevent collisions between transcription and replication machineries (Fig. 8g). Importantly, our data revealed that cells become more dependent on this secondary ELOF1 pathway when canonical TCR fails, which suggests that the additive impact of the second ELOF1 pathway may be partially masked in TCR-proficient cells. (Fig. 8c,e). Elucidating the components and the mechanism involved in the compensatory ELOF1-dependent pathway are important goals for future research.

Together, our results identified ELOF1 as a transcription-coupled DNA repair factor that promotes CSB-dependent TCR by directing RNAPII ubiquitylation and, at the same time, acts in a compensatory second pathway as a more general sensor of transcription stress during DNA replication (Fig. 8g).

Online content

Any methods, additional references, Nature Research reporting summaries, source data, extended data, supplementary information, acknowledgements, peer review information; details of author contributions and competing interests; and statements of data and code availability are available at https://doi.org/10.1038/s41556-021-00688-9.

Received: 24 June 2020; Accepted: 26 April 2021;
Published online: 9 June 2021

References

1. Brueckner, F., Hennecke, U., Carell, T. & Cramer, P. CPD damage recognition by transcribing RNA polymerase II. *Science* **315**, 859–862 (2007).
2. Nakazawa, Y. et al. Ubiquitination of DNA damage-stalled RNAPII promotes transcription-coupled repair. *Cell* **180**, 1228–1244.e24 (2020).
3. Tufegdžić Vidaković, A. et al. Regulation of the RNAPII pool is integral to the DNA damage response. *Cell* **180**, 1245–1261.e21 (2020).
4. Nakazawa, Y. et al. Mutations in *UVSSA* cause UV-sensitive syndrome and impair RNA polymerase IIo processing in transcription-coupled nucleotide-excision repair. *Nat. Genet.* **44**, 586–592 (2012).
5. Schwertman, P. et al. UV-sensitive syndrome protein UVSSA recruits USP7 to regulate transcription-coupled repair. *Nat. Genet.* **44**, 598–602 (2012).
6. van der Weegen, Y. et al. The cooperative action of CSB, CSA, and UVSSA target TFIIH to DNA damage-stalled RNA polymerase II. *Nat. Commun.* **11**, 2104 (2020).
7. Laugel, V. et al. Mutation update for the *CSB/ERCC6* and *CSA/ERCC8* genes involved in Cockayne syndrome. *Hum. Mutat.* **31**, 113–126 (2010).
8. Xu, J. et al. Structural basis for the initiation of eukaryotic transcription-coupled DNA repair. *Nature* **551**, 653–657 (2017).
9. Jaspers, N. G. et al. Anti-tumour compounds illudin S and irofulven induce DNA lesions ignored by global repair and exclusively processed by transcription- and replication-coupled repair pathways. *DNA Repair (Amst.)* **1**, 1027–1038 (2002).
10. Mair, B. et al. Essential gene profiles for human pluripotent stem cells identify uncharacterized genes and substrate dependencies. *Cell Rep.* **27**, 599–615.e12 (2019).
11. Yu, X. et al. Up-regulation of human prostaglandin reductase 1 improves the efficacy of hydroxymethylacylfulvene, an antitumor chemotherapeutic agent. *J. Pharmacol. Exp. Ther.* **343**, 426–433 (2012).
12. Adam, S., Polo, S. E. & Almouzni, G. Transcription recovery after DNA damage requires chromatin priming by the H3.3 histone chaperone HIRA. *Cell* **155**, 94–106 (2013).
13. Oksenych, V. et al. Histone methyltransferase DOT1L drives recovery of gene expression after a genotoxic attack. *PLoS Genet.* **9**, e1003611 (2013).
14. Boeing, S. et al. Multiomic analysis of the UV-induced DNA damage response. *Cell Rep.* **15**, 1597–1610 (2016).
15. Daniels, J. P., Kelly, S., Wickstead, B. & Gull, K. Identification of a crenarchaeal orthologue of Elf1: implications for chromatin and transcription in Archaea. *Biol. Direct* **4**, 24 (2009).
16. Ehara, H. et al. Structural insight into nucleosome transcription by RNA polymerase II with elongation factors. *Science* **363**, 744–747 (2019).
17. Ehara, H. et al. Structure of the complete elongation complex of RNA polymerase II with basal factors. *Science* **357**, 921–924 (2017).
18. Prather, D., Krogan, N. J., Emili, A., Greenblatt, J. F. & Winston, F. Identification and characterization of Elf1, a conserved transcription elongation factor in *Saccharomyces cerevisiae*. *Mol. Cell. Biol.* **25**, 10122–10135 (2005).
19. Veloso, A. et al. Rate of elongation by RNA polymerase II is associated with specific gene features and epigenetic modifications. *Genome Res.* **24**, 896–905 (2014).
20. Mayne, L. V. & Lehmann, A. R. Failure of RNA synthesis to recover after UV irradiation: an early defect in cells from individuals with Cockayne's syndrome and xeroderma pigmentosum. *Cancer Res.* **42**, 1473–1478 (1982).

21. Perdiz, D. et al. Distribution and repair of bipyrimidine photoproducts in solar UV-irradiated mammalian cells. Possible role of Dewar photoproducts in solar mutagenesis. *J. Biol. Chem.* **275**, 26732–26742 (2000).
22. Epanchintsev, A. et al. Cockayne's syndrome A and B proteins regulate transcription arrest after genotoxic stress by promoting ATF3 degradation. *Mol. Cell* **68**, 1054–1066.e6 (2017).
23. Bugai, A. et al. P-TEFb activation by RBM7 shapes a pro-survival transcriptional response to genotoxic stress. *Mol. Cell* **74**, 254–267 e210 (2019).
24. Geijer, I. et al. NCB-M43309B. *Nat. Cell Biol.* doi:Placeholder (2021).
25. Zhang, X. et al. Mutations in *UVSSA* cause UV-sensitive syndrome and destabilize ERCC6 in transcription-coupled DNA repair. *Nat. Genet.* **44**, 593–597 (2012).
26. Fei, J. & Chen, J. KIAA1530 protein is recruited by Cockayne syndrome complementation group protein A (CSA) to participate in transcription-coupled repair (TCR). *J. Biol. Chem.* **287**, 35118–35126 (2012).
27. Olivieri, M. et al. A genetic map of the response to DNA damage in human cells. *Cell* **182**, 481–496 e421 (2020).
28. de Vivo, A. et al. The OTUD5–UBR5 complex regulates FACT-mediated transcription at damaged chromatin. *Nucleic Acids Res.* **47**, 729–746 (2019).

Methods

Cell lines. All cell lines (listed in Supplementary Table 1) were cultured at 37 °C in an atmosphere of 5% CO_2 in DMEM (Thermo Fisher Scientific) supplemented with penicillin–streptomycin (Sigma) and 10% fetal bovine serum (Bodinco BV or Thermo Fisher Scientific (Gibco)). U2OS Flp-In/T-REx cells (here on called U2OS (FRT)), which were generated using the Flp-InTM/T-RExTM system (Thermo Fisher Scientific), were a gift from D. Durocher[29].

Construction of RPE1-TetOn-Cas9-PuroS-*TP53*-KO cells. Human RPE1-hTERT cells were acquired from the American Type Culture Collection (ATCC, CRL-4000). Lentiviral particles of pLVX-Tre3G-Cas9 plasmid (Clontech, Cas9 from vector Lenti-Cas9-2A-Blast (Addgene)) were produced in HEK293T cells using the Lenti-X HT packaging system (Clontech). Transduced RPE1-hTERT cells were selected using 10 μg ml^{-1} puromycin and 400 μg ml^{-1} G418 to generate RPE1-TetOn-Cas9 (ref. [30]). To create KO cells, Cas9 expression was induced by 100 ng ml^{-1} doxycycline (Dox; Sigma-Aldrich) followed by transfection using RNAiMAX (Invitrogen) with 10 nM tracrRNA (Integrated DNA Technologies, IA) and 10 nM synthetic crRNA targeting *TP53* and the *Streptomyces* puromycin-*N*-acetyltransferase *PAC1* gene (sgRNAs listed in Supplementary Table 2). The population was selected for *TP53*-KO cells by selection on 10 μM nutlin-3 (Selleck Chemicals, TX) for 1 week. Single-cell clones were selected based on their sensitivity to 1 μg ml^{-1} puromycin, and KO of *TP53* was confirmed by Sanger sequencing and western blotting. Cas9 activity of the RPE1-TetOn-Cas9-PuroS-*TP53*-KO cell line (RPE1-iCas9) was assayed by transducing cells with lentivirus produced using vector pXPR-011 (Addgene)[31] containing eGFP, sgGFP and puromycin *N*-acetyltransferase (plasmids are listed in Supplementary Table 3). After transduction, transduced cells were selected by puromycin (3 μg ml^{-1}; Sigma) and eGFP expression was assayed every 4 h for up to 1 week in the absence and presence of doxycycline (100 ng ml^{-1}; Sigma) in an IncuCyte Zoom automated live-cell imaging platform (Sartorius).

CRISPR–Cas9 screens. For every screen, three populations of RPE1-iCas9 were transduced at a multiplicity of infection of ~0.2 with a 1:1,000 dilution of TKOv3-in-pLCKO lentiviral library in medium containing 8 μg ml^{-1} hexadimethrine bromide (Sigma-Aldrich). The library was a gift from K. Chan, A. Tong and J. Moffat (Donnelly Centre, University of Toronto, Canada). After 24 h of transduction, puromycin (5 μg ml^{-1}; Sigma-Aldrich) was added to select for transduced cells. After all cells in non-transduced control populations had died and dishes with transduced populations had reached 90% confluence, a $t=0$ sample was taken for each of the three populations. From the remaining cells of each population, 30×10^6 cells (corresponding to a library representation of >400) were grown as a control population, and additionally 30×10^6 cells were grown in the presence of illudin S for the drug screens (at a concentration of 25 nM for the screen in RPE1-iCas9, 2 nM for the screen in RPE1-iCas9 *CSB*-KO and 5 nM for the screen in RPE1-iCas9 *ELOF1*-KO). Doxycycline (200 ng ml^{-1}) was added to the medium of all replicates from $t=0$ onwards to induce expression of Cas9. After three doublings, 30×10^6 cells of each population were subcultured. After 12 doublings, all populations were collected.

Sequencing and analysis of CRISPR screens. Genomic DNA was isolated from each population using a Blood and Cell Culture DNA Maxi kit (Qiagen). A total of 3 μg genomic DNA of each population was amplified using a KAPA HiFi ReadyMix PCR kit (Roche) with the TKO outer forward and reverse primers (primers are listed in Supplementary Table 4) followed by a second PCR assay using reverse primers with different Illumina i7 index sequences for each sample to identify the sample after pooled sequencing as described by Hart et al.[32]. The second PCR products of each pool were purified using a QIAquick PCR Purification kit (Qiagen). RNA-seq samples were added to 10% to create balanced reads for the first 21 nucleotides sequenced. Up to 12 samples were sequenced in a single HiSeq4000 lane in a SR50 run using standard reagents and conditions, and reads were mapped to the TKOv3 library sequences, not allowing any mismatches. The screen data were analysed using the software drugZ (v.1.1.0.2)[33], and the $\log_2$(fold change) was calculated by first normalizing all samples to an equal number of total reads (pseudocount +1), then calculating the median fold-change per guide for the three replicate screen samples, and finally calculating the $\log_2$ of the median fold-change of all guides targeting the gene. For the network analysis, the physical interactions of differentially depleted genes were extracted from the gene interaction database GeneMANIA. Functional pathway analysis was performed using Reactome (v.72). The interaction network was built and visualized in Cytoscape (v.3.7). Node colours were adjusted based on the FDR. Node border colours were customized based on enriched pathways.

Generation of KO cells. Cells were either transfected with Cas9-2A-GFP (pX458; Addgene, 48138) containing a gRNA from the TKOv3 library (Addgene, 125517) or co-transfected with Cas9-2A-GFP (pX458; Addgene, 48138) together with pLV-U6g-PPB encoding a gRNA from the LUMC/Sigma-Aldrich sgRNA library using Lipofectamine 2000 (Invitrogen) (sgRNAs are listed in Supplementary Table 2 and plasmids in Supplementary Table 3). Cells were FACS sorted on BFP/GFP and plated at low density, after which individual clones were isolated. Alternatively, cells were selected with puromycin (1 μg ml^{-1}) for 3 days and seeded at low density, after which individual clones were isolated. Isolated KO clones were verified by western blot analysis and/or Sanger sequencing as previously described[6] (primers are listed in Supplementary Table 4).

Plasmids. The neomycin-resistance gene in pcDNA5/FRT/TO-Neo (Addgene, 41000) was replaced with a puromycin-resistance gene. Fragments spanning GFP-N1 (Clontech) including the multiple cloning site were inserted into pcDNA5/FRT/TO-puro. ELOF1^{WT} was amplified by PCR and inserted into pcDNA5/FRT/TO-puro-GFP-N1. ELOF1 mutants were generated by site-directed mutagenesis PCR (primers are listed in Supplementary Table 4). A region spanning the PGK promoter was amplified by PCR and used to replace the CMV promoter in pEGFP-C1-IRES-PURO[34]. The ELOF1^{WT}-GFP and ELOF1$^{S72K/D73K}$-GFP genes were inserted into pPGK-EGFP-C1-IRES-PURO to replace EGFP-C1. All sequences were verified by Sanger sequencing.

Generation of stable cell lines. U2OS (FRT) *ELOF1*-KO clone 3-12 was selected and subsequently used to stably express inducible GFP-tagged proteins by co-transfecting a pCDNA5/FRT/TO-Puro plasmid encoding GFP-tagged fusion proteins (5 μg) together with a pOG44 plasmid encoding the Flp recombinase (0.5 μg) using Lipofectamine 2000 (Invitrogen) (plasmids are listed in Supplementary Table 3). Cells expressing inducible GFP-tagged proteins were selected by incubation with 1 μg ml^{-1} puromycin and 4 μg ml^{-1} blasticidin S. Expression of these GFP-tagged proteins was induced by the addition of 2 μg ml^{-1} doxycycline for 24 h.

Compounds. In the indicated experiments, 10 μM MG132 (Cayman Chemical, 13697), 20 mM *N*-ethylmaleimide (NEM) (Pierce, 23030) and 10 μM FT671 (Medchem Express, HY-107985) was used.

Immunoprecipitation for co-immunoprecipitation. Cells were mock treated or irradiated with UV-C light (20 J m^{-2}) and collected 1 h after treatment. Chromatin-enriched fractions were prepared by incubating the cells for 20 min on ice in IP buffer (IP-130 for endogenous RNAPII immunoprecipitation and IP-150 for GFP immunoprecipitation) followed by centrifugation and removal of the supernatant. For endogenous RNAPII immunoprecipitation, the chromatin-enriched cell pellets were lysed in IP-130 buffer (30 mM Tris (pH 7.5), 130 mM NaCl, 2 mM $MgCl_2$, 0.5% Triton X-100, protease inhibitor cocktail (Roche), 250 U ml^{-1} benzonase nuclease (Novagen) and 2 μg RNAPII-S2 (ab5095, Abcam)) for 2–3 h at 4 °C. For GFP immunoprecipitation, the chromatin-enriched cell pellets were lysed in IP-150 buffer (50 mM Tris (pH 7.5), 150 mM NaCl, 0.5% NP-40, 2 mM $MgCl_2$, protease inhibitor cocktail (Roche) and 500 U ml^{-1} benzonase nuclease (Novagen)) for 1 h at 4 °C. Protein complexes were pulled down by 1.5 h incubation with Protein A agarose beads (Millipore) or GFP-Trap A beads (Chromotek). For subsequent analysis by western blotting, the beads were washed six times with IP-130 buffer for endogenous RNAPII immunoprecipitation and EBC-2 buffer (50 mM Tris (pH 7.5), 150 mM NaCl, 1 mM EDTA, 0.5% NP-40 and protease inhibitor cocktail (Roche)) for GFP immunoprecipitation. The samples were prepared by boiling in Laemmli–SDS sample buffer.

Mass spectrometry (MS). After pull-down, the beads were washed four times with EBC-2 buffer without NP-40 and two times with 50 mM ammonium bicarbonate followed by overnight digestion using 2.5 μg trypsin at 37 °C under constant shaking. Peptides were desalted using a Sep-Pak tC18 cartridge by washing with 0.1% acetic acid. Finally, peptides were eluted with 0.1% formic acid/60% acetonitrile and lyophilized as previously described[35]. Samples were analysed on a Orbitrap Exploris 480 mass spectrometer (Thermo Fisher) coupled to an Ultimate 3000 UHPLC system (Thermo Fisher). Digested peptides were separated using a 50-cm-long fused-silica emitter (FS360-75-15-N-5-C50, New Objective) in-house packed with 1.9 μM C18-AQ beads (Reprospher-DE, Pur, Dr. Maisch, Ammerburch-Entringen) and heated to 50 °C in a Column Oven for ESI/nano spray (Sonation). Peptides were separated by liquid chromatography using a gradient from 2% to 32% acetonitrile with 0.1% formic acid for 40 min followed by column re-conditioning for 20 min. Scan range for MS was from 300 to 1,600 m/z. Data-dependent acquisition mode was used with a Top Speed method, resolution of 60,000 and tandem mass spectra (MS/MS) cycles of 3 s. Internal calibration was enabled based on lock mass corresponding to polysiloxane (445.12003 m/z). Higher-collisional dissociation normalized collision energy was set to 28%, and only precursor ions with charges between 2 and 6 were considered to trigger MS/MS events. Precursors selected for MS/MS analysis were dynamically excluded for 30 s.

MS data analysis. Raw MS data were further analysed using MaxQuant (v.1.6.14) as previously described[36] and using standard settings with the following modifications. Maximum missed cleavages by trypsin was set to 4. Searches were performed against an in silico-digested database from the human proteome, including isoforms and canonical proteins (UniProt, accessed 8 June 2020) plus GFP protein. Oxidation (M), Acetyl (Protein N-term), GlyGly (K) and Phospho (STY) were set as variable modifications with a maximum of 3. Carbamidomethyl

(C) was disabled as fixed modification. Label-free quantification was activated, including calculation of iBAQ and not enabling Fast LFQ. The match between runs feature was activated with default parameters. MaxQuant output data were further processed in the Perseus Computational Platform (v.1.6.14) as previously described[37]. LFQ intensity values were $\log_2$-transformed, and potential contaminants and proteins identified by site only or reverse peptide were removed. Samples were grouped in experimental categories, and proteins not identified in 4 out of 4 replicates in at least one group were also removed. Missing values were imputed using normally distributed values with a 1.8 downshift ($\log_2$) and a randomized 0.3 width ($\log_2$) considering whole matrix values. Two-sided *t*-tests were performed to compare groups. Data were exported from Perseus and further processed in Microsoft Excel 2016 for comprehensive visualization.

Western blotting. Proteins were separated on 4–12% Criterion XT Bis-Tris gels (Bio-Rad, 3450124) in NuPAGE MOPS running buffer (NP0001-02, Thermo Fisher Scientific) and blotted onto polyvinylidenedifluoride membranes (IPFL00010, EMD Millipore). Membranes were blocked with blocking buffer (Rockland, MB-070-003) for 1 h at room temperature. Membranes were then probed with antibodies as indicated (antibodies are listed in Supplementary Table 5). Proteins stained with HRP-conjugated secondary antibodies were detected using western Lightning Plus-ECL (PerkinElmer, NEL103001EA).

Clonogenic survival assays. Cells were seeded at low density and mock treated or exposed to a dilution series of illudin S (Santa Cruz, sc-391575) or CD437 (Stem Cell, 72722) for 72 h. On day 10, the cells were washed with 0.9% NaCl and stained with methylene blue. Colonies of more than 20 cells were scored.

Dose–response curves. Cells were seeded in 96-well plates (1,000 cells per well for RPE1-iCas9) in 150 µl of medium. At 24 h after seeding, drugs were added manually dissolved in 50 µl of medium (cisplatin) or printed directly into the plate by a Tecan D300e digital dispenser (illudin S and irofulven). Phenylarsine oxide (PAO; Sigma-Aldrich) was used at 10 µM as a control for zero cell viability. After 72 h of drug exposure, cell viability was assayed by adding 30 µl of CellTiter-Blue (Promega) in the medium to each well. Plates were incubated for 4 h at 37 °C, and plate fluorescence (560 excitation/590 emission) was measured on a BioTek plate reader. Relative viability was calculated for each well from the fluorescence measurements as follows: (value – (value(PAO))/((value(untreated) – (value(PAO)). A four-parameter dose–response curve was fit to the viability values using Graphpad Prism 8 (v.8.4.2).

Recovery of RNA synthesis (RRS). For the RRS following DRB treatment, cells were treated with 100 µM DRB (Sigma, D1916) for 2 h. Then, either during the DRB treatment or following DRB washout, the cells were pulse-labelled with 400 µM 5-EU (Jena Bioscience) for 1 h. For the RRS following UV irradiation, cells were irradiated with UV-C light (9 J m^{-2} or 12 J m^{-2}), allowed to recover for the indicated time periods and pulse-labelled with 400 µM 5-EU for 1 h followed by a 15-min medium-chase with DMEM without supplements. Cells were fixed with 3.7% formaldehyde in PBS for 15 min, permeabilized with 0.5% Triton X-100 in PBS for 10 min at room temperature and blocked in 1.5% BSA (Thermo Fisher) in PBS. Nascent RNA was visualized by Click-iT chemistry, labelling the cells for 1 h with a mix of 60 µM atto azide Alexa 594 (Atto Tec), 4 mM copper sulfate (Sigma), 10 mM ascorbic acid (Sigma) and 0.1 µg ml^{-1} 4,6-diamidino-2-phenylindole (DAPI) in a 50 mM Tris buffer. Cells were washed extensively with PBS and mounted in Polymount (Brunschwig).

Unscheduled DNA synthesis (UDS). Cells were locally irradiated with UV-C light (5 µm filter; 30 J m^{-2}) and subsequently pulse-labelled with 20 µM EdU (VWR) and 1 µM FuDR (Sigma Aldrich) for either 1 h or 4 h followed by a 30-min medium-chase with DMEM without supplements. Cells were fixed with 3.7% formaldehyde in PBS for 15 min, permeabilized with 0.5% Triton X-100 in PBS for 20 min at room temperature and blocked in 3% BSA (Thermo Fisher) in PBS. The incorporated EdU was coupled to atto azide Alexa Fluor 647 using Click-iT chemistry according to the manufacturer's instructions (Invitrogen). After coupling, the cells were post-fixed with 2% formaldehyde for 10 min and subsequently blocked with 100 mM glycine. DNA was denatured with 0.5% NaOH for 5 min, followed by blocking with 10% BSA (Thermo Fisher) for 15 min. Next, the cells were incubated with an antibody against CPDs for 2 h, followed by secondary antibodies 1 h and DAPI for 5 min (antibodies are listed in Supplementary Table 5). Cells were mounted in Polymount (Brunschwig).

Proximity Ligation Assay (PLA). Cells were locally irradiated with UV-C light (5 µm filter; 100 J m^{-2}; 1 h recovery), washed with CSK buffer (100 mM NaCl, 300 mM sucrose, 3 mM $MgCl_2$ 10 mM PIPES (pH 6.8)) followed by a pre-extraction with CSK buffer containing 0.25% Triton X-100 for 5 min. Cells were fixed with 3.7% formaldehyde in PBS for 15 min and permeabilized with 0.5% Triton X-100 for 10 min at room temperature. The PLA was performed according to the manufacturer's specifications using Duolink in Situ (Sigma) with the indicated antibodies (antibodies are listed in Supplementary Table 5), and signal intensities were quantified using Image J.

DNA fibre assay. Cells were treated with 5 nM or 25 nM illudin S for 15 min before labelling. Cells were sequentially incubated for 20 min with 25 µM chlorodeoxyuridine (CldU) followed by 20 min with 250 µM iododeoxyuridine (IdU). Next, cells were lysed in spreading buffer (200 mM Tris-HCl (pH 7.4), 50 mM EDTA and 0.5% SDS) on Superfrost microscope slides. Fibres were spread by slightly tilting slides followed by fixation in methanol:acetic acid (3:1). After denaturation of DNA by 2.5 M HCl for 75 min and blocking in PBS with 1% BSA and 0.1% Tween-20, slides were incubated with antibodies against BrdU (antibodies are listed in Supplementary Table 5). After fixing using 4% paraformaldehyde, slides were incubated with secondary antibodies and mounted with Prolong Gold Antifade Mountant (Invitrogen). Fibre lengths were measured using ImageJ, and values were converted into kilobases using the conversion factor 1 µm = 2.59 kb (ref. [38]).

γH2AX foci. Cells were either mock treated or treated with 5 nM illudin S for 15 h. Cells were incubated with 10 µM EdU (Jena Bioscience) for 20 min, fixed with 2% paraformaldehyde and permeabilized with 70% ice-cold ethanol. Cells were blocked with 3% BSA containing 0.3% Triton X-100. Next, the cells were incubated with an antibody against γH2AX for 1.5 h, followed by secondary antibodies 1 h (antibodies are listed in Supplementary Table 5). Next, EdU-positive cells were visualized by incubating for 30 min with EdU Click-iT reaction cocktail (50 mM Tris-HCl (pH 7.6), 150 mM NaCl, 1 µM picolyl azide 5/6-FAM (CLK-1180, Jena Bioscience), 4 mM $CuSO_4$ and 2 mg ml^{-1} sodium-L-ascorbate). Cells were mounted using ProLong Gold Antifade Mountant with DAPI (Invitrogen), and γH2AX foci per cell were quantified using Image J.

Microscopy analysis of fixed cells. Images of fixed samples were acquired on a Zeiss AxioImager M2 or D2 widefield fluorescence microscope equipped with 63x PLAN APO (1.4 NA) oil-immersion objectives (Zeiss) and an HXP 120 metal-halide lamp used for excitation. Images were recorded using ZEN 2012 (Blue edition, v.1.1.0.0) software and analysed using Image J (v.1.48).

DRIP–qPCR. Cells were irradiated with UV-C light (9 J m^{-2}) and incubated in conditioned medium for 3 h. DNA was extracted by incubating the cells overnight at 37 °C in TE buffer containing 0.625% SDS and 0.1 mg ml^{-1} proteinase K (Thermo Fisher Scientific, EO0491) followed by phenol–chloroform extraction and ethanol precipitation. The DNA was enzymatically digested with the following cocktail of enzymes and compounds at 37 °C overnight as previously described[39]: *HindIII*, *EcoRI*, *XbaI*, *SspI* and *BsrGI*, BSA, NEB buffer 2.1 (New England Biolabs) and spermidine (0.1 M; Sigma-Aldrich, 05292-1ML-F). The DNA was purified using phenol–chloroform and precipitated with ethanol. For the control of the immunoprecipitated material, 10 µg of each sample was separated in an independent tube and treated with RNase H (NEB) overnight at 37 °C. The DRIP procedure was performed as previously described with some modifications[40]. One-tenth of the purified DNA was used as input. For the immunoprecipitation step, 8 µg of DNA was incubated with 3 µg of S9.6 antibody (Kerafast, ENH001) in 1× binding buffer (10 mM sodium phosphate (pH 7.0), 140 mM NaCl and 0.05% Triton X-100) overnight at 4 °C, followed by pulldown of DNA–RNA hybrids with Protein A Dynabeads (Thermo Fisher, 10002D) for 2 h at 4 °C. The samples were extensively washed, after which the samples were eluted with elution buffer (50 mM Tris (pH 8.0), 10 mM EDTA (pH 8.0) and 0.5% SDS). Both the input and the immunoprecipitation samples were treated with proteinase K and incubated for 45 min at 55 °C. The samples were purified using phenol–chloroform and precipitated with ethanol. qPCR was performed using SYBR Green mastermix (Bio-Rad) with the indicated primers (primers are listed in Supplementary Table 4). The immunoprecipitation efficiency as the percentage of input at each locus was calculated as previously described[40].

Protein expression and purification. Cloning, protein expression and purification of *X. laevis* CSB and CSA-DDB1-CUL4A-RBX1 (CRL4^{CSA}) was done as previously described[6]. Coding sequences of *X. laevis ELOF1* and *RAD23B* for bacterial expression were ordered as codon-optimized gene blocks from Integrated DNA Technologies and cloned into pOPINK vectors (Addgene, 41143) containing the indicated affinity tags. Proteins were expressed in *Escherichia coli* OverExpress C41(DE3) chemically competent cells (Sigma) grown at 37 °C in LB medium supplemented with appropriate antibiotics. At an optical density (OD_{600}) of 0.5–0.6, protein expression was induced with 0.5 mM IPTG for 18–20 h at 18 °C. For the expression of ELOF1, $ZnSO_4$ was added to a final concentration of 20 µM at the time of induction. Protein purifications were performed at 4 °C. Cells were lysed by sonication in lysis buffer (25 mM HEPES (pH 8.0) 300 mM NaCl, 10% glycerol, 2 mM dithiothreitol (DTT), 20 µM $ZnSO_4$ (ELOF1 only)) containing one EDTA-free complete protease inhibitor tablet (Roche) and 1 mg ml^{-1} lysozyme (Sigma), and cleared by centrifugation for 1 h at 35,000 r.p.m. The cleared lysate was incubated with 1–2 ml equilibrated glutathione sepharose 4B resin (GE Healthcare) for 1 h at 4 °C on a rotating wheel. The resin was extensively washed with GST high-salt wash buffer (25 mM HEPES (pH 8.0), 500 mM NaCl, 5% glycerol, 2 mM DTT and 10 µM $ZnSO_4$ (ELOF1 only)). For the purification of GST and GST-tagged ELOF1, proteins were eluted with GST high-salt wash buffer supplemented with 20 mM reduced L-glutathione (Sigma). For the purification

of untagged ELOF1 and RAD23B, the resin was washed with gel-filtration buffer (25 mM HEPES (pH 8.0), 200 mM NaCl, 5% glycerol, 2 mM DTT and 10 μM $ZnSO_4$ (ELOF1 only)) and the GST tag was cleaved overnight on the resin with GST-tagged PreScission protease. Both GST-tagged and untagged proteins were further purified by gel filtration (Superdex 75) in gel filtration buffer. Peak fractions were concentrated with 5 ml of 3 MWCO spin concentrators (Millipore), frozen in liquid nitrogen and stored at −80 °C. Endogenous *X. laevis* RNAPII complex was purified from egg extract (HSS; high-speed supernatant) using the monoclonal 8WG16 antibody immobilized on protein G sepharose 4 fast flow resin (GE Healthcare). After overnight incubation at 4 °C, the resin was washed with wash buffer (25 mM HEPES (pH 7.5), 12.5 mM $MgCl_2$, 0.1 mM EDTA, 10% glycerol, 0.1 mM DTT and 0.01% NP-40) containing 400 mM KCl followed by wash buffer containing 200 mM KCl. The protein was eluted with wash buffer containing 200 mM KCl and 1.5 mg ml^{-1} RNAPII CTD peptide (H_2N-PTSPSYSPTSPSYSPTSPSYS-OH; New England Peptide) and further purified by gel filtration (Superose 6 Increase) in Superose 6 gel filtration buffer (25 mM HEPES (pH 7.5), 150 mM NaCl, 10% glycerol and 2 mM DTT). Peak fractions were pooled, concentrated with 5 ml of 50 MWCO spin concentrators (Millipore), frozen in liquid nitrogen and stored at −80 °C.

Pull-down using immobilized GST and GST–ELOF1. Purified GST and GST-tagged *X. laevis* ELOF1 were immobilized on equilibrated glutathione sepharose 4B resin (GE Healthcare) for 1 h at 4 °C. The beads were washed with GST pull-down buffer (10 mM HEPES (pH 7.7), 50 mM KCl, 2.5 mM $MgCl_2$, 250 mM sucrose, 0.2 mg ml^{-1} BSA and 0.02% Tween) and incubated with the indicated purified proteins for 1 h at 4 °C. Subsequently, the resin was washed three times with GST pull-down buffer. After the final wash, the beads were resuspended in Laemmli–SDS sample buffer before SDS–PAGE analysis and western blotting.

In vitro ubiquitylation assay. In vitro ubiquitylation assays were performed as previously described[6]. In short, in vitro neddylated recombinant xlCRL4^{CSA} was incubated at room temperature with purified ELOF1 or CSB, E1, UBE2D2, ubiquitin and ATP before SDS–PAGE and western blot analysis.

ChIP-seq. Cells were mock treated or irradiated with UV-C light (9 J m^{-2}) and incubated in conditioned medium for different periods of time (1, 4, 8 and 16 h). Cells were crosslinked with 0.5 mg ml^{-1} disuccinimidyl glutarate (Thermo Fisher) in PBS for 45 min at room temperature. Cells were washed with PBS and crosslinked with 1% paraformaldehyde for 20 min at room temperature. Fixation was stopped by adding 1.25 M glycin in PBS to a final concentration of 0.1 M for 3 min at room temperature. Cells were washed with cold PBS and lysed and collected in a buffer containing 0.25% Triton X-100, 10 mM EDTA (pH 8.0), 0.5 mM EGTA (pH 8.0) and 20 mM HEPES (pH 7.6). Chromatin was pelleted for 5 min at 400×*g* and incubated in a buffer containing 150 mM NaCl, 1 mM EDTA (pH 8.0), 0.5 mM EGTA (pH 8.0) and 50 mM HEPES (pH 7.6) for 10 min at 4 °C. Chromatin was again pelleted for 5 min at 400×*g* and resuspended in ChIP buffer (0.15% SDS, 1% Triton X-100, 150 mM NaCl, 1 mM EDTA (pH 8.0), 0.5 mM EGTA (pH 8.0) and 20 mM HEPES (pH 7.6)) to a final concentration of 15×10^6 cells per ml. Chromatin was sonicated to approximately 1 nucleosome using a Bioruptor waterbath sonicator (Diagenode). Chromatin from ~5×10^6 cells was incubated with 3 μg antibody (antibodies are listed in Supplementary Table 5) overnight at 4 °C, followed by a 1.5 h of protein–chromatin pull-down with a 1:1 mix of protein A and protein G Dynabeads (Thermo Fisher, 10001D and 10003D). ChIP samples were extensively washed followed by decrosslinking for 4 h at 65 °C in the presence of proteinase K. DNA was purified using a Qiagen minElute kit. For ser2-RNAPII, ChIP-seq sample libraries were prepared from 1 ng ChIPed DNA using a NEBNext Ultra II DNA Library Prep kit for Illumina (NEB, E7645S) and index primer sets (NEB, E7335S). Strand-biased library amplification was performed using high-fidelity KAPA HiFi enzyme (Roche, KK2102). The prepared libraries were sequenced on an Illumina HiSeq 2500 system (Illumina), resulting in 150-bp paired-end reads. For the remaining ChIP-seq samples, libraries were prepared using a KAPA HyperPrep kit (Roche) and A-T-mediated ligation of full Y-shaped IDT adapters. Samples were sequenced in a 150-bp paired-end run on an Illumina HiSeq X system (Macrogen).

Bru-seq. For Bru-seq after DRB treatment, cells were pretreated with DRB (100 μM) for 3.5 h. Then, cells were washed with PBS and incubated with 2 mM BrU at 37 °C for 30 or 60 min, as indicated, per experiment. For Bru-seq after UV irradiation, cells were irradiated with UV-C light (9 J m^{-2}) and incubated in conditioned medium for different periods of time (3, 8 and 24 h) before being incubated with 2 mM BrU at 37 °C for 30 min. All Bru-seq samples were subsequently lysed in TRIzol reagent (Invitrogen), and BrU-containing RNA was isolated as previously described[41]. Complementary DNA libraries were made from the BrU-labelled RNA using an Illumina TruSeq library kit and paired-end 151-bp sequenced using the Illumina NovaSeq platform at the University of Michigan Advanced Genomics Core. Single-end or paired-end sequencing data were used for downstream analyses.

ATAC-seq. For each experimental condition, 50,000 cells were collected and washed with cold PBS containing protease inhibitors (Roche). The cells were resuspended in 50 μl Transposase mixture, containing 1× Tagment DNA buffer (Illumina kit, 20034197), 0.5 μl Tagment DNA enzyme (Illumina kit, 20034197) and 200 ng μl^{-1} digitonin (Promega, G9441), and incubated at 37 °C for 30 min. Fragmented DNA was purified using a Qiagen minElute kit (28204). Libraries were prepared by PCR using NEBNext High-Fidelity 2× PCR master mix (New England Biolabs, M0541) and a Nextera XT index kit v2 (Illumina). Samples were sequenced in a 150-bp paired-end run on an Illumina HiSeq X system (Macrogen).

RNA-seq and data analysis. Cells were irradiated with UV-C light (9 J m^{-2}) or mock treated and collected 24 h later. Total RNA was isolated using a RNeasy mini kit (Qiagen) according to the manufacturer's protocol. Up to 5×10^6 cells per sample were lysed in RLT buffer. For quantification purposes, 24 ng of the eight ArrayControl RNA Spikes (Thermo Fisher Scientific) were added to each sample at this stage (3 ng per spike). Samples were purified using a KAPA mRNA HyperPrep kit (Roche) and prepared for sequencing using a TruSeq RNA Library Prep kit v2 (Illumina) according to the manufacturer's instructions, and sequenced in an SR50 run in a single lane on an Illumina HiSeq4000. For RNA-seq data analysis, obtained sequencing reads were cleaned by 5′-end quality trimming and Illumina-adapter clipping by Trimmomatic (v.0.32)[42]. Pre-alignment quality control of the cleaned sequencing reads was done with FastQC (v.0.11.8). The alignment to reference genome hg19 of trimmed sequencing reads was done with Hisat2, guided by gene annotation in the refGene UCSC table[43]. The generated SAM files were converted to the binary counterpart BAM, followed by BAM sorting and indexing with SAMtools (v.1.10)[44]. Counting reads to the UCSC's genomic features hg19 was performed by Subread and featureCounts[45]. Differential expression analysis was performed using edgeR (v.3.14.0)[46]. Only genes with at least 2 counts per million in at least 33% of samples were included in the analysis. Data were normalized for sample-specific effects by the trimmed mean of *M*-values. This was followed by estimating the dispersion and determining the differentially expressed genes using a general linear model. FDR-adjusted *P* values of <0.05 were considered significant.

ChIP-seq, Bru-seq and ATAC-seq data analyses. For ser2-RNAPII ChIP-seq, low-quality sequence reads and adapters were filtered out by Trimmomatic (v.3.36)[42]. The trimmed reads were aligned to the human reference genome (GRC h37/hg19) with the Burrows–Wheeler Aligner (BWA-v.0.7.12-r1039)[47]. Biobambam2 (v.2.0.72)[48] was used to remove duplicate reads from the aligned reads. Sequence reads were locally realigned, and base-quality scores were recalibrated with the IndelRealigner and BaseRecalibrator programs in Genome Analysis Toolkit (GATK-v.3.5)[49].

For pan-RNAPII ChIP-seq, Bru-seq and ATAC-seq, a sequencing-quality profile was generated using FastQC (v.0.11.2). If needed, sequences were trimmed using TrimGalore (v.0.6.5). Reads were aligned to the Human Genome 38 using bwa-mem tools (BWA (v.0.7.16a)[47]. Only high-quality reads (>q30) were included in the analyses and duplicates were removed using Samtools (v.1.6) with fixmate -m and markdup -r settings (Supplementary Table 6). Bam files were converted into stranded TagDirectories and UCSC genome tracks using HOMER tools (v.4.8.2)[50]. Example genome tracks were generated in IGV (v.2.4.3). A list of 49,948 genes was obtained from the UCSC genome database (https://genome.ucsc.edu/cgi-bin/hgTables) selecting the knownCanonical table containing the canonical TSSs per gene. To prevent contamination of binding profiles, genes should be non-overlapping with at least 2 kb between genes. Subsequent selection of sets of genes is described per analysis.

For ChIP-seq, binding profiles within selected areas of individual genes (for example around the TSS or the TTS) were defined using the AnnotatePeaks.pl tool of HOMER using the default normalization to 10 million reads. Metagene profiles were defined using the makeMetaGeneProfile.pl tool of HOMER using default settings. Read densities in input samples were subtracted from individual ChIP-seq datasets to background-correct our data, in which negative values were converted to 0, to prevent the use of impossible negative read densities in further calculations. Individual datasets were subsequently processed into heatmaps or binding profiles using R (v.3.5.3) and Rstudio (v.1.1.423)[51]. ChIP-seq binding and metagene profiles were averaged per set of genes, and profiles were normalized to area under the curve (unless described otherwise) to allow proper comparison of the profiles without effects of overall differences in read density.

ATAC-seq and Bru-seq heatmaps were generated as described for ChIP-seq analyses, except for the input subtraction. Bru-seq-aggregated profiles presented in Fig. 3d and Extended Data Fig. 4d were defined using the AnnotatePeaks.pl tool of HOMER using the default normalization to 10 million reads, as for ChIP-seq except for input subtraction. Genes were selected on size and strongest binding of RNAPII at the TSS in undamaged condition, as for ChIP-seq. Read counts at 200 bp was put to 0, and averaged binding profiles were subsequently normalized to nascent transcript levels, as quantified by 5-EU labelling, relative to the control in their specific cell type. For example, WT cells 3 h after UV irradiation showed 35% RNA relative to WT control cells, so we multiplied the expression of the bins by 0.35.

For ChIP-seq, ATAC-seq and Bru-seq analyses, genes were selected based on their lengths for the different analyses (either 3–100 kb, 25–50 kb, 50–100 kb or greater than 100 kb), and were further selected based on the strongest binding of RNAPII in mock-treated WT cells, as indicated per analysis.

Strand-bias analyses and recovery index. Pull-down of RNAPII from damaged genes results in a relative overrepresentation of damaged transcribed strands in the ChIP-seq samples. The inability of high-fidelity DNA polymerases to amplify damaged DNA strands therefore results in unequal PCR amplification (strand bias) of the transcribed and non-transcribed strand during ChIP-seq library sample prep. ChIP-seq reads were quantified in transcribed and non-transcribed strands of genes of 3–100 kb (removing small genes that are unlikely to be damaged in our approach and long genes that are unlikely to be repaired within the time frame of our analyses) with a minimal gap of 2 kb between genes using the AnnotatePeaks.pl tool of HOMER with the default normalization to 10 million reads. We focused on the top 3,000 genes that showed strongest binding of RNAPII at the TSS in WT undamaged condition to select for actively transcribed genes. A strand specificity index (SSI) was subsequently calculated per gene with the following equation (as described before[2])

$$\text{Strand specificity index} = \frac{\text{reads in ``transcribed'' strand} - \text{reads in ``non-transcribed'' strand}}{\text{reads in ``transcribed'' strand} + \text{reads in ``non-transcribed'' strand}}$$

Depending on whether genes are present on the + or – strand of DNA, a strand bias results in either positive or negative SSI values, varying around 0 (representing no strand-bias). To quantify the amount of damage and correlated level of recovery, we defined a recovery index (RI). For this, we generated frequency distributions of per-gene SSIs. While SSIs frequencies follow a single Gaussian distribution in non-biased ChIP-seq samples, the SSI frequencies in biased ChIP-seq samples are expected to follow a mixed Gaussian distribution composed of three normal distributions: one distribution representing genes without strand bias (with $\mu_0 = 0$), and two Gaussian distributions representing strand-biased genes on either the + or – strands of DNA, with μ_1 and μ_2 symmetrically positioned around μ_0 ($-\mu_1 = \mu_2$). The mean distance that the strand-biased Gaussian distributions deviate from 0 (which is represented by $-\mu_1$ or μ_2) was defined as the RI. The three Gaussian distributions were fitted using normalmixEM of the mixtools package in R[52].

RNAPII wave-front analyses. DRB treatment inhibits the release of protomer-proximal RNAPII into the gene, which results in a run-off of all elongating RNAPII molecules from transcribed genes. After DRB release, RNAPII molecules restart transcription from the TSS with an average speed of ~2 kb min^{-1} in WT cells[53]. To define the speed of RNAPII molecules, a RNAPII wave-front was defined in BruDRB-seq samples as the average distance from the TSS that newly released RNAPII molecules reach within the indicated time period (30–60 min after DRB release). Per gene, a positive transcription level was defined as the average BrU read count per kb within the first 20 kb of a gene. Per gene, the front of the RNAPII pool was subsequently defined as the shortest distance from the TSS where in at least five consecutive kb the BrU read count per kb dropped below 20% of this positive transcription level. Wave-fronts per gene were subsequently recalculated to speed of RNAPII in kb min^{-1} and averaged per BruDRB-seq repeat.

Statistics and reproducibility. Most experiments were confirmed in multiple cell lines and using complementary approaches. The genome-wide CRISPR–Cas9 screens were performed in three independent replicate populations. The ChIP-seq and ATAC-seq experiments were repeated independently twice, except for the pan-RNAPII ChIP-seq U2OS *CSB*-KO 20 J m^{-2} at 8 h, which was performed once. The Bru-seq and BruDRB-seq experiments were repeated independently twice, expect for the BruDRB-seq 30 min, which was repeated three times. RNA-seq experiments were independently repeated three times. All experiments yielding micrographs, pull-down experiments and drug-sensitivity assays were performed independently at least twice and often three times as indicated in the legends. The MS experiments were performed in quadruplicate. Statistical analysis was carried out using two-sided *t*-tests to compare groups ($P < 0.05$).

Reporting Summary. Further information on research design is available in the Nature Research Reporting Summary linked to this article.

Data availability

Both raw and processed ChIP-seq, Bru-seq, ATAC-seq and RNA-seq data shown in main Figs. 2–4 and Extended Data Figs. 3–9 have been deposited into the Gene Expression Omnibus (GEO) under GSE149760. The mass spectrometry proteomics data shown in main Fig. 1 and Extended Data Fig. 2 have been deposited into the ProteomeXchange Consortium via the PRIDE partner repository[54] (https://www.ebi.ac.uk/pride/) with the dataset identifier PXD024051. Additionally, publicly available reference datasets of the Hg38 genome and hg19 genome and the known Canonical gene table from the UCSC genome database (https://genome.ucsc.edu/cgi-bin/hgTables; hg38 genome, lifted-over to hg19 when needed) and gene interactions from the GeneMANIA database (https://genemania.org/) have been obtained and used in this manuscript. Published structural information has been obtained for *Saccharomyces cerevisiae* RAD26 bound to RNAPII https://www.rcsb.org/ PBD: 5VVS) and *Komagataella pastoris* ELF1 bound to RNAPII (PDB: 5XOG). Source data are provided with this paper. All other data supporting the findings of this study are available from the corresponding authors upon reasonable request.

Code availability

Custom code used for the analysis of NGS data was written in R and is available from GitHub (https://git.lumc.nl/dvandenheuvel/van-der-weegen-et-al_elof_ncb2021.git).

References

29. Panier, S. et al. Tandem protein interaction modules organize the ubiquitin-dependent response to DNA double-strand breaks. *Mol. Cell* **47**, 383–395 (2012).
30. Benedict, B. et al. WAPL-dependent repair of damaged DNA replication forks underlies oncogene-induced loss of sister chromatid cohesion. *Dev. Cell* **52**, 683–698.e7 (2020).
31. Doench, J. G. et al. Rational design of highly active sgRNAs for CRISPR–Cas9-mediated gene inactivation. *Nat. Biotechnol.* **32**, 1262–1267 (2014).
32. Hart, T. et al. High-Resolution CRISPR screens reveal fitness genes and genotype-specific cancer liabilities. *Cell* **163**, 1515–1526 (2015).
33. Colic, M. et al. Identifying chemogenetic interactions from CRISPR screens with drugZ. *Genome Med.* **11**, 52 (2019).
34. Typas, D. et al. The de-ubiquitylating enzymes USP26 and USP37 regulate homologous recombination by counteracting RAP80. *Nucleic Acid Res.* **43**, 6919–6933 (2015).
35. Rappsilber, J., Mann, M. & Ishihama, Y. Protocol for micro-purification, enrichment, pre-fractionation and storage of peptides for proteomics using StageTips. *Nat. Protoc.* **2**, 1896–1906 (2007).
36. Tyanova, S., Temu, T. & Cox, J. The MaxQuant computational platform for mass spectrometry-based shotgun proteomics. *Nat. Protoc.* **11**, 2301–2319 (2016).
37. Tyanova, S. et al. The Perseus computational platform for comprehensive analysis of (prote)omics data. *Nat. Methods* **13**, 731–740 (2016).
38. Parra, I. & Windle, B. High resolution visual mapping of stretched DNA by fluorescent hybridization. *Nat. Genet.* **5**, 17–21 (1993).
39. Garcia-Rubio, M., Barroso, S. I. & Aguilera, A. Detection of DNA–RNA hybrids in vivo. *Methods Mol. Biol.* **1672**, 347–361 (2018).
40. Sanz, L. A. & Chedin, F. High-resolution, strand-specific R-loop mapping via S9.6-based DNA–RNA immunoprecipitation and high-throughput sequencing. *Nat. Protoc.* **14**, 1734–1755 (2019).
41. Andrade-Lima, L. C., Veloso, A., Paulsen, M. T., Menck, C. F. & Ljungman, M. DNA repair and recovery of RNA synthesis following exposure to ultraviolet light are delayed in long genes. *Nucleic Acids Res.* **43**, 2744–2756 (2015).
42. Bolger, A. M., Lohse, M. & Usadel, B. Trimmomatic: a flexible trimmer for Illumina sequence data. *Bioinformatics* **30**, 2114–2120 (2014).
43. Kim, D., Langmead, B. & Salzberg, S. L. HISAT: a fast spliced aligner with low memory requirements. *Nat. Methods* **12**, 357–360 (2015).
44. Li, H. et al. The Sequence Alignment/Map format and SAMtools. *Bioinformatics* **25**, 2078–2079 (2009).
45. Liao, Y., Smyth, G. K. & Shi, W. featureCounts: an efficient general purpose program for assigning sequence reads to genomic features. *Bioinformatics* **30**, 923–930 (2014).
46. Robinson, M. D., McCarthy, D. J. & Smyth, G. K. edgeR: a Bioconductor package for differential expression analysis of digital gene expression data. *Bioinformatics* **26**, 139–140 (2010).
47. Li, H. Aligning sequence reads, clone sequences and assembly contigs with BWA-MEM. Preprint at https://arxiv.org/abs/1303.3997 (2013).
48. Tischler, G. & Leonard, S. biobambam: tools for read pair collation based algorithms on BAM files. *Source Code Biol. Med.* **9**, 13 (2014).
49. McKenna, A. et al. The Genome Analysis Toolkit: a MapReduce framework for analyzing next-generation DNA sequencing data. *Genome Res.* **20**, 1297–1303 (2010).
50. Heinz, S. et al. Simple combinations of lineage-determining transcription factors prime *cis*-regulatory elements required for macrophage and B cell identities. *Mol. Cell* **38**, 576–589 (2010).
51. R Development Core Team. R: a Language and Environment for Statistical Computing. (R Foundation for Statistical Computing, 2019).
52. Benaglia, T., Hunter, C. D. & Young, D. R. D mixtools: an R Package for analyzing finite mixture models. *J. Stat. Softw.* **32**, 1–29 (2009).
53. Danko, C. G. et al. Signaling pathways differentially affect RNA polymerase II initiation, pausing, and elongation rate in cells. *Mol. Cell* **50**, 212–222 (2013).
54. Perez-Riverol, Y. et al. The PRIDE database and related tools and resources in 2019: improving support for quantification data. *Nucleic Acids Res.* **47**, D442–D450 (2019).

Acknowledgements

We acknowledge A. Kragten, J. Balk, J. Poell, K. Kato, M. Shimada, S. Kloet, M. Paulsen, M. Vukic, D. Warmerdam, A. Ramadhin and L. Daxinger for help during this project. We also thank J. Moffat, K. Chan and A. Tong for sharing the pLCKO-TKOv3 library before publication. We thank the Amsterdam UMC NGS sequencing facilities for support. We thank P. van Veelen and A. de Ru for MS equipment maintenance. This work was funded

by a LUMC Research Fellowship, a NWO-ENW-M grant (OCENW.KLEIN.090) and a NWO-VIDI grant (ALW.016.161.320) to M.S.L., a Leiden University Fund (LUF) grant to D.v.d.H. (W18355-2-EM), a KWF/Alpe Young Investigator 10701 grant to J.d.L., a CCA proof-of-concept grant to K.d.L. and R.W., an Amsterdam UMC Innovation Grant (CRISPR Expertise Center, 2019) to R.W., UM1 HG009382 and R01 CA213214 NCI grants to M.L., a KWF Young Investigator grant 11367 to R.G.-P., and an ERC starting grant 310913 to A.C.O.V. J.C.W. was supported by NIH grant HL098316 and is a Howard Hughes Medical Institute (HHMI) Investigator and an American Cancer Society Research Professor. T.E.T.M. was supported by an EMBO Long-term fellowship (ALTF 1316-2016) and a HHMI fellowship of The Jane Coffin Childs Memorial Fund for Medical Research.

Author contributions

Y.v.d.W. generated plasmids, U2OS and RPE1-iCas9 single KO and dKO cells, U2OS Flp-In cell-lines, performed clonogenic survivals, co-IP experiments, RRS and DRB-RRS experiments, western blot analyses, in situ PLA experiments, generated samples for pan-RNAPII ChIP-seq, ser2-RNAPII ChIP-seq, ATAC-seq, BruDRB-seq and Bru-seq, generated the figures and wrote the paper. K.d.L. optimized, performed and analysed all CRISPR screens and RNA-seq experiments, performed and analysed drug-sensitivity assays, generated gene-gene interaction network and Venn diagrams, performed γH2AX foci and DNA fibre experiments and helped write the paper. D.v.d.H. performed co-IP experiments, developed tools and analysed pan-RNAPII ChIP-seq, ser2-RNAPII ChIP-seq, ATAC-seq, BruDRB-seq, Bru-seq and helped write the paper. Y.N. performed co-IP experiments and generated TCR-seq libraries. T.E.T.M. generated recombinant xlELOF1, xlCSB and xlCRL4^{CSA}, purified xlRNAPII and performed pull-down and in vitro ubiquitylation assays. J.J.M.v.S. created the RPE1-iCas9 cell line, performed CRISPR screens, performed γH2AX foci and DNA fibre analyses. M.S.M.A. performed and analysed DRIP–qPCR. I.V.N. analysed BruDRB-seq and Bru-seq. D.E.C.B. generated stable cell lines and performed clonogenic survival assays. R.G.-P. analysed the MS with support from A.C.O.V. N.H.M.K. generated U2OS single KO clones, Flp-In cell-lines, performed clonogenic survivals and co-IP experiments. A.P.W. performed the unscheduled DNA synthesis experiments and generated plasmids. K.R. processed and analysed the RNA-seq data, performed gene–gene interaction network analysis, and performed and analysed CRISPR screens. Y.H. analysed ser2-RNAPII ChIP-seq. J.d.L. supervised J.J.M.v.S.; J.C.D. supervised K.R.; J.C.W. supervised T.E.T.M.; S.M.N. supervised M.S.M.A.; M.L. supervised I.V.N. and analysed BruDRB-seq and Bru-seq. T.O. supervised Y.N. and Y.H. and analysed Ser2-RNAPII ChIP-seq. R.M.F.W. supervised K.d.L., co-supervised K.R. and J.J.M.v.S., conceived, coordinated and supervised the project and helped write the paper. M.S.L. supervised Y.v.d.W., D.v.d.H., D.E.C.B., N.H.M.K. and A.P.W., conceived, coordinated and supervised the project, generated all cryo-electron microscopy images and wrote the paper.

Competing interests

The authors declare no competing interests.

Additional information

Extended data is available for this paper at https://doi.org/10.1038/s41556-021-00688-9.

Supplementary information The online version contains supplementary material available at https://doi.org/10.1038/s41556-021-00688-9.

Correspondence and requests for materials should be addressed to R.M.F.W. or M.S.L.

Peer review information *Nature Cell Biology* thanks Dong Wang and the other, anonymous, reviewer(s) for their contribution to the peer review of this work. Peer reviewer reports are available.

Reprints and permissions information is available at www.nature.com/reprints.

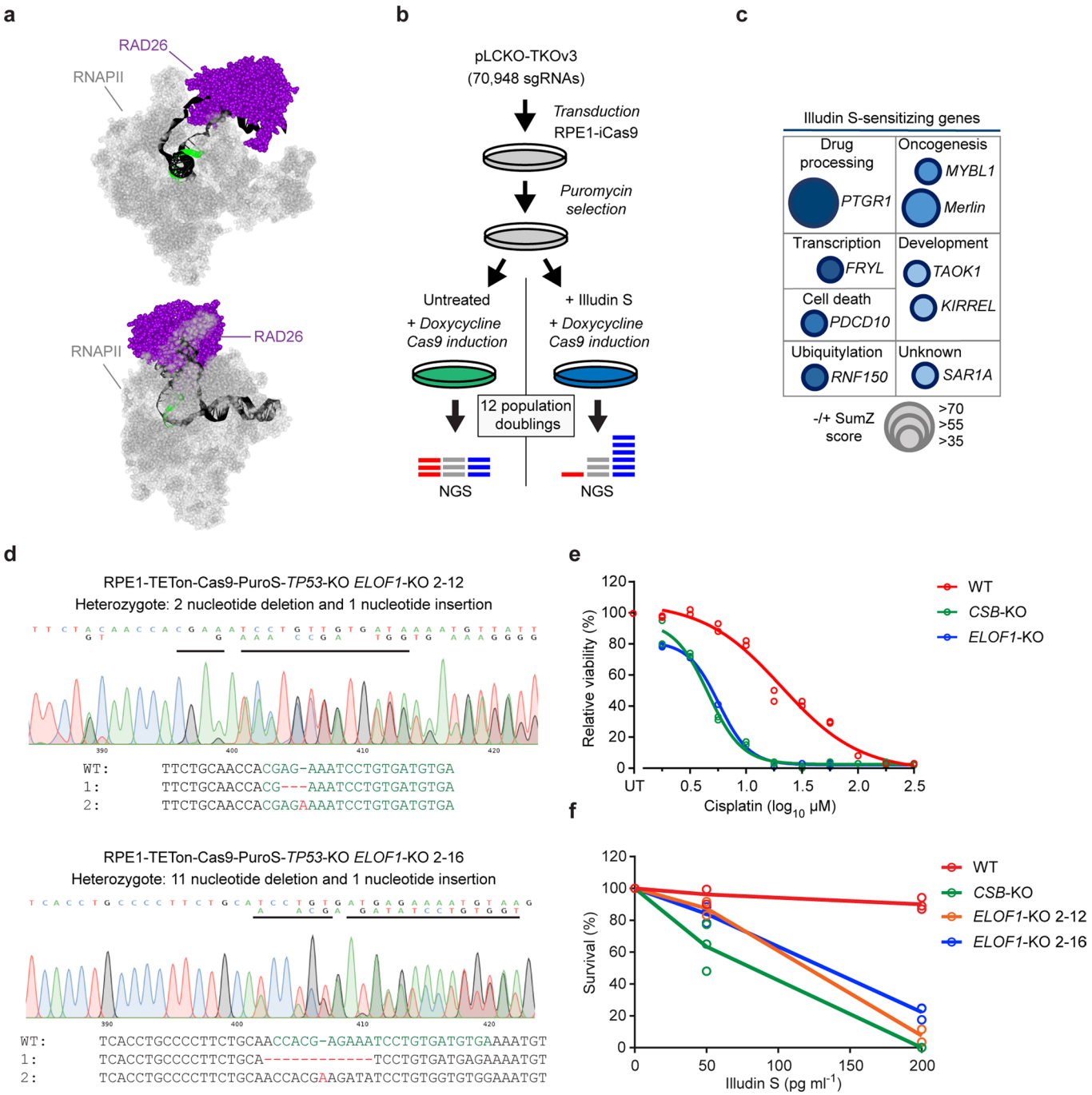

Extended Data Fig. 1 | Human ELOF1 protects cells against transcription stress. a, Front-view and side-view of the yeast orthologue of CSB, *Saccharomyces cerevisiae* RAD26 (purple), bound to RNAPII (grey) (PDB: 5VVS). **b**, Schematic representation of the CRISPR/Cas9 screen in RPE1-iCas9 cells in the presence of Illudin S (IC60; 25 nM). **c**, Network analysis of highly significant hits representing genes that promote Illudin S toxicity. Grey lines reflect known protein-protein interactions (Cytoscape, BioGRID). **d**, Sanger sequencing of the indicated RPE1-iCas9 single *ELOF1*-KO clones. **e**, 72 h drug sensitivity assay of indicated RPE1-iCas9 KO clones. The experiment has been performed twice and each symbol represents the median of 6 technical replicates of an independent experiment. UT, untreated **f**, Clonogenic Illudin S survival of the indicated RPE1-iCas9 cells. The experiment has been performed three times (except for *ELOF1*-KO 2-12 where the experiment has been done twice) and each symbol represents the mean of 2 technical replicates of an independent experiment. Numerical data are provided in Source data extended data Fig. 1.

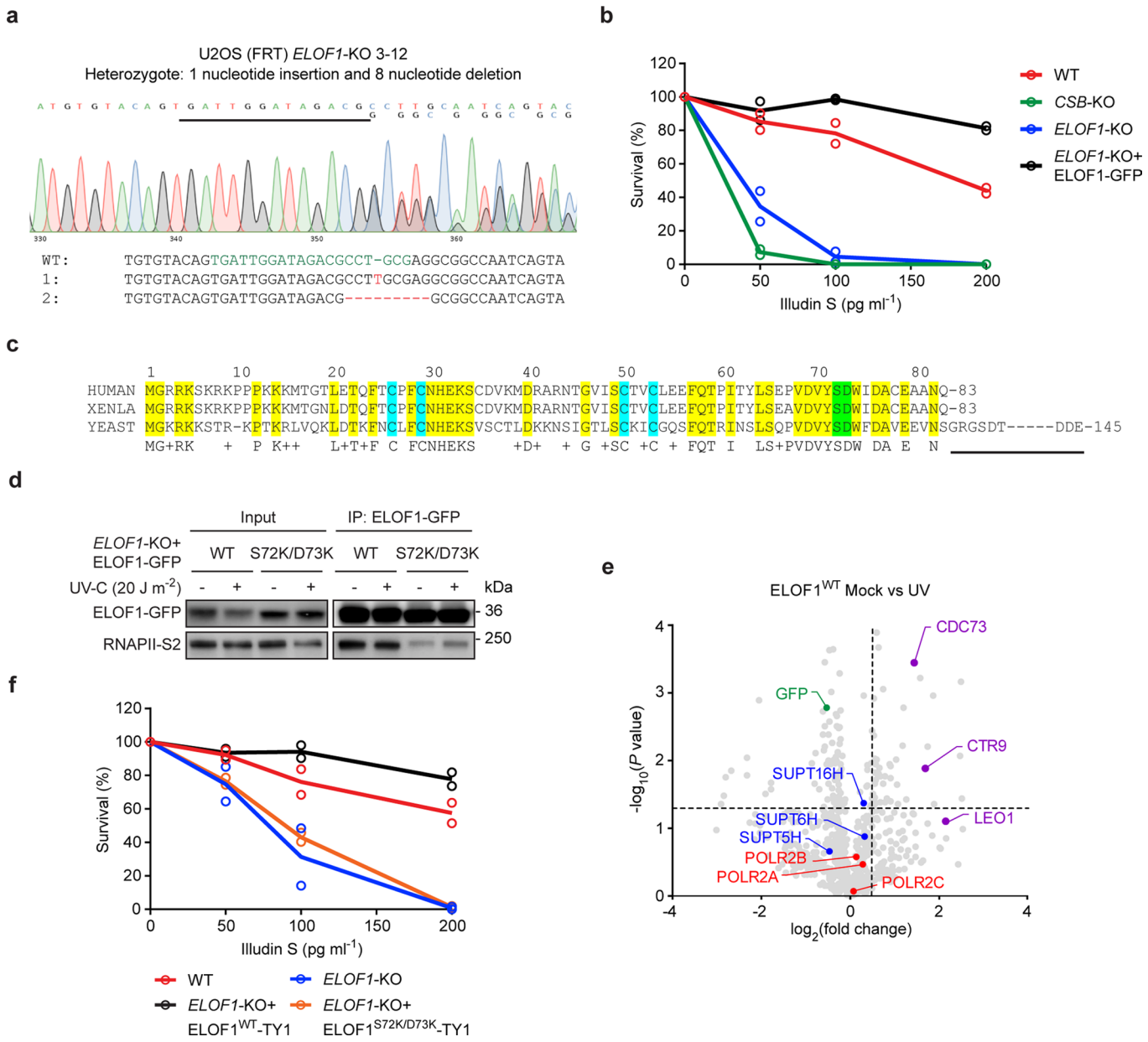

Extended Data Fig. 2 | Human ELOF1 and yeast ELF1 show similar RNAPII-binding modes. a, Sanger sequencing of the indicated U2OS (FRT) *ELOF1*-KO clone. **b**, Clonogenic Illudin S survival of U2OS (FRT) WT, *CSB*-KO, *ELOF1*-KO, and *ELOF1*-KO complemented with ELOF1^{WT}-GFP. The experiment has been performed twice and each symbol represents the mean of 2 technical replicates of an independent experiment. **c**, Alignment of human ELOF1, *Xenopus leavis* ELOF1, and *Saccharomyces cerevisiae* ELF1. Conserved residues are indicated in yellow, zinc-finger cysteines in magenta, residues involved in the RPB1 or RPB2 interaction in green. Note that the C-terminus of *Saccharomyces cerevisiae* ELF1 (83–145) is absent in human ELOF1 and *Xenopus leavis* ELOF1. (**d**) Co-immunoprecipitation (IP) of ELOF1^{WT}-GFP and ELOF1$^{S72K/D73K}$-GFP on the combined soluble and chromatin fraction. Data shown represent 4 independent experiments. (**e**) Volcano plot depicting the statistical differences between 4 replicates of the MS analysis on ELOF1^{WT}-GFP pull-down in mock treated and UV-irradiated samples. The fold change (log_2) is plotted on the x-axis and the significance (t-test -log_{10}(*P* value)) is plotted on the y-axis. RNAPII subunits are indicated in red, elongation factors are indicated in blue, GFP is indicated in green, and PAF1 subunits are indicated in purple. (**f**) Clonogenic Illudin S survival of U2OS (FRT) WT, *ELOF1*-KO, and TY1-tagged ELOF1 rescue cell lines. The experiment has been performed twice and each symbol represents the mean of 2 technical replicates of an independent experiment. Uncropped blots and numerical data are provided in Source data extended data Fig. 2.

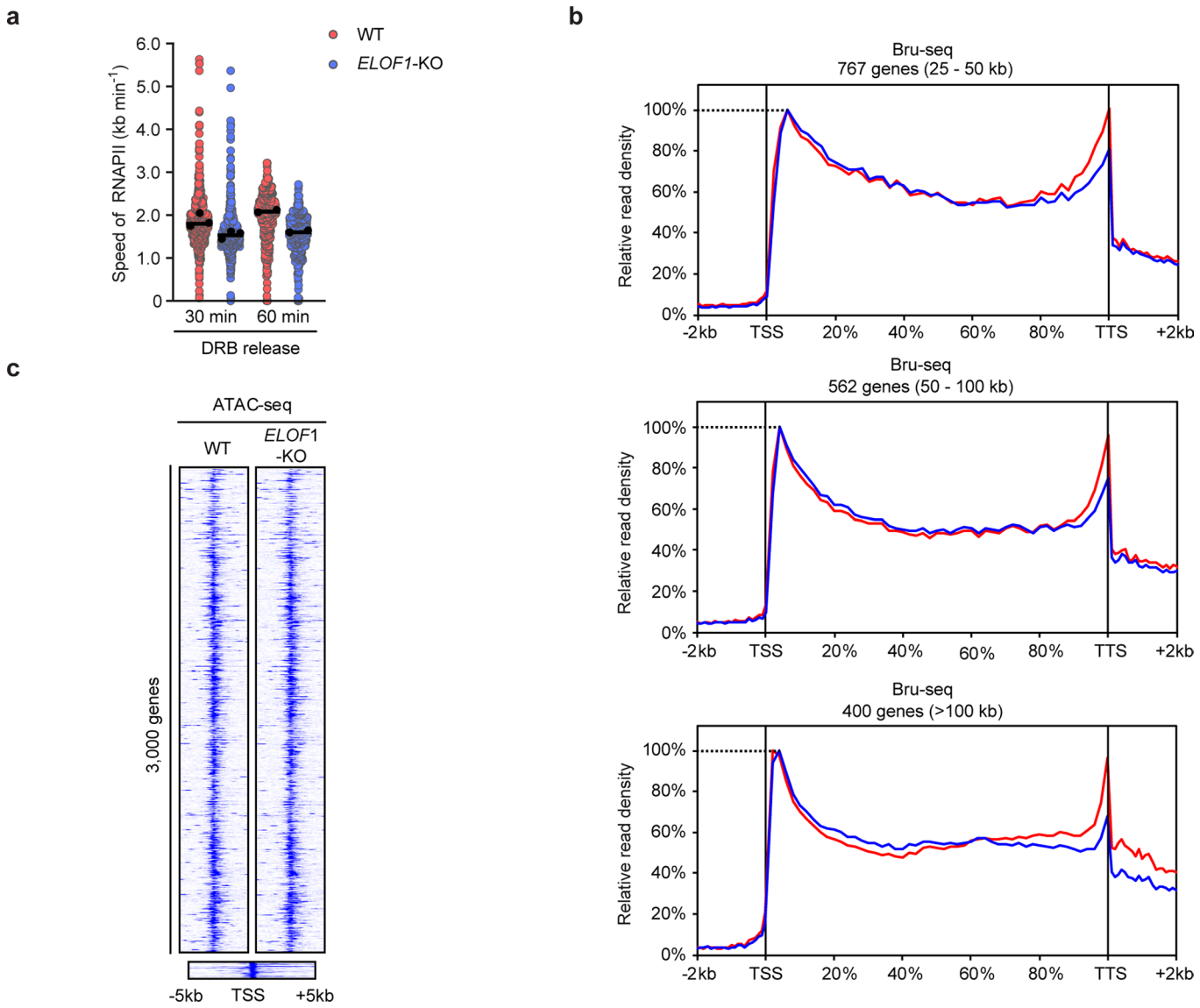

Extended Data Fig. 3 | ELOF1 promotes transcription elongation. a, Calculated speed of RNAPII, quantified by wave-front analyses, in WT (red) or *ELOF1*-KO (blue) cells 30 min (*n=3* experiments) or 60 min (*n=2* experiments) after DRB release. Data represents the median per condition (black line) and median within individual replicates (black circles). **b**, Metaplots of BrU signal (nascent transcription) from 2 kb before the TSS to 2 kb after the TTS in 767 genes between 25–50 kb (upper), 562 genes between 50–100 kb (middle), or 400 genes of >100 kb in WT (red) or *ELOF1*-KO (blue) cells. Profiles are normalized to 100% at promoter-proximal BrU peaks instead of area under the curve for better comparison of transcription profiles. Profiles are averages of 2 independent replicates. **c**, Heatmaps of ATAC-seq data around the TSS (−5 kb until +5 kb) of 3,000 genes of 3–100 kb in unirradiated RPE1-iCas9 cells (WT or *ELOF1*-KO). Numerical data are provided in Source data extended data Fig. 3.

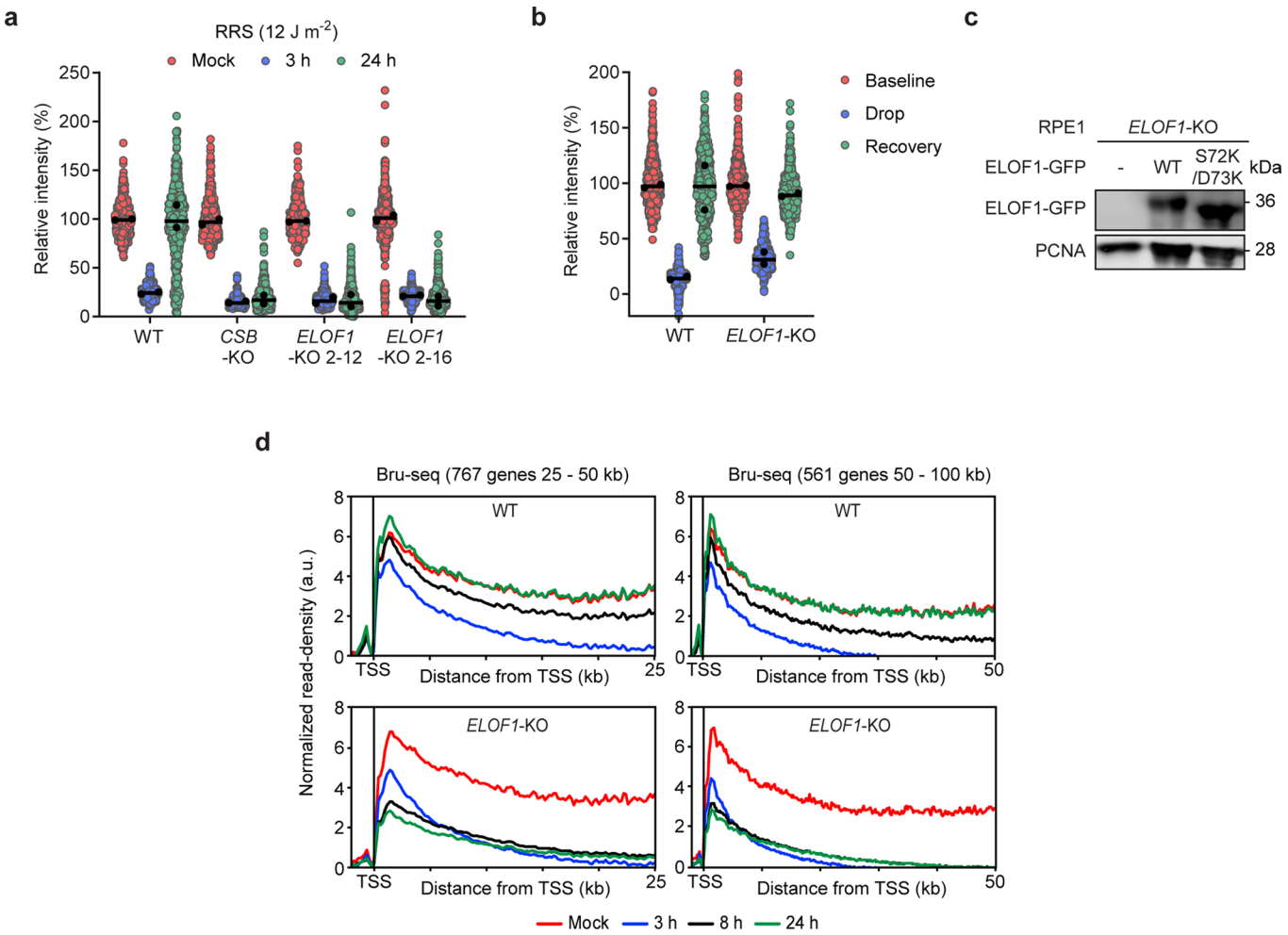

Extended Data Fig. 4 | ELOF1 promotes genome-wide transcription recovery. a, Quantification of 5-EU levels of the indicated RPE1-iCas9 cells normalized to mock-treated levels for each cell line. Cells were either mock-treated or UV-irradiated (3 h or 24 h; 12 J m^{-2}). The experiment has been performed twice and each black circle represents the median of 2 technical replicates of an independent experiment, >80 cells collected per technical replicate. The black line represents the median of all the cells collected. **b**, Quantification of 5-EU levels normalized to the baseline level before DRB treatment for each condition. The experiment has been performed twice and each black circle represents the median of 2 technical replicates of an independent experiment, >80 cells collected per technical replicate. The black line represents the median of all the cells collected. **c**, Western blot analysis of RPE1-iCas9 *ELOF1*-KO cells complemented with GFP-tagged versions of ELOF1. Data shown represent 3 independent experiments. **d**, Metaplots of BrU signal (nascent transcription) in 767 genes between 25–50 kb, or in 561 genes between 50–100 kb in WT (upper) or *ELOF1*-KO (lower) cells after mock treatment (red), or 3 h (blue), 8 h (black), and 24 h (green) after UV irradiation (9 J m^{-2}). Profiles are averages of 2 independent replicates. Uncropped blots and numerical data are provided in Source data extended data Fig. 4.

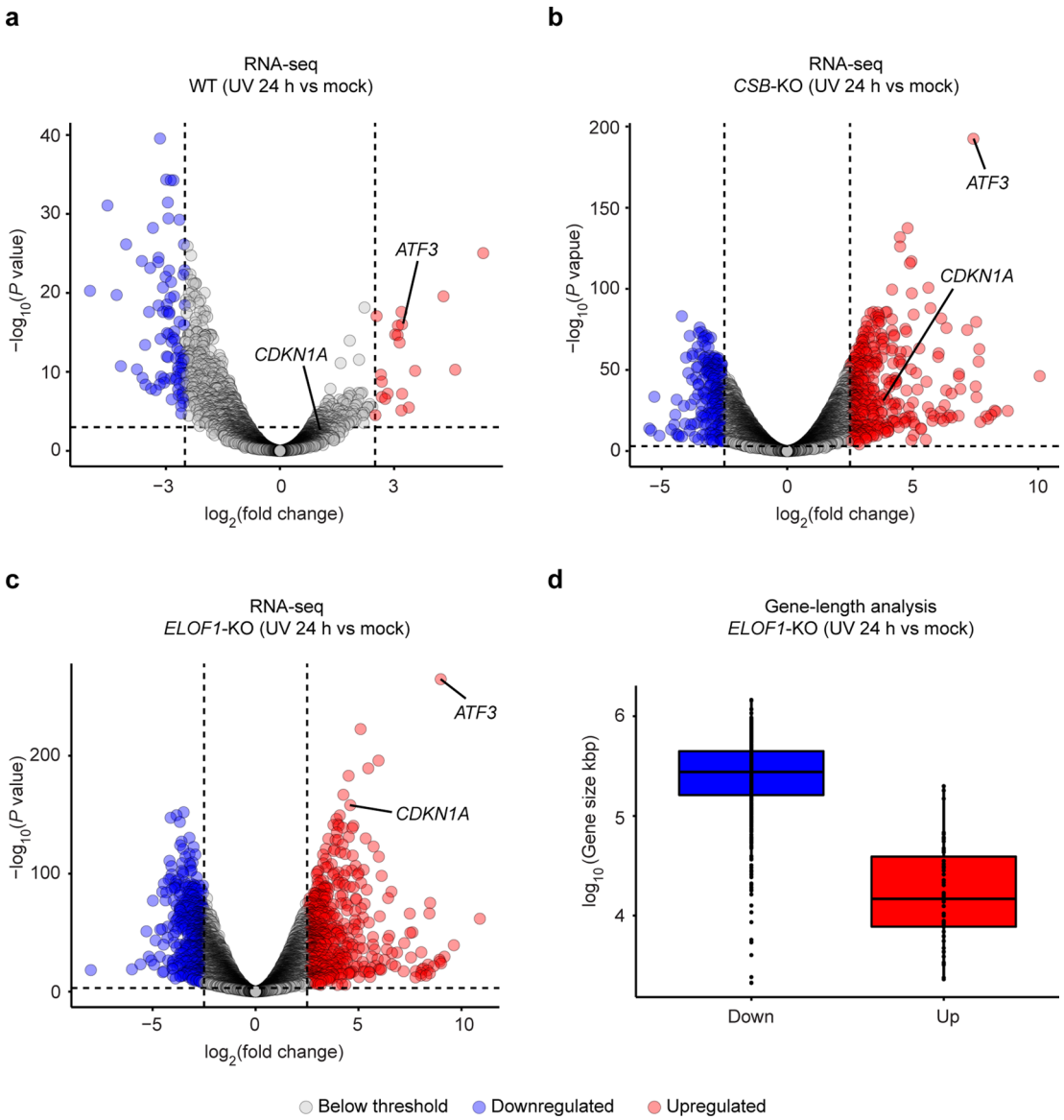

Extended Data Fig. 5 | Global gene-expression changes in response to UV irradiation. Volcano plots of RNA-seq in the indicated RPE1-iCas9 cell lines depicting the downregulation (blue) or upregulation (red) of gene expression in response to UV irradiation (24 h; 9 J m^{-2}). The fold change (log_2) is plotted on the x-axis and the significance (-log_{10} *P* value) is plotted on the y-axis. **a**, WT, (**b**) *CSB*-KO, (**c**) *ELOF1*-KO. Only genes indicating at least 2 counts per million (CPM) in at least 33% of samples were included in the analysis. FDR-adjusted *P* values < 0.05 were considered significant. Two short UV-response genes (*ATF3*, *CDKN1A*) are highlighted. **d**, Box plot depicting the gene length of the 650 most significantly downregulated genes (in blue) or the 650 most significantly upregulated genes (in red). The horizontal line represents the median (center); Upper Bound: gene length scores larger than 75% of all data points; Lower Bound: gene lengths scores shorter than 75% of all data points. Points above and below the box represent the outliers.

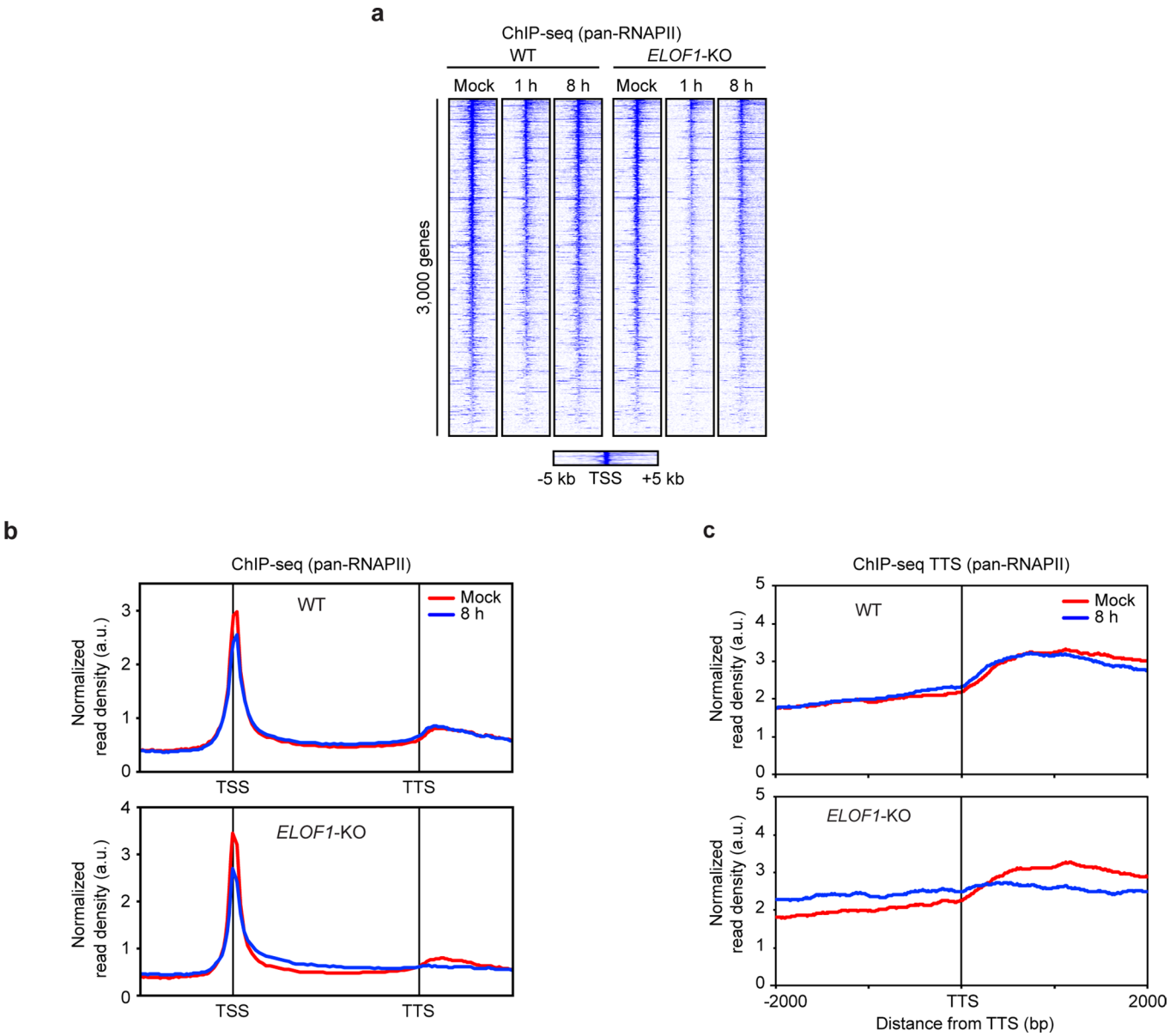

Extended Data Fig. 6 | Genome-wide redistribution of RNAPII in response to UV irradiation. a, Heatmaps of pan-RNAPII ChIP-seq data around the TSS of 3,000 genes of 3–100 kb, ranked according to RNAPII signal in mock-treated WT cells. Heatmaps of the same genes are shown after UV irradiation (9 J m^{-2}) in WT or *ELOF1*-KO cells. **b**, Averaged metaplots of pan-RNAPII ChIP-seq of 3,000 genes of 3–100 kb from the TSS until the TTS in the indicated RPE1-iCas9 cells after mock-treatment (red) or at 8 h (blue) after UV irradiation (9 J m^{-2}). (**c**) As in **b** showing the area around the TTS (−2 kb until +2 kb).

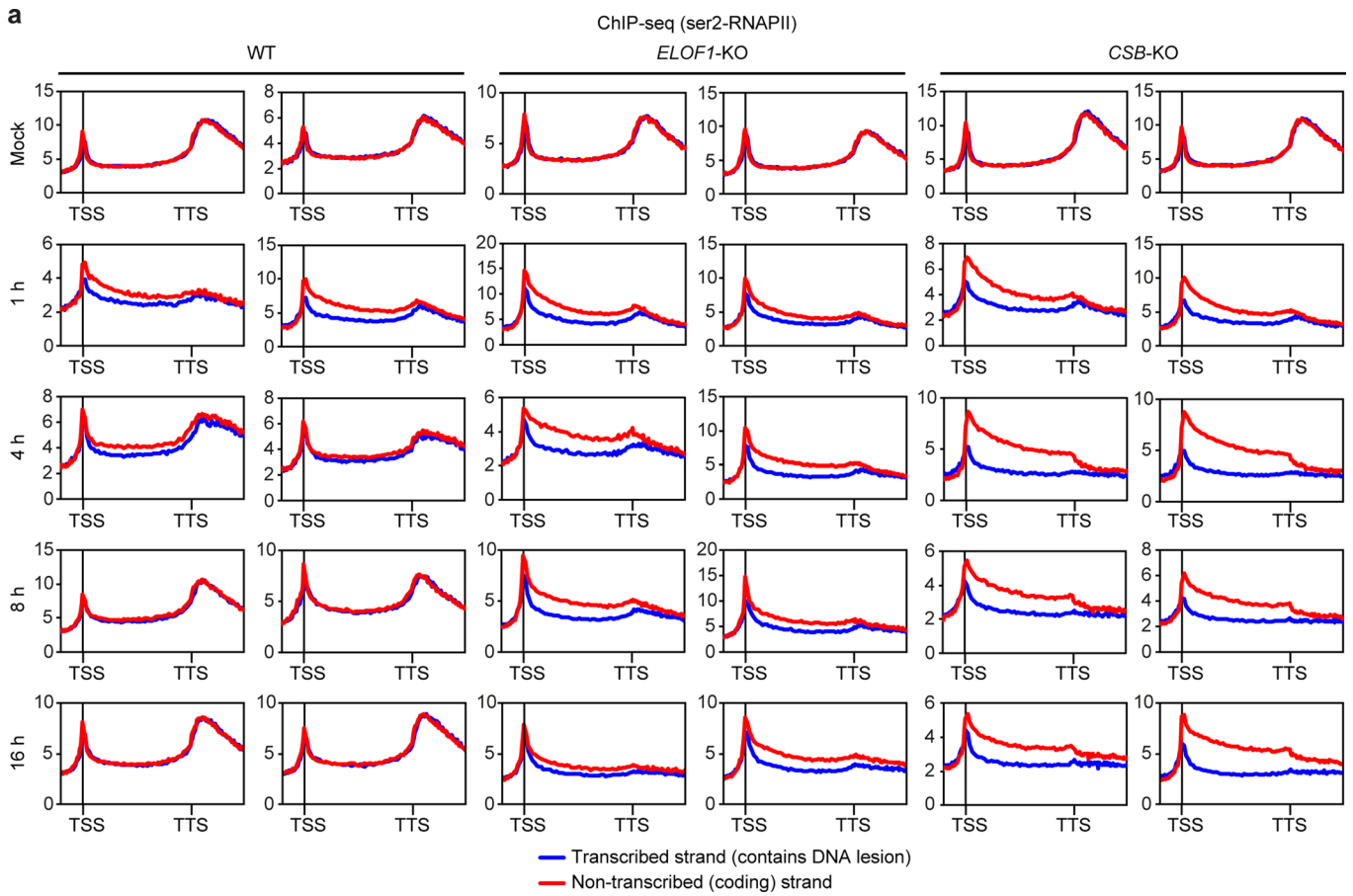

Extended Data Fig. 7 | Metaplots of TCR-seq using a Ser2-RNAPII antibody. a, Individual metaplots (two replicates for each condition) of ser2-RNAPII TCR-seq of 3,000 genes for 3–100 kb from the TSS until the TTS (−5 kb and +5 kb, respectively) in the indicated RPE1-iCas9 cells after mock-treatment or at 1 h, 4 h, or 8 h after UV irradiation (9 J m^{-2}). The coding (non-transcribed) strand in shown in red, while the template (transcribed) strand is shown in blue.

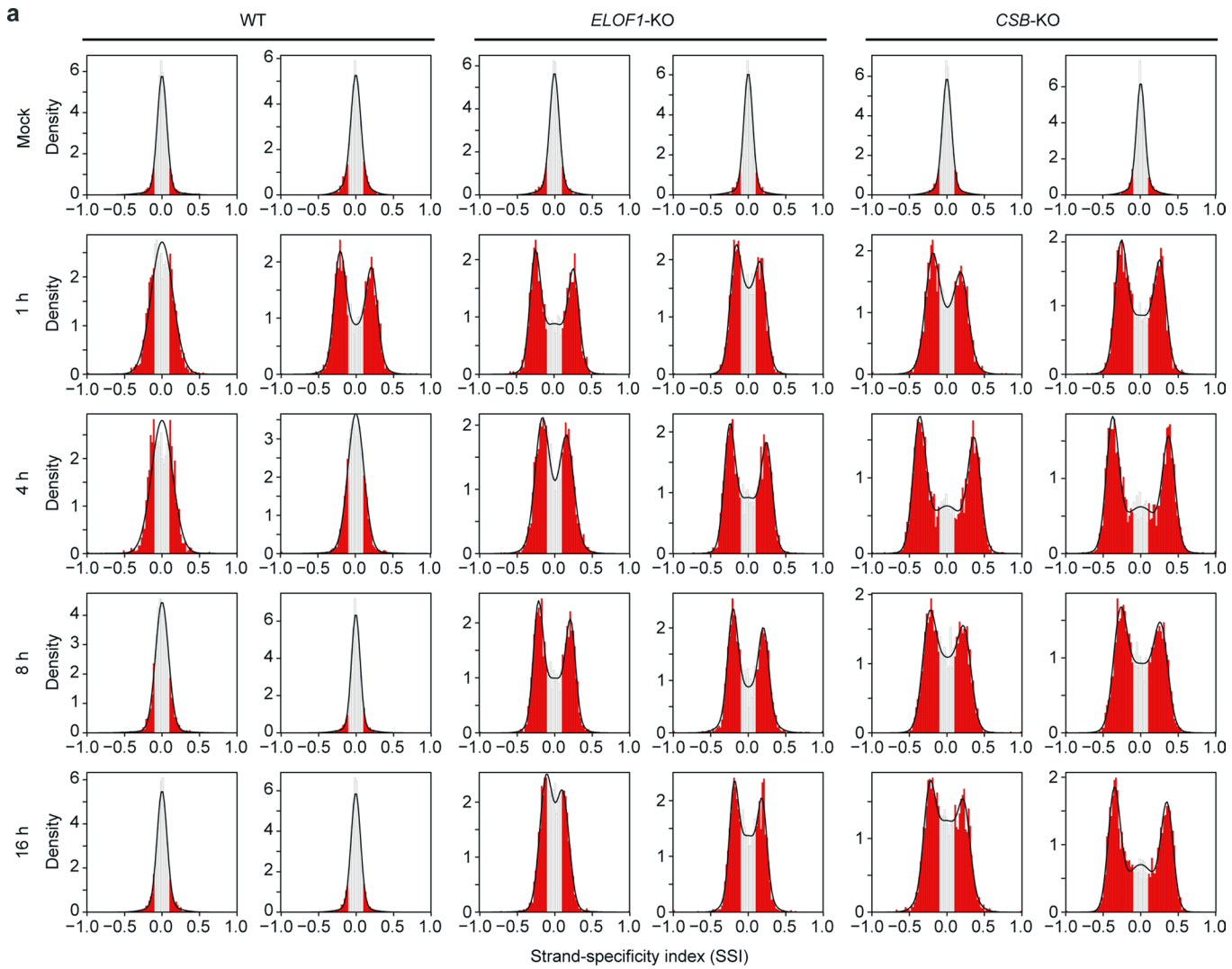

Extended Data Fig. 8 | Histogram plots of TCR-seq using a Ser2-RNAPII antibody. a, Frequency distribution plots of the gene-by-gene ser2-RNAPII strand-specificity index (SSI). SSIs below −0.1 or above 0.1 are presented in red. A unimodal distribution indicates no strand-bias (and thus no DNA damage in the template strand), while a trimodal distribution reflects a strand-bias caused by DNA damage in the template strand.

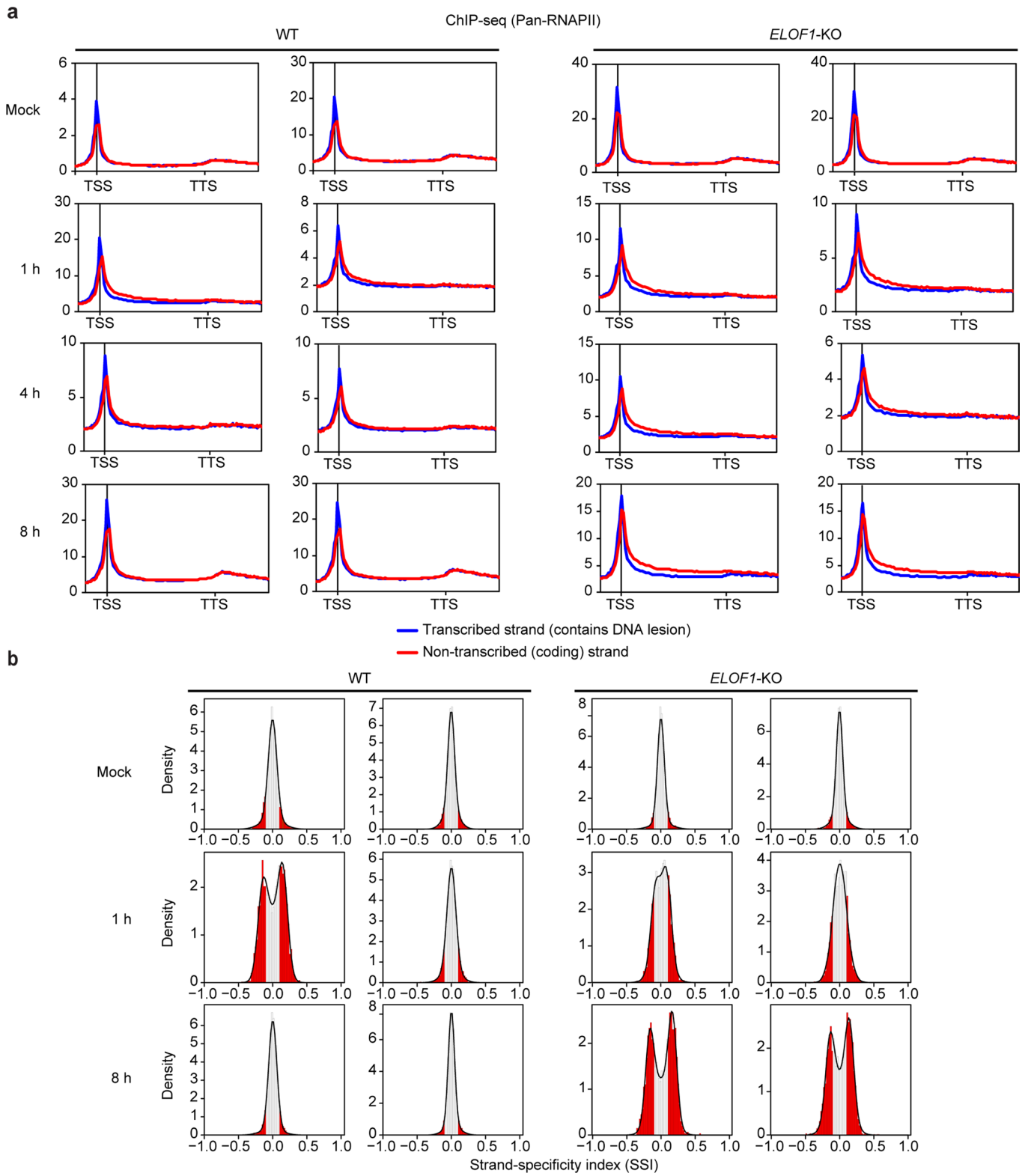

Extended Data Fig. 9 | Validation of TCR-seq with a pan-RNAPII antibody. a, Individual metaplots (two replicates for each condition) of pan-RNAPII TCR-seq of 3,000 genes of 3–100 kb from the TSS until the TTS (−5 kb and +5 kb, respectively) in the indicated RPE1-iCas9 cells after mock-treatment or at 1 h, 4 h, or 8 h after UV irradiation (9 J m^{-2}). The coding (non-transcribed) strand in shown in red, while the template (transcribed) strand is shown in blue. **b**, Frequency distribution plots of the gene-by-gene pan-RNAPII strand-specificity index (SSI). SSIs below −0.1 or above 0.1 are presented in red. A unimodal distribution indicates no strand-bias (and thus no DNA damage in the template strand), while a trimodal distribution reflects a strand-bias caused by DNA damage in the template strand.

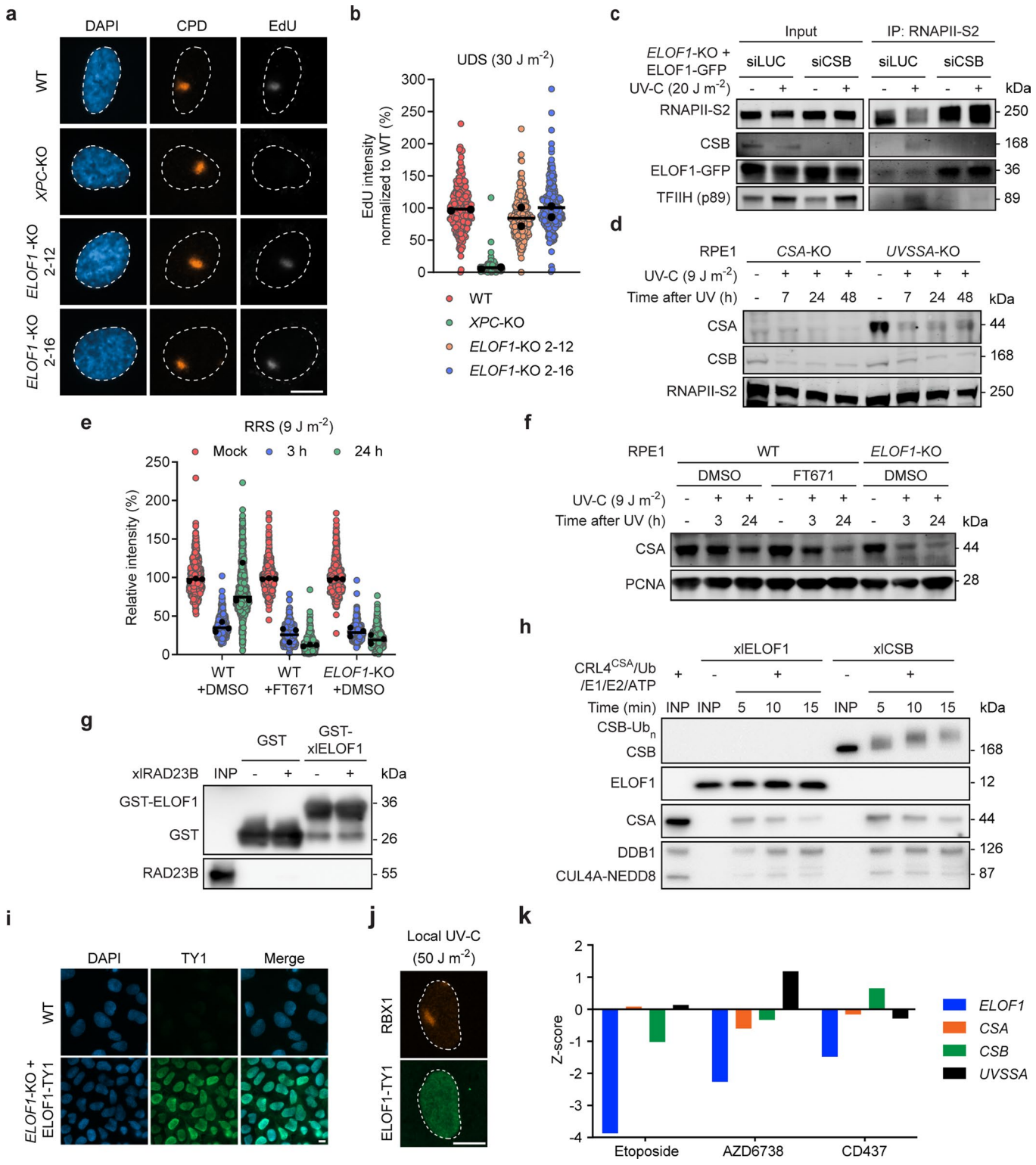

Extended Data Fig. 10 | See next page for caption.

Extended Data Fig. 10 | ELOF1 is not involved in global genome repair. a-b, Unscheduled DNA synthesis (UDS) in the indicated RPE1-iCas9 cells following local UV irradiation (30 J m^{-2}; 1 h). DNA damage was identified by CPD staining. **a**, Representative images (Scale bar, 10 μm) and (**b**) quantification of EdU levels normalized to WT cells. The experiment has been performed twice and each black circle represents the median of 2 technical replicates of an independent experiment, >80 cells collected per technical replicate. The black line represents the median of all the cells collected. **c**, Endogenous RNAPIIo Co-IP on U2OS (FRT) *ELOF1*-KO cells complemented with $ELOF1^{WT}$-GFP after knockdown of CSB (siCSB) or as a control luciferase (siLUC). Data shown represent 2 independent experiments. **d**, Western blot analysis of CSA protein levels in the indicated RPE1-iCas9 cells after mock treatment, or 7 h, 24 h, and 48 h after UV irradiation (9 J m^{-2}; *n=2*). **e**, Quantification of 5-EU levels of the indicated RPE1-iCas9 cells normalized to mock-treated levels for each cell line. Cells were either mock-treated or UV-irradiated (3 h or 24 h; 9 J m^{-2}). 10 μM FT671 (USP7 inhibitor) was added to the indicated cells 24 h prior to UV irradiation. The experiment has been performed three times and each black circle represents the median of 2 technical replicates of an independent experiment, >50 cells collected per technical replicate. The black line represents the median of all the cells collected. **f**, Western blot analysis of CSA protein levels from e. **g**, GST pull-down of immobilized recombinant *Xenopus laevis* (xl) ELOF1 incubated with recombinant xlRAD23B. Data shown represent 2 independent experiments. **h**, In vitro ubiquitylation of recombinant xlELOF1 and xlCSB with recombinant $xlCRL4^{CSA}$, E1, E2, ubiquitin, and ATP. In vitro ubiquitylation reactions were stopped at the indicated times. Data shown represent 3 independent experiments. (**i**) Representative images of staining with TY1 antibodies in U2OS (FRT) WT cells and *ELOF1*-KO cells complemented with TY1-tagged ELOF1. Data shown represent 2 independent experiments. **j**, Representative image of staining with TY1 and RBX1 antibodies at 1 h after local UV irradiation (50 J m^{-2}) in U2OS (FRT) *ELOF1*-KO cells complemented with TY1-tagged ELOF1. Data shown represent 2 independent experiments. **k**, Results of mining a recent CRISPR screen repository[27]. Shown are the Z-scores for the indicated sgRNAs (targeting *ELOF1* (blue), *CSA* (orange), *CSB* (green), *UVSSA* (black) after exposure to the indicated genotoxic agents. Uncropped blots and numerical data are provided in Source data extended data fig. 10.

nature research

Corresponding author(s): M.S. Luijsterburg
R.M.F. Wolthuis

Last updated by author(s): Apr 22, 2021

Reporting Summary

Nature Research wishes to improve the reproducibility of the work that we publish. This form provides structure for consistency and transparency in reporting. For further information on Nature Research policies, see our Editorial Policies and the Editorial Policy Checklist.

Statistics

For all statistical analyses, confirm that the following items are present in the figure legend, table legend, main text, or Methods section.

n/a	Confirmed	
☐	☒	The exact sample size (*n*) for each experimental group/condition, given as a discrete number and unit of measurement
☐	☒	A statement on whether measurements were taken from distinct samples or whether the same sample was measured repeatedly
☒	☐	The statistical test(s) used AND whether they are one- or two-sided *Only common tests should be described solely by name; describe more complex techniques in the Methods section.*
☒	☐	A description of all covariates tested
☒	☐	A description of any assumptions or corrections, such as tests of normality and adjustment for multiple comparisons
☐	☒	A full description of the statistical parameters including central tendency (e.g. means) or other basic estimates (e.g. regression coefficient) AND variation (e.g. standard deviation) or associated estimates of uncertainty (e.g. confidence intervals)
☒	☐	For null hypothesis testing, the test statistic (e.g. *F*, *t*, *r*) with confidence intervals, effect sizes, degrees of freedom and *P* value noted *Give P values as exact values whenever suitable.*
☒	☐	For Bayesian analysis, information on the choice of priors and Markov chain Monte Carlo settings
☒	☐	For hierarchical and complex designs, identification of the appropriate level for tests and full reporting of outcomes
☒	☐	Estimates of effect sizes (e.g. Cohen's *d*, Pearson's *r*), indicating how they were calculated

Our web collection on statistics for biologists contains articles on many of the points above.

Software and code

Policy information about availability of computer code

Data collection	Microscopy images were acquired using a Zeiss AxioImager M2 or D2 widefield fluorescence microscope and ZEN 2012 software (blue edition, version 1.1.0.0). Western blot images were acquired using a Odyssey CLx with Image studio lite software (v5.2) or for western blot with ECL a Amersham Imager 680.
Data analysis	Microscopy images were analyzed in Image J (1.48v). CRISPR screen: Drugz (v1.1.0.2) (Colic et al., 2019) was used to analyse Crispr/Cas9 screen data. Functional pathway analysis was performed using Reactome (v72). Cytoscape (v3.7) was used to build and visualize the interaction networks. RNA-seq: Trimmomatic (v0.32) (Bolger et al., 2014) was used to trim sequences. FastQC (v0.11.8) was used to generate a quality profile. Hisat2 (v2.2.0) was used to align sequences to the Human Genome. BAM sorting and indexing was done with SAMtools (v1.10). Differential expression analysis was performed using edgeR (v3.14.0). Ser2-RNAPII ChIP-seq: Trimmomatic (v3.36) (Bolger et al., 2014) was used to filter out low-quality sequence reads. The BWA tool (BWA-v0.7.12-r1039) (Li, 2013) was used to align sequencing reads to the Human Genome. Biobambam2 (v2.0.72) (Tischler and Leonard, 2014) was used to remove duplicate reads from the aligned reads. Sequence reads were locally realigned and base-quality scores were recalibrated with the IndelRealigner and BaseRecalibrator programs in Genome Analysis Toolkit (GATK-v3.5) (McKenna et al., 2010). Pan-RNAPII ChIP-seq, Bru-seq, and ATAC-seq: FastQC (v0.11.2) was used to generate a quality profile. Sequences were trimmed using TrimGalore (v0.6.5). The BWA tool (BWA-v0.7.16a) (Li, 2013) was used to align sequencing reads to the Human Genome. duplicates were removed using Sam tools (v1.6) (Li et al., 2009). Example genome tracks were generated using IGV (v2.4.3). ChIP-seq, Bru-seq, ATAC-seq: HOMER (v4.8.2) (Heinz et al., 2010) was used to convert bam files into TagDirectories and to define binding profiles (Heinz et al., 2010), using the settings described in the methods section of the manuscript. R (v3.5.3) and Rstudio (v1.1.423) (Team, 2019) were used to perform remaining customized analyses, using tools commonly available in R software and using the settings described in the methods section of the manuscript. Mass spectrometry data was analyzed using MaxQuant software (v1.6.14) and analysis output was further processed in the Perseus (v1.6.14) computational platform and further processed in Microsoft Excel 2016 for comprehensive visualization. Graphs were plotted and analyzed using Graphpad Prism 8 (v8.4.2).

Custom code used for the analysis of NGS data was written in R and is available from GitHub (https://git.lumc.nl/dvandenheuvel/van-der-weegen-et-al_elof_ncb2021.git).

For manuscripts utilizing custom algorithms or software that are central to the research but not yet described in published literature, software must be made available to editors and reviewers. We strongly encourage code deposition in a community repository (e.g. GitHub). See the Nature Research guidelines for submitting code & software for further information.

Data

Policy information about availability of data

All manuscripts must include a data availability statement. This statement should provide the following information, where applicable:

- Accession codes, unique identifiers, or web links for publicly available datasets
- A list of figures that have associated raw data
- A description of any restrictions on data availability

Both raw and processed ChIP-seq, Bru-seq, ATAC-seq, and RNA-seq data shown in main Figure 2 – 4 and Extended Data Figure 3 – 9 are deposited in the Gene Expression Omnibus (GEO) under GSE149760. The mass spectrometry proteomics data shown in main figure 1 and Extended Data Figure 2 are deposited to the ProteomeXchange Consortium via the PRIDE partner repository (https://www.ebi.ac.uk/pride/) with the dataset identifier PXD024051. Additionally, publicly available reference datasets of the Hg38 genome and hg19 genome and the knownCanonical gene table from the UCSC genome database ((https://genome.ucsc.edu/cgi-bin/hgTables; hg38 genome, lifted-over to hg19 when needed)) and gene interactions from the GeneMANIA database (https://genemania.org/) have been obtained and used in this manuscript. Published structural information has been obtained for S. cerevisiae RAD26 bound to RNAPII (https://www.rcsb.org/ PBD: 5VVS) and K. pastoris ELF1 bound to RNAPII (PDB: 5XOG). Source data are provided with this study. All other data supporting the findings of this study are available from the corresponding author on reasonable request.

Field-specific reporting

Please select the one below that is the best fit for your research. If you are not sure, read the appropriate sections before making your selection.

☒ Life sciences ☐ Behavioural & social sciences ☐ Ecological, evolutionary & environmental sciences

For a reference copy of the document with all sections, see nature.com/documents/nr-reporting-summary-flat.pdf

Life sciences study design

All studies must disclose on these points even when the disclosure is negative.

Sample size	No statistical method was used to predetermine sample size. Sample sizes were chosen for the different experimental approaches based on the technical difficulty and throughput of the individual assays, the chosen sample sizes are consistent with previous publications.
Data exclusions	Data were only excluded from the study when internal controls indicated evident technical errors such as a lack of proper locus enrichment in ChIP-seq.
Replication	All replication attempts were successful. The number of replicate experiments are indicated in the figure legends of the manuscript and at least two replicates were performed for each individual approach. Most results were confirmed in multiple cell lines and using complementary approaches. - Hits in the CRISPR/Cas9 screen were verified by analysis of knockout cells - Knockout cells were confirmed by sequencing and if specific antibodies were available also with western blot analyses - Drug sensitivity was confirmed by Clonogenic survival assays and proliferation assays - Strand specificity index (SSI) findings for the Ser2 ChIP-seq were confirmed with Pan RNAPII ChIP-seq - Recovery of RNA synthesis (RRS) after DRB treatment or UV irradiation was confirmed with Bru-seq - Mass spec findings were confirmed by reciprocal immunoprecipitation and western blot analyses - Interactions found with proximity ligation assays (PLA) were confirmed with in vitro pull-down assays
Randomization	There was no allocation of test subjects for any experiments, thus randomization was not applicable to our study
Blinding	Data analyses were performed by unbiased software programs/algorithms blinding was therefore not applicable to our study

Reporting for specific materials, systems and methods

We require information from authors about some types of materials, experimental systems and methods used in many studies. Here, indicate whether each material, system or method listed is relevant to your study. If you are not sure if a list item applies to your research, read the appropriate section before selecting a response.

Materials & experimental systems

n/a	Involved in the study
☐	☒ Antibodies
☐	☒ Eukaryotic cell lines
☒	☐ Palaeontology and archaeology
☒	☐ Animals and other organisms
☒	☐ Human research participants
☒	☐ Clinical data
☒	☐ Dual use research of concern

Methods

n/a	Involved in the study
☐	☒ ChIP-seq
☒	☐ Flow cytometry
☒	☐ MRI-based neuroimaging

Antibodies

Antibodies used

Cas9 (Mouse) - Cell signalling, (7A9-3A3 #14697); RRID:AB_2750916; Lot #2
CSA/ERCC8 (Mouse) - Santa Cruz (D2 sc-376981); Lot #10816
CSA/ERCC8 (Rabbit) - Abcam (EPR9237 ab137033); RRID:AB_2783825; Lot #GR155793-4
CSB/ERCC6 (Goat) - Santa Cruz (E-18 SC-10459); RRID:AB_668957; Lot #A2114
CSB/ERCC6 (Rabbit) - Santa Cruz (H-300 sc25370); RRID:AB_668958; Lot #I1012
CSB/ERCC6 (Mouse) - Bio Matrix Research (553C5a) ;Lot #BMR00638
GFP (Mouse) - Roche (7.1-13.1 11814460001); RRID:AB_390913; Lot #27575600
GFP (Mouse) - Santa Cruz (B2); RRID:AB_627695; Lot #sc-9996
GFP (Rabbit) - Abcam (ab290); RRID:AB_303395; Lot #GR3251545-1
p62/GTF2H1 (Mouse) - Santa Cruz (G10 sc-48431); RRID:AB_2247962; Lot #J1706
p89/XPB/ERCC3 (Mouse) - Millipore (15TF2-1B3 MABE1123); Lot #Q2589558
p89/XPB/ERCC3 (Mouse) - Santa Cruz (G10); RRID:AB_10649033; Lot #sc-271500
UVSSA (Mouse) - Abnova, (B01P); RRID:AB_10716149; Lot #H00057654-B01P
RNAPII-S2 (Rabbit) - Abcam (ab5095); RRID:AB_304749; Lot #GR3231908-7
RNAPII-S2 (Rat) - Milipore (3E10); RRID:AB_10627998; Lot #04-1571
RNAPII-Total (Rabbit) - Bethyl; RRID:AB_2620600; Lot #A304-405A
ATF3 (Rabbit) - Abcam (EPR19488); RRID:AB_2734728; Lot #ab207434
γH2aX (Mouse) - Millipore (JBW301); RRID:AB_309864; Lot #05-636
Tubulin (Mouse) - Sigma (DM1A T6199); RRID:AB_477583; Lot #048M4751V
Mouse IgG (H+L) CF770 (Goat) - Biotium (#20077); RRID: AB_10852670; Lot #17C0928
Rabbit IgG (H+L) CF680 (Goat) - Biotium (VWR #20067); RRID:AB_10871686; Lot #18C1120
Goat IgG (H+L) CF680 (Donkey) - Thermo fisher Scientific (A-21084); RRID:AB_2535741; Lot #1778374
Mouse IgG (HRP) (Goat) - Abcam (ab6789); RRID:AB_955439; Lot #GR3234199-2
Rabbit IgG (HRP) (Goat) - Abcam (ab6721); RRID:AB_955447
Rat IgG (HRP) (Goat) - Cell signaling (ab7077); RRID:AB_10694715
Mouse IgG (HRP) (Horse) - Cell signaling (ab7076); RRID:AB_330924
Mouse Alexa 555 (Goat) - Thermo fisher Scientific (A-21424); RRID:AB_141780
CPD (Mouse) - Cosmo Bio (TDM-2 CAC-NM-DND-001); RRID:AB_1962813; Lot #TM-C-014
FK2 (Mouse) - Life Sciences (BML-PW8810-0500); Batch: x08714
Rabbit Alexa 488 (Goat) - Thermo fisher Scientific (A-11034); RRID:AB_2576217
Mouse Alexa 488 (Donkey) - Jackson Immuno Research (715-545-150); RRID:AB_2340846
Rat Alexa 555 (Goat) - Invitrogen (A-21434); RRID:AB_141733
Mouse Cy3 (Donkey) - Jackson Immuno Research (715-165-150); RRID:AB_2340813
TY1 (Mouse) - Diagenode, C15200054 (Mab-054-050)
RBX1 (Rabbit) - Cell signalling (D3J5I) ; RRID:AB_2797769
XPC (Rabbit) - Novus biologicals (#NB100-58801) ;RRID:AB_877776; Lot #A1
PCNA (Mouse) - Santa Cruz (PC10); RRID:AB_628110
s9.6 (Mouse) - Kerafast (#ENH001); RRID:AB_2687463
BrdU (Mouse) - BD Biosciences (#B44); RRID:AB_2313824
BrdU (Rat) - Novus Biologicals (BU1/75 (ICR1)); RRID:AB_341913
FLAG (Rabbit) - New England Peptide; antigen: C(dPEG4)DYKDDDDK
xlCSA (Rabbit) - New England Peptide; antigen: CHRTHINPAFEDAWSSSEDES
xlELOF1 (Rabbit) - Pocono Rabbit Farm and Laboratory; antigen: recombinant full-length xlELOF1
xlRAD23B (Rabbit) - Pocono Rabbit Farm and Laboratory; antigen: recombinant full-length xlRAD23B
RPB1 (Mouse) - Thermo fisher Scientific (8WG16); RRID:AB_795353
RPB2 (Rabbit) - Thermo fisher Scientific; RRID:AB_2645754
GST (Mouse) - Cell Signaling (26H1); RRID:AB_2189875

Validation

The following antibodies were validated in knockout cells: CSA/ERCC8 (Rabbit) - Abcam (EPR9237 ab137033), CSA/ERCC8 (Mouse) - Santa Cruz (D2 sc-376981), CSB/ERCC6 (Goat) - Santa Cruz (E-18 SC-10459), CSB/ERCC6 (Rabbit) - Santa Cruz (H-300 sc25370), XPC (Rabbit) - Novus biologicals (#NB100-58801)

The following antibodies were validated in Co-IP experiments: p62/GTF2H1 (Mouse) - Santa Cruz (G10 sc-48431), p89 (Mouse) - Millipore (15TF2-1B3 MABE1123), p89/XPB/ERCC3 (Mouse) - Santa Cruz (G10 sc-271500), UVSSA (Mouse) - Abnova, (H00057654-B01P), RNAPII-S2 (Rabbit) - Abcam (ab5095), RNAPII-S2 (Rat) - Milipore (3E10 #04-1571), FK2 (mouse) -, FLAG (Rabbit) - New England Peptide; antigen: C(dPEG4)DYKDDDDK, xlCSA (Rabbit) - New England Peptide; antigen: CHRTHINPAFEDAWSSSEDES, xlELOF1 (Rabbit) - Pocono Rabbit Farm and Laboratory; antigen: recombinant full-length xlELOF1, xlRAD23B (Rabbit) - Pocono Rabbit Farm and Laboratory; antigen: recombinant full-length xlRAD23B, RPB1 (Mouse) - Thermo fisher Scientific (8WG16)

RPB2 (Rabbit) - Thermo fisher Scientific, GST (Mouse) - Cell Signaling (26H1)

The following antibody is a commonly used loading control: Tubulin (Mouse) - Sigma (T6199)

The following antibody was validated by local UV-C irradiation experiments: CPD (Mouse) - Cosmo Bio (TDM-2 CAC-NM-DND-001)

The following antibodies were validated by westernblot: Cas9 (Mouse) - Cell Signalling technology (7A9-3A3 #14697), GFP (Mouse) - Roche (7.1-13.1 11814460001), GFP (Rabbit) - Abcam (ab290), GFP (Mouse) - Santa Cruz (B2 sc-9996), ATF3 (Rabbit) - Abcam (EPR19488 ab207434), γH2aX (Mouse) - Millipore (JBW301 05-636), PCNA (Mouse) - Santa Cruz (PC10)

This antibody was validated in ChIP-seq experiments: RPB1-total - Bethyl (A304-405A)

The following antibody was vailidated in IF experiments: TY1 (Mouse) - Diagenode, C15200054 (Mab-054-050)

Eukaryotic cell lines

Policy information about cell lines

Cell line source(s)	U2OS(FRT) (Panier et al., 2012) U2OS(FRT) CSB-KO (1-12) (van der Weegen et al., 2020) U2OS(FRT) ELOF1-KO (3-12) This study U2OS(FRT) ELOF1-KO (3-12) + ELOF1-GFP-N1 This study U2OS(FRT) ELOF1-KO (3-12) + ELOF1S72K/D73K-GFP This study U2OS(FRT) ELOF1-KO (3-12) + ELOF1-TY1-N1 This study U2OS(FRT) ELOF1-KO (3-12) + ELOF1S72K/D73K-TY1-N1 This study RPE1-iCas9 This study RPE1-iCas9 CSB-KO (1-15) This study RPE1-iCas9 ELOF1-KO (2-12) This study RPE1-iCas9 ELOF1-KO (2-16) This study RPE1-iCas9 UVSSA-KO (3-9) This study RPE1-iCas9 PTGR1-KO (11) This study RPE1-iCas9 XPC-KO This study RPE1-iCas9 CSB-KO (15)/ELOF1-KO (2-20) This study RPE1-iCas9 CSB-KO (15)/CSA-KO (3-21) This study RPE1-iCas9 ELOF1-KO (2-16) + ELOF1-GFP-N1 This study RPE1-iCas9 ELOF1-KO (2-16) + ELOF1S72K/D73K-GFP This study Human RPE1-hTERT ATCC (CRL-4000™)
Authentication	Cells were authenticated by STR profiling. All knockout cells were validated by Western blot analysis and/or DNA sequencing
Mycoplasma contamination	All cell lines were routinely tested for mycoplasma and were nested negative
Commonly misidentified lines (See ICLAC register)	No commonly misidentified cell lines were used in this study

ChIP-seq

Data deposition

☒ Confirm that both raw and final processed data have been deposited in a public database such as GEO.

☒ Confirm that you have deposited or provided access to graph files (e.g. BED files) for the called peaks.

Data access links *May remain private before publication.*	Both raw and processed ChIP-seq, BrU-seq, ATAC-seq, and RNA-seq data are deposited in the Gene Expression Omnibus (GEO; https://www.ncbi.nlm.nih.gov/geo/). The data can be accessed by using the following details: Dataset identifier: GSE149760 Password: obmhawiqvnenxal)
Files in database submission	Raw data ATAC-seq: WTMock-1_1.fastq.gz WTMock-1_2.fastq.gz WTMock-2_1.fastq.gz WTMock-2_2.fastq.gz ELOF1-KOMock-1_1.fastq.gz ELOF1-KOMock-1_2.fastq.gz ELOF1-KOMock-2_1.fastq.gz ELOF1-KOMock-2_2.fastq.gz BruDRB-seq: 638-MP-10_trimmed_S_R1_001.fastq.gz

638-MP-12_trimmed_S_R1_001.fastq.gz
2048-MP-1_GAGATTCC-AGGATAGG_S206_R1_001.fastq.gz
2048-MP-1_GAGATTCC-AGGATAGG_S206_R2_001.fastq.gz
2048-MP-2_ATTCAGAA-TCAGAGCC_S208_R1_001.fastq.gz
2048-MP-2_ATTCAGAA-TCAGAGCC_S208_R2_001.fastq.gz
2048-MP-3_GAATTCGT-CTTCGCCT_S209_R1_001.fastq.gz
2048-MP-3_GAATTCGT-CTTCGCCT_S209_R2_001.fastq.gz
2048-MP-4_CTGAAGCT-TAAGATTA_S210_R1_001.fastq.gz
2048-MP-4_CTGAAGCT-TAAGATTA_S210_R2_001.fastq.gz
2048-MP-5_TAATGCGC-ACGTCCTG_S211_R1_001.fastq.gz
2048-MP-5_TAATGCGC-ACGTCCTG_S211_R2_001.fastq.gz
2048-MP-6_CGGCTATG-GTCAGTAC_S212_R1_001.fastq.gz
2048-MP-6_CGGCTATG-GTCAGTAC_S212_R2_001.fastq.gz
1068-MP-10_TAATGCGC-CAGGACGT_S10_R1_001.fastq.gz
1068-MP-10_TAATGCGC-CAGGACGT_S10_R2_001.fastq.gz
1068-MP-12_AGCGATAG-TATAGCCT_S12_R1_001_fastq.gz
1068-MP-12_AGCGATAG-TATAGCCT_S12_R2_001.fastq.gz

Bru-seq:
638-MP-1_trimmed_S_R1_001.fastq.gz
638-MP-2_trimmed_S_R1_001.fastq.gz
638-MP-3_trimmed_S_R1_001.fastq.gz
638-MP-4_trimmed_S_R1_001.fastq.gz
638-MP-5_trimmed_S_R1_001.fastq.gz
638-MP-6_trimmed_S_R1_001.fastq.gz
638-MP-7_trimmed_S_R1_001.fastq.gz
638-MP-8_trimmed_S_R1_001.fastq.gz
1068-MP-1_CGGCTATG-TAATCTTA_S1_R1_001_fastq.gz
1068-MP-1_CGGCTATG-TAATCTTA_S1_R2_001_fastq.gz
1068-MP-2_TCCGCGAA-CAGGACGT_S2_R1_001_fastq.gz
1068-MP-2_TCCGCGAA-CAGGACGT_S2_R2_001_fastq.gz
1068-MP-3_TCTCGCGC-GTACTGAC_S3_R1_001.fastq.gz
1068-MP-3_TCTCGCGC-GTACTGAC_S3_R2_001.fastq.gz
1068-MP-4_TCCGGAGA-TATAGCCT_S4_R1_001.fastq.gz
1068-MP-4_TCCGGAGA-TATAGCCT_S4_R2_001.fastq.gz
1068-MP-5_CGCTCATT-ATAGAGGC_S5_R1_001.fastq.gz
1068-MP-5_CGCTCATT-ATAGAGGC_S5_R2_001.fastq.gz
1068-MP-6_GAGATTCC-CCTATCCT_S6_R1_001.fastq.gz
1068-MP-6_GAGATTCC-CCTATCCT_S6_R2_001.fastq.gz
1068-MP-7_ATTCAGAA-GGCTCTGA_S7_R1_001.fastq.gz
1068-MP-7_ATTCAGAA-GGCTCTGA_S7_R2_001.fastq.gz
1068-MP-8_GAATTCGT-AGGCGAAG_S8_R1_001.fastq.gz
1068-MP-8_GAATTCGT-AGGCGAAG_S8_R2_001.fastq.gz

Ser2 ChIP-seq:
A002664-1_R1.fastq.gz
A002664-1_R2.fastq.gz
A002665-2_R1.fastq.gz
A002665-2_R2.fastq.gz
A002664-2_R1.fastq.gz
A002664-2_R2.fastq.gz
A002665-3_R1.fastq.gz
A002665-3_R2.fastq.gz
A002664-3_R1.fastq.gz
A002664-3_R2.fastq.gz
A002665-4_R1.fastq.gz
A002665-4_R2.fastq.gz
A002664-4_R1.fastq.gz
A002664-4_R2.fastq.gz

Diana_ChIP_WT_UV_3E10_S8_R1_001.fastq.gz
A002664-5_R1.fastq.gz
A002664-5_R2.fastq.gz
A002665-5_R1.fastq.gz
A002665-5_R2.fastq.gz
A002664-6_R1.fastq.gz
A002664-6_R2.fastq.gz
A002665-6_R1.fastq.gz
A002665-6_R2.fastq.gz
A002664-7_R1.fastq.gz
A002664-7_R2.fastq.gz
A002665-7_R1.fastq.gz
A002665-7_R2.fastq.gz
A002664-8_R1.fastq.gz
A002664-8_R2.fastq.gz
A002665-8_R1.fastq.gz

A002665-8_R2.fastq.gz
A002664-9_R1.fastq.gz
A002664-9_R2.fastq.gz
A002665-9_R1.fastq.gz
A002665-9_R2.fastq.gz
A002664-10_R1.fastq.gz
A002664-10_R2.fastq.gz
A002665-10_R1.fastq.gz
A002665-10_R2.fastq.gz
A002664-11_R1.fastq.gz
A002664-11_R2.fastq.gz
A002665-11_R1.fastq.gz
A002665-11_R2.fastq.gz
A002664-12_R1.fastq.gz
A002664-12_R2.fastq.gz
A002665-12_R1.fastq.gz
A002665-12_R2.fastq.gz
A002664-13_R1.fastq.gz
A002664-13_R2.fastq.gz
A002665-13_R1.fastq.gz
A002665-13_R2.fastq.gz
A002664-14_R1.fastq.gz
A002664-14_R2.fastq.gz

Diana_ChIP_ELOF1-KO_UV_3E10_S10_R1_001.fastq.gz
A002665-1_R1.fastq.gz
A002665-1_R2.fastq.gz
A002665-14_R1.fastq.gz
A002665-14_R2.fastq.gz

Pan RNAPII ChIP-seq:
WT_input_1.fastq.gz
WT_input_2.fastq.gz
WTinputChIP_1.fastq.gz
WTinputChIP_2.fastq.gz
WT_mock_1_1.fastq.gz
WT_mock_1_2.fastq.gz
WT_mock_2_1.fastq.gz
WT_mock_2_2.fastq.gz
WT1hrs-1ChIP_1.fastq.gz
WT1hrs-1ChIP_2.fastq.gz
WT1hrs-2ChIP_1.fastq.gz
WT1hrs-2ChIP_2.fastq.gz
WT_UV_1_1.fastq.gz
WT_UV_1_2.fastq.gz
WT_UV_2_1.fastq.gz
WT_UV_2_2.fastq.gz
ELOF1_input_1.fastq.gz
ELOF1_input_2.fastq.gz
ELOF1-KOinputCh_1.fastq.gz
ELOF1-KOinputCh_2.fastq.gz
ELOF1_mock_1_1.fastq.gz
ELOF1_mock_1_2.fastq.gz
ELOF1_mock_2_1.fastq.gz
ELOF1_mock_2_2.fastq.gz
ELOF1-KO1hrs-1C_1.fastq.gz
ELOF1-KO1hrs-1C_2.fastq.gz
ELOF1-KO1hrs-2C_1.fastq.gz
ELOF1-KO1hrs-2C_2.fastq.gz
ELOF1_UV_1_1.fastq.gz
ELOF1_UV_1_2.fastq.gz
ELOF1_UV_2_1.fastq.gz
ELOF1_UV_2_2.fastq.gz
PAF1-RPB-20180724-RPB1-CSB-KO-noUV-15775_R1.fastq.gz
PAF1-RPB-20180724-RPB1-CSB-KO-noUV-15775_R2.fastq.gz
PAF1-RPB-20180926-RPB1-CSB-KO-noUV-16185_R1.fastq.gz
PAF1-RPB-20180926-RPB1-CSB-KO-noUV-16185_R2.fastq.gz
PAF1-RPB-20180724-RPB1-CSB-KO-6J8h-15777_R1.fastq.gz
PAF1-RPB-20180724-RPB1-CSB-KO-6J8h-15777_R2.fastq.gz
PAF1-RPB-20180926-RPB1-CSB-KO-6J8hUV-16186_R1.fastq.gz
PAF1-RPB-20180926-RPB1-CSB-KO-6J8hUV-16186_R2.fastq.gz
PAF1-RPB-20180724-RPB1-CSB-KO-20J8h-15776_R1.fastq.gz
PAF1-RPB-20180724-RPB1-CSB-KO-20J8h-15776_R2.fastq.gz

RNA-seq:
CSB-MCK1_S2_R1_001.fastq.gz

CSB-MCK2_S3_R1_001.fastq.gz
CSB-MCK3_S4_R1_001.fastq.gz
CSB-UV1_S5_R1_001.fastq.gz
CSB-UV2_S6_R1_001.fastq.gz
CSB-UV3_S7_R1_001.fastq.gz
ELOF1-MCK1_S8_R1_001.fastq.gz
ELOF1-MCK2_S9_R1_001.fastq.gz
ELOF1-MCK3_S43_R1_001.fastq.gz
ELOF1-UV1_S11_R1_001.fastq.gz
ELOF1-UV2_S12_R1_001.fastq.gz
ELOF1-UV3_S13_R1_001.fastq.gz
WT-MCK1_S15_R1_001.fastq.gz
WT-MCK2_S16_R1_001.fastq.gz
WT-MCK3_S17_R1_001.fastq.gz
WT-UV1_S18_R1_001.fastq.gz
WT-UV2_S19_R1_001.fastq.gz
WT-UV3_S20_R1_001.fastq.gz

Genome browser session
(e.g. UCSC)

not applicable

Methodology

Replicates

The number of replicates are indicated in Table S9 and related figure legends.

Sequencing depth

All ChIP-seq and ATAC-seq samples were sequenced in paired-end with 150nt sequencing reads. All BrU-seq samples were sequenced in paired-end (although used single-end) with 151nt sequencing reads. Details on sequencing depth and uniquely mapped high quality reads are described in Table S9 and added below.

ATAC-seq (RPE1-iCas9):
WT mock-treated (n=2)
ATACseq_WTMock_Rep1_TagDir: 35,639,384
ATACseq_WTMock_Rep2_TagDir: 29,958,690

ELOF1-KO mock-treated (n=2)
ATACseq_ELOFKOMock_Rep1_TagDir: 28,438,534
ATACseq_ELOFKOMock_Rep2_TagDir: 33,176,750

BruDRB-seq (RPE1-iCas9):
WT 30 minutes DRB release (n=3)
BrUseqRep2_WT30m_SSPE_TagDir: 36,625,983
BrUseqRep3_WT30mDRB_SSPE_TagDir: 78,198,211
BrUseqRep4_WT30mDRB_SSPE_TagDir: 85,459,459

WT 60 minutes DRB release (n=2)
BrUseqRep4_WT60mDRB_SSPE_TagDir: 94,504,592
BrUseqRep5_WT60mDRB_SSPE_TagDir: 99,951,101

ELOF1-KO 30 minutes DRB release (n=3)
BrUseqRep2_ELOFKO30m_SSPE_TagDir: 36,297,661
BrUseqRep3_ELOFKO30mDRB_SSPE_TagDir: 100,792,041
BrUseqRep4_ELOFKO30mDRB_SSPE_TagDir: 105,691,482

ELOF1-KO 60 minutes DRB release (n=2)
BrUseqRep4_ELOFKO60mDRB_SSPE_TagDir: 97,294,170
BrUseqRep5_ELOFKO60mDRB_SSPE_TagDir: 97,772,962

Bru-seq (RPE1-iCas9):
WT mock-treated (n=2)
BrUseqRep2_WT0h_SSPE_TagDir: 46,498,167
BrUseqRep3_WT0h_SSPE_TagDir: 95,200,816

WT 3 hours after 9J/m2 (n=2)
BrUseqRep2_WT3h_SSPE_TagDir: 30,486,325
BrUseqRep3_WT3h_SSPE_TagDir: 91,314,465

WT 8 hours after 9J/m2 (n=2)
BrUseqRep2_WT8h_SSPE_TagDir: 30,832,534
BrUseqRep3_WT8h_SSPE_TagDir: 100,310,116

WT 24 hours after 9J/m2 (n=2)
BrUseqRep2_WT24h_SSPE_TagDir: 46,960,735
BrUseqRep3_WT24h_SSPE_TagDir: 92,145,990

ELOF1-KO mock-treated (n=2)

BrUseqRep2_ELOFKO0h_SSPE_TagDir: 43,875,250
BrUseqRep3_ELOFKO0h_SSPE_TagDir: 100,894,444

ELOF1-KO 3 hours after 9J/m2 (n=2)
BrUseqRep2_ELOFKO3h_SSPE_TagDir: 34,909,758
BrUseqRep3_ELOFKO3h_SSPE_TagDir: 82,382,104

ELOF1-KO 8 hours after 9J/m2 (n=2)
BrUseqRep2_ELOFKO8h_SSPE_TagDir: 35,829,345
BrUseqRep3_ELOFKO8h_SSPE_TagDir: 73,302,725

ELOF1-KO 24 hours after 9J/m2 (n=2)
BrUseqRep2_ELOFKO24h_SSPE_TagDir: 35,592,827
BrUseqRep3_ELOFKO24h_SSPE_TagDir: 68,288,654

RNAPII S2 ChIP-seq (RPE1-iCas9):
WT mock-treated (n=2)
DataTOgi_WTrep1_mock_SSPE_TagDir: 37,516,272
DataTOgi_WTrep2_mock_SSPE_TagDir: 38,571,922

WT 1 hour after 9J/m2 (n=2)
DataTOgi_WTrep1_1h_SSPE_TagDir: 34,409,419
DataTOgi_WTrep2_1h_SSPE_TagDir: 38,789,028

WT 4 hours after 9J/m2 (n=2)
DataTOgi_WTrep1_4h_SSPE_TagDir: 28,093,367
DataTOgi_WTrep2_4h_SSPE_TagDir: 32,867,919

WT 8 hours after 9J/m2 (n=2)
DataTOgi_WTrep1_8h_SSPE_TagDir: 33,947,077
DataTOgi_WTrep2_8h_SSPE_TagDir: 17,812,398

WT 16 hours after 9J/m2 (n=2)
DataTOgi_WTrep1_16h_SSPE_TagDir: 35,102,378
DataTOgi_WTrep2_16h_SSPE_TagDir: 45,062,679

CSB-KO mock-treated (n=2)
DataTOgi_CSBKOrep1_mock_SSPE_TagDir: 37,986,546
DataTOgi_CSBKOrep2_mock_SSPE_TagDir: 40,640,212

CSB-KO 1 hour after 9J/m2 (n=2)
DataTOgi_CSBKOrep1_1h_SSPE_TagDir: 38,447,432
DataTOgi_CSBKOrep2_1h_SSPE_TagDir: 36,096,454

CSB-KO 4 hours after 9J/m2 (n=2)
DataTOgi_CSBKOrep1_4h_SSPE_TagDir: 33,023,511
DataTOgi_CSBKOrep2_4h_SSPE_TagDir: 34,115,863

CSB-KO 8 hours after 9J/m2 (n=2)
DataTOgi_CSBKOrep1_8h_SSPE_TagDir: 38,924,552
DataTOgi_CSBKOrep2_8h_SSPE_TagDir: 39,151,481

CSB-KO 16 hours after 9J/m2 (n=2)
DataTOgi_CSBKOrep1_16h_SSPE_TagDir: 34,581,457
DataTOgi_CSBKOrep2_16h_SSPE_TagDir: 43,678,724

ELOF1-KO mock-treated (n=2)
DataTOgi_ELOFKOrep1_mock_SSPE_TagDir: 40,784,609
DataTOgi_ELOFKOrep2_mock_SSPE_TagDir: 43,805,221

ELOF1-KO 1 hour after 9J/m2 (n=2)
DataTOgi_ELOFKOrep1_1h_SSPE_TagDir: 35,849,282
DataTOgi_ELOFKOrep2_1h_SSPE_TagDir: 46,626,951

ELOF1-KO 4 hours after 9J/m2 (n=2)
DataTOgi_ELOFKOrep1_4h_SSPE_TagDir: 34,899,234
DataTOgi_ELOFKOrep2_4h_SSPE_TagDir: 43,369,451

ELOF1-KO 8 hours after 9J/m2 (n=2)
DataTOgi_ELOFKOrep1_8h_SSPE_TagDir: 51,291,185
DataTOgi_ELOFKOrep2_8h_SSPE_TagDir: 9,676,403

ELOF1-KO 16 hours after 9J/m2 (n=2)
DataTOgi_ELOFKOrep1_16h_SSPE_TagDir: 39,626,707
DataTOgi_ELOFKOrep2_16h_SSPE_TagDir: 42,524,194

Pan RNAPII ChIP-seq (RPE1-iCas9):
WT input (n=2)
WT_input_rep1_SPPE_TagDir: 59,447,372
WT_input_rep2_SSPE_TagDir: 75,872,035

WT mock-treated (n=2)
WT_mock_rep1_SPPE_TagDir: 43,702,697
WT_mock_rep2_SPPE_TagDir: 60,297,146

WT 1 hour after 9J/m2 (n=2)
WT_UV1h_rep1_SSPE_TagDir: 62,042,662
WT_UV1h_rep2_SSPE_TagDir: 82,059,258

WT 8 hours after 9J/m2 (n=2)
WT_UV_rep1_SPPE_TagDir: 52,616,690
WT_UV_rep2_SPPE_TagDir: 76,526,696

ELOF1-KO input (n=2)
ELOF1_input_rep1_SPPE_TagDir: 40,511,010
ELOF1_input_rep2_SSPE_TagDir: 80,121,992

ELOF1-KO mock-treated (n=2)
ELOF1_mock_rep1_SPPE_TagDir: 61,798,796
ELOF1_mock_rep2_SPPE_TagDir: 61,770,248

ELOF1-KO 1 hour after 9J/m2 (n=2)
ELOF1_UV1hrs_rep1_SPPE_TagDir: 70,975,828
ELOF1_UV1hrs_rep2_SPPE_TagDir: 76,828,850

ELOF1-KO 8 hours after 9J/m2 (n=2)
ELOF1_UV_rep1_SPPE_TagDir: 64,798,363
ELOF1_UV_rep2_SPPE_TagDir: 50,474,378

Pan RNAPII ChIP-seq (U2OS (FRT)):
CSB-KO mock-treated (n=2)
CSB-KO_mock_1: 60,090,350
CSB-KO_mock_2: 33,989,141

CSB-KO 8 hours after 6J/m2 (n=2)
CSB-KO_UV_6J8h_1: 55,433,652
CSB-KO_UV_6J8h_2: 31,234,277

CSB-KO 8 hours after 20J/m2 (n=1)
CSB-KO_UV_20J8h: 61,679,092

RNA-seq :
WT mock-treated (n=3)
RNAseq_WT_Mock_rep1: 16,570,265
RNAseq_WT_Mock_rep2: 20,535,747
RNAseq_WT_Mock_rep3: 20,356,970

WT 24 hours after 9J/m2 (n=3)
RNAseq_WT_UV_rep1: 30,231,046
RNAseq_WT_UV_rep2: 18,430,293
RNAseq_WT_UV_rep3: 22,828,990

ELOF1-KO mock-treated (n=2)
RNAseq_ELOFKO_Mock_rep1: 22,250,155
RNAseq_ELOFKO_Mock_rep2: 18,412,158

ELOF1-KO 24 hours after 9J/m2 (n=3)
RNAseq_ELOFKO_UV_rep1: 33,575,741
RNAseq_ELOFKO_UV_rep2: 20,292,635
RNAseq_ELOFKO_UV_rep3: 22,376,948

CSB-KO mock-treated (n=3)
RNAseq_CSBKO_Mock_rep1: 26,689,782
RNAseq_CSBKO_Mock_rep2: 23,198,147
RNAseq_CSBKO_Mock_rep3: 20,027,395

CSB-KO 24 hours after 9J/m2 (n=3)
RNAseq_CSBKO_UV_rep1: 23,039,563
RNAseq_CSBKO_UV_rep2: 12,906,509
RNAseq_CSBKO_UV_rep3: 22,359,479

Antibodies	RNAPII-S2 (Rat) - Milipore (3E10); RRID:AB_10627998; Lot #04-1571 RNAPII-Total (Rabbit) - Bethyl; RRID:AB_2620600; Lot #A304-405A For both antibodies we used 3µg antibody per ChIP-seq experiment
Peak calling parameters	Peak calling was performed using the freely available HOMER software
Data quality	Data quality for individual replicates was confirmed by Trimmomatic and FastQC. Duplicate ChIP-seq reads or reads with low quality were subsequently removed using Biobambam2 and Samtools with the "fixmate -m" and "markdup -r" tools. BrU-seq and ATAC-seq, reads were aligned to the Human Genome 38 (Hg38) using bwa-mem tools (BWA (Version 0.7.16a)) Quality of obtained results were further validated by performing replicate experiments and by testing the reversal of phenotypes over time.
Software	RNAPII-S2 ChIP-seq: Trimmomatic (v3.36), BWA (BWA-v0.7.12-r1039), Biobambam2 (v2.0.72), Genome Analysis Toolkit (GATK-v3.5), HOMER (v4.8.2) RNAPII ChIP-seq, BrU-seq and ATAC-seq: FastQC (Version 0.11.2), BWA (BWA-v0.7.16a), SAM (v1.6), HOMER (v4.8.2), IGV (Version 2.4.3), R (Version 3.5.3), Rstudio (Version 1.1.423) RNA-seq: Trimmomatic (version 0.39), FastQC (version 0.11.9), Hisat2 (version 2.2.0), SAMtools (version 1.1.0), edgeR (version 3.28.1)